

DAMAGE TOLERANCE PREDICTIONS FOR SPAR WEB CRACKING
IN A DIMINISHING STRESS FIELD

by

Randal Evan Heller

A thesis submitted to the faculty of
The University of Utah
in partial fulfillment of the requirements for the degree of

Master of Science

Department of Mechanical Engineering

The University of Utah

December 2011

Report Documentation Page				Form Approved OMB No. 0704-0188	
Public reporting burden for the collection of information is estimated to average 1 hour per response, including the time for reviewing instructions, searching existing data sources, gathering and maintaining the data needed, and completing and reviewing the collection of information. Send comments regarding this burden estimate or any other aspect of this collection of information, including suggestions for reducing this burden, to Washington Headquarters Services, Directorate for Information Operations and Reports, 1215 Jefferson Davis Highway, Suite 1204, Arlington VA 22202-4302. Respondents should be aware that notwithstanding any other provision of law, no person shall be subject to a penalty for failing to comply with a collection of information if it does not display a currently valid OMB control number.					
1. REPORT DATE 01 DEC 2011		2. REPORT TYPE N/A		3. DATES COVERED -	
4. TITLE AND SUBTITLE Damage Tolerance Predictions for Spar Web Cracking in a Diminishing Stress Field				5a. CONTRACT NUMBER	
				5b. GRANT NUMBER	
				5c. PROGRAM ELEMENT NUMBER	
6. AUTHOR(S) Randal Evan Heller				5d. PROJECT NUMBER	
				5e. TASK NUMBER	
				5f. WORK UNIT NUMBER	
7. PERFORMING ORGANIZATION NAME(S) AND ADDRESS(ES) Department of Mechanical Engineering, University of Utah A-10 Systems Program Office Hill AFB Utah				8. PERFORMING ORGANIZATION REPORT NUMBER	
9. SPONSORING/MONITORING AGENCY NAME(S) AND ADDRESS(ES)				10. SPONSOR/MONITOR'S ACRONYM(S)	
				11. SPONSOR/MONITOR'S REPORT NUMBER(S)	
12. DISTRIBUTION/AVAILABILITY STATEMENT Approved for public release, distribution unlimited					
13. SUPPLEMENTARY NOTES The original document contains color images.					
14. ABSTRACT					
15. SUBJECT TERMS					
16. SECURITY CLASSIFICATION OF:			17. LIMITATION OF ABSTRACT UU	18. NUMBER OF PAGES 128	19a. NAME OF RESPONSIBLE PERSON
a. REPORT unclassified	b. ABSTRACT unclassified	c. THIS PAGE unclassified			

Copyright © Randal Evan Heller 2011

All Rights Reserved

THE UNIVERSITY OF UTAH GRADUATE SCHOOL

SUPERVISORY COMMITTEE APPROVAL

of a thesis submitted by

Randal Evan Heller

This thesis has been read by each member of the following supervisory committee and by a majority vote has been found to be satisfactory.

Date

Chair: David W. Hoeppe

Date

Daniel O. Adams

Date

Mark L. Thomsen

ABSTRACT

Current United States Air Force (USAF) Damage Tolerance Analysis (DTA) methodology yields short crack growth lives for webs in built-up beams as used in the construction of wing spars. This results in very short inspection intervals for these types of structures. Inspection data from fleet usage and fatigue tests do not support the analytically-based assertion that spar webs are as damage tolerant critical as typically predicted. Current analytical methods involve short edge distances predicting failure when the crack reaches the edge-of-part. In reality, there is remaining residual strength in the spar web.

Current continuing damage methods allow for cracks that grow up into the part after the lower ligament fails. The assumption for this secondary cracking has been to use the same driving force as in the initial crack. However, the high driving force from bending found near the extreme fiber diminishes as the crack grows toward the neutral axis.

This paper utilizes the test results from two specimens to help validate an analytical approach toward crack growth predictions in spar webs. The goal of this approach is to extend short inspection intervals currently required on some USAF aircraft.

I would like to thank my wife, Mindy, for all of her encouragement and support during this long effort. Without you, I never would have started. Thanks to my children, Evan, Austin and Erin for your patience during the long hours away from home that this effort required. Thanks also to Dr. Paul Clark and Dr. Mark Thomsen of the United States Air Force. You rekindled my love of learning and convinced me that I had what it takes to tackle graduate work. A final thanks to Dr. David Hoeppner of the University of Utah Mechanical Engineering department. You have inspired me to pursue professional development and to strive to blend wisdom, skill, and ethics in all of my engineering endeavors.

TABLE OF CONTENTS

ABSTRACT	iii
LIST OF FIGURES	vii
LIST OF TABLES	viii
ACKNOWLEDGMENTS	ix
1 INTRODUCTION	1
1.1 Evolution of USAF Aircraft Structural Design Philosophies.....	1
1.2 Current Aircraft Structural Design Philosophy	5
1.3 Research Project Outline	8
1.4 Research Project Objective	16
2 FATIGUE TESTING OF SIMULATED SPARS	18
2.1 Tension Specimen	18
2.2 Bending Specimen	20
3 STRESSCHECK [®] 2D CRACK PATH PREDICTIONS	29
3.1 StressCheck [®] Crack Path Procedure	29
3.2 StressCheck [®] Crack Path Model Results	35
4 AFGROW CRACK GROWTH PREDICTIONS	41
4.1 A-10 DTA Ground Rules and Program Inputs	41
4.2 Tension Model Crack Growth Predictions	44
4.3 Bending Model Crack Growth Predictions	48
5 DISCUSSION	59
5.1 Fatigue Crack Growth Testing Observations	59
5.2 StressCheck [®] Modeling Observations	61
5.3 AFGROW Modeling Observations	62

6 SUMMARY	64
6.1 Conclusions	64
6.2 Recommendations	65

APPENDICES

A TENSION SPECIMEN PHOTOGRAPHS.....	67
B BENDING SPECIMEN PHOTOGRAPHS	74
C SHAPE DESIGNER SECTION DATA.....	81
D A-10 DTA GROUND RULES FOR A-10A RECONFIGURED POST DESERT STORM	88
E AFGROW INPUT FILE SCREENSHOTS.....	99
REFERENCES	124

LIST OF FIGURES

1 A-10 Thunderbolt II aircraft.	9
2 Spar web crack identification.	11
3 Typical razor-cut and pre-crack.	14
4 Tension specimen test setup.	19
5 Tension specimen crack growth curve.	21
6 Tension specimen failure.	21
7 Anomalous Crack in tension specimen at 13,762 cycles.	22
8 Tension specimen repair for anomalous crack.	22
9 Bending specimen test setup.	23
10 Bending specimen at failure.	25
11 Bending specimen crack growth curve.	25
12 Intentional cracks in bending specimen.	26
13 Bending test article tested incorrect hole.	26
14 Anomalous crack in bending specimen.	27
15 Beam idealization for StressCheck® models.	30
16 Crack definition in idealized StressCheck® model.	31
17 Tension model geometry.	31
18 StressCheck® tension model.	33
19 Bending model geometry.	33
20 Normal constraint at pivot holes in bending model.	34

21 Typical bearing load in holes of bending model.....	34
22 StressCheck® bending model.	34
23 Baseline crack path prediction in tension specimen.	35
24 Crack path prediction compared to tension specimen crack.....	36
25 Second tension model with anomalous crack included.	37
26 Improved correlation to test when anomalous crack is modeled.	38
27 Crack path prediction compared to bending specimen crack.	40
28 NASGRO material file inputs for 7075-T6 aluminum.	43
29 AFGROW model for primary ligament crack – baseline condition.	46
30 AFGROW model for secondary crack – baseline condition.	46
31 AFGROW model for continuing damage crack – baseline condition.	46
32 Beta correction versus crack length for tension specimen.....	47
33 User-defined beta versus crack length for tension specimen.	49
34 AFGROW model for user-defined beta.....	50
35 Crack growth comparison - tension specimen.	51
36 Crack life comparison - tension specimen.	52
37 AFGROW model for through crack at a hole.	52
38 Beta correction versus crack length for bending specimen.	53
39 User-defined beta versus crack length for bending specimen.	54
40 Crack growth comparison - bending specimen.....	57
41 Crack life comparison - bending specimen.	58
42 Tension specimen failed web.	68
43 View A tension specimen.....	69
44 View B tension specimen.....	69
45 View C tension specimen.	70

46 View D tension specimen.	70
47 View E tension specimen.....	71
48 View F tension specimen.....	71
49 View G tension specimen.	72
50 View H tension specimen.	72
51 View I tension specimen.....	73
52 Bending specimen failed web.....	75
53 View A bending specimen.	76
54 View B bending specimen.	77
55 View C bending specimen.....	77
56 View D bending specimen.....	78
57 View E bending specimen.	78
58 View F bending specimen.....	79
59 View G bending specimen.....	79
60 View H bending specimen.	80
61 View I bending specimen.....	80
62 Shape Designer SaaS beam geometry.	82
63 Shape Designer SaaS beam properties.	83
64 Shape Designer SaaS cap geometry.	84
65 Shape Designer SaaS cap properties.	85
66 Shape Designer SaaS idealized beam geometry	86
67 Shape Designer SaaS idealized beam properties	87
68 AFGROW input file – tension model 1 - ligament crack – baseline.	100
69 AFGROW input file – tension model 2 - IFS for secondary crack – baseline.	101
70 AFROW input file – tension model 3 - secondary crack – baseline.	102

71 AFGROW input file – tension model 4 - continuing damage crack – baseline.	103
72 AFGROW input file – tension model 1 - ligament crack – beta correction. . .	104
73 AFGROW input file – tension model 2 - IFS for secondary crack – beta correction.	105
74 AFROW input file – tension model 3 - secondary crack – beta correction. . .	106
75 AFGROW input file – tension model 4 - continuing damage crack – beta correction.	107
76 AFGROW input file – tension model 1 - ligament crack – user-defined beta.	108
77 AFGROW input file – tension model 2 - IFS for secondary crack – user-defined beta.	109
78 AFROW input file – tension model 3 - secondary crack – user-defined beta.	110
79 AFGROW input file – tension model 4 - continuing damage crack – user-defined beta.	111
80 AFGROW input file – bending model 1 - ligament crack – baseline.	112
81 AFGROW input file – bending model 2 - IFS for secondary crack – baseline.	113
82 AFROW input file – bending model 3 - secondary crack – baseline.	114
83 AFGROW input file – bending model 4 - continuing damage crack – baseline.	115
84 AFGROW input file – bending model 1 - ligament crack – beta correction. .	116
85 AFGROW input file – bending model 2 - IFS for secondary crack – beta correction.	117
86 AFROW input file – bending model 3 - secondary crack – beta correction. .	118
87 AFGROW input file – bending model 4 - continuing damage crack – beta correction.	119
88 AFGROW input file – bending model 1 - ligament crack – user-defined beta.	120
89 AFGROW input file – bending model 2 - IFS for secondary crack – user-defined beta.	121
90 AFROW input file – bending model 3 - secondary crack – user-defined beta.	122
91 AFGROW input file – bending model 4 - continuing damage crack – user-defined beta.	123

LIST OF TABLES

<u>Table</u>	<u>Page</u>
1 Beta corrections for tension model	47
2 User-defined beta values for tension model	50
3 Beta corrections for bending model.	55
4 User-defined beta values for bending model	56

ACKNOWLEDGMENTS

I would like to thank my graduate committee, Dr. David W. Hoepfner, Dr. Daniel Adams, and Dr. Mark L. Thomsen for their support and encouragement through this research project. It is impossible to overstate the support Dr. Thomsen gave to me, most especially for funding the testing portion of this project.

Thanks to Mr. Meir Levy of the Northrop Grumman Corporation for his assistance in testing the spar web specimens. A special thanks to Mr. Ken Grube of Northrop Grumman for his invaluable contributions to the structural integrity of the A-10 Thunderbolt II aircraft, the structure of which is the model for this project.

Thank you to the USAF's Aircraft Structural Integrity Program (ASIP) Analysis Group at Hill Air Force Base for your support and patience during my graduate studies.

Thank you to Dr. Ken Griffin and Dr. Hal Burnside at Southwest Research Institute for approving and funding this graduate work.

1 INTRODUCTION

1.1 Evolution of USAF Aircraft Structural Design Philosophies

The United States Air Force was founded as an independent entity on September 18, 1947 breaking its ties to the United States Army that dated back to the inception of the United States Army Signal Corp's Aeronautical Division on August 1, 1907. However, the Air Force's Aircraft Structural Integrity Program (ASIP) wasn't established until May 1958. How was the Air Force able to function for 51 years without an organized structural integrity program? To answer that question the history of aircraft development must be considered.

1.1.1 Aircraft Development in the Army Air Corps

The early years of aircraft development were characterized by rapid innovation in propulsion and structural efficiency and the obsolescence of aircraft before life limits became a factor. These improvements along with the lower costs of acquisition and operation of successive types and models of engines were often sufficient to make prior production aircraft economically obsolete.¹ Materials used in early airplane construction, primarily wood and fabric, were less susceptible to fatigue, so static strength concerns predominated.

Early aluminum designs relied on alloying with copper-dominated non-aluminum metals that provided an acceptable mix of strength and durability.¹ Airframe fatigue was still not the overriding concern to airplane designers. Thus,

structures designed during this period typically had ultimate strength requirements, but did not have service-life requirements. Uncertainties in loads, materials and methods led to a safety factor of 1.5 on aircraft limit loads, and this strength requirement has remained in place in both civil and military design requirements. The capability of the newly-manufactured airplane structure to meet static strength requirements was demonstrated by analysis and supported by test evidence.²

1.1.2 Aircraft Structural Development

in the United States Air Force

In the 1940s fatigue of metals was a known phenomenon, but systematic fatigue analyses had not yet become part of the aircraft structural integrity paradigm. Unbeknownst to designers and operators, the risks from fatigue were increasing. Ironically, the increased risk from fatigue came from improvements in the strength of aluminum alloys. During the 1950s aircraft manufacturers evolved from the copper-based aluminum alloys to zinc-based. These new zinc-based alloys possessed superior tensile strength properties, but suffered from reduced durability, corrosion and fracture toughness properties. Further compounding the problem was refined stress analysis methods together with detailed full-scale static testing of structural components which lowered previously-conservative margins of safety in fatigue-prone structure. The knowledge of actual operating conditions also became more extensive because of advances in instrumentation. These flight conditions provided more precise static strength analysis based on ultimate design conditions calculated from

conditions actually measured in flight.² Commercial airplane operators endured the loss of three De Havilland Comets during the early 1950s, but it wasn't until after the fatigue-related loss of two B-47 bombers on March 13, 1958, followed by a third B-47's in-flight wing separation only a month later that Air Force leadership saw an irrefutable need for an organized structural integrity program. In May 1958 the ASIP was established with the following three objectives: control structural failure of operational aircraft, determine methods of accurately predicting aircraft service life, and to provide design and test approaches that would avoid structural fatigue problems in future aircraft.¹ In November 1958 Air Force Chief of Staff, General Curtis LeMay, signed a policy directive that directed major operational commands to work with the Air Force's engineers in implementing ASIP.

The first structural life paradigms adopted by the Air Force were the "safe life" and the "fail safe" approaches. In a safe-life paradigm, structure is designed to perform through its entire design service life without detrimental effects from fatigue. The "safe life" of the aircraft was established by dividing the number of successful test-simulated flight hours by a factor (four was commonly used by the USAF).³ The purpose of the factor was to account for the many uncertainties that exist in materials and manufacturing quality. During an aircraft's safe life, the cumulative probability of failure is less than 1 in 1000 over the safe life of operation.⁴ This concept was the analytical basis for all new U.S. Air Force aircraft designed during the 1960s.³ However, it was recognized through experience that defects in the fleet could appear much sooner than the analyzed

and test-demonstrated life.² Because inspection was not required as a part of the safe life approach, small cracks and defects could escape detection and grow unchecked with dramatic consequences.³ Attempts to design for a certain life were gradually changed to control fatigue life by limiting major component service lives. The use of imprecise and inaccurate fatigue analyses coupled with inherent material scatter characteristics often resulted in unnecessarily short lives and many sound structures were retired prematurely.² In fact, as many as 99.9% of all structures managed under safe life were retired from service long before their useful lives had been reached.⁴ These inherent problems with the safe life paradigm were thought to be addressed by the fail safe paradigm.

The fail safe paradigm derives structural safety through redundancy. Structure is designed such that the failure of any critical member will result in the safe redistribution of load to an adjacent member. Consequently, the emphasis for this approach was multiple-load-path structure with strength requirements for the partial or complete failure of a single structural element. Fail safe concepts have been generally effective, correctly guarding against the types of failures for which it was intended. However, single-load-path structure did not benefit from fail safe precautions, and even multiple-load-path structure was susceptible to multi-site damage, where several adjacent structural details may contain cracks. Fail-safe construction is still absolutely necessary, but has not prevented several notable fatal crashes by structural failures due to fatigue.⁵

One such notable failure occurred in 1969 when the Air Force lost a new F-111 aircraft after only 107 hours of flying time. It was ultimately determined

that the structural failure of the F-111 was caused by an initial defect in the D6AC steel pivot fitting, a single-load-path element, that secured the wing to the aircraft.⁶ This initial defect caused a fatigue crack to form and routine flying caused the crack to grow to a critical length in a fraction of the time predicted by designers. The shortcomings highlighted by the F-111 failure were instrumental in adoption of the current structural analysis and maintenance paradigm, that of “damage tolerance”.

1.2 Current Aircraft Structural Design Philosophy

1.2.1 Damage Tolerance Design Philosophy

The USAF led the transition from the safe-life design approach to the physics-based fracture mechanics methods in the United States. The 1969 F-111 failure was one of the main catalysts in the transition of the USAF to the damage tolerance design philosophy in 1975.⁷

The damage tolerance design philosophy uses a deterministic fracture-mechanics-based approach to crack growth coupled with an assumption of an initial discontinuity state to determine the total life of a part. Integral to the damage tolerance paradigm is the requirement to periodically inspect structures for signs of growth of these assumed flaws. Damage tolerance uses Linear Elastic Fracture Mechanics (LEFM) to determine the life of a component and its residual strength due to the presence of a flaw or crack. The objective of the damage tolerance approach is to be able to sustain required loads in the presence of cracks, accidental damage, discrete damage, or environmental degradation until such a time that such damage can be detected and repaired.²

The advantage of the damage tolerance methodology is that cracked structure is treated and analyzed in an appropriate fashion whereas the previous methods only allowed for the immediate removal of cracked structure.⁸

1.2.2 Damage Tolerance and ASIP in the Modern Air Force

Newly-developed aircraft in today's Air Force are designed under a number of guiding documents. Foremost amongst them is the Joint Services Specification Guide (JSSG 2006)⁹. The ASIP's defining document is MIL-STD-1530C, which "defines the requirements necessary to achieve structural integrity in USAF aircraft while managing cost and schedule risks through a series of disciplined, time-phased tasks."¹⁰ MIL-STD-1530C defines the five program tasks of ASIP: Task I, Design Information, Task II, Design Analyses and Development Testing, Task III, Full-Scale Testing, Task IV, Certification and Force Management Development, and Task V, Force Management Execution. Damage tolerance requirements are found throughout the five tasks.

In Task I, the requirements to develop a durability and damage tolerance control program are given. Task II requires the generation of the damage tolerance analysis. Task III includes the damage tolerance testing requirements. Task IV includes the Force Structural Maintenance Plan (FSMP), the document that combines Damage Tolerance Analysis (DTA) results with Non-Destructive Inspection (NDI) requirements. Task V includes the Loads/Environment Spectrum Survey (L/ESS) which is used to help determine when an update to the DTA is required, and also provides for periodic updates of the FSMP.

In this new damage tolerance paradigm, traditional life limits are constantly being redefined. Schijve¹¹ notes:

Ideas about the lifetime have changed over the years. As an example, in the fifties, the lifetime of a transport aircraft was supposed to be about 10 years because it was thought that the aircraft would be obsolete after 10 years. Later, it turned out that this argument was too pessimistic, and a lifetime of 20 years was adopted as a more realistic target. In the eighties and ninetens, (sic) aircraft older than 20 years could still be economically flown. The term “aging aircraft” was introduced for these aircraft which refers to safety issues which can occur if maintenance is below standards.

Grandt¹² comments:

The fact that these structures have reached “old age” with potential for further productive use is testimony to the soundness of their original design and construction and continuous maintenance upkeep on the structure. Indeed, premature retirement could be an unnecessary waste of these valuable assets, *provided they can continue to be employed in a manner that protects the public safety.*

Determining the “effective age” of such structures can be problematic, however, as “calendar time” does not provide a complete indication of structural health. A component’s actual life depends on the severity of fatigue, corrosion, and other time dependent damage that develops in service. Moreover, the formation of fatigue cracks and/or corrosion depends upon the nature of prior usage as well as on the effectiveness of structural maintenance, repairs, and modifications.

The Air Force is being required to field and maintain aircraft longer now than at any time in their history. In fact, many aircraft in the fleet with years or even decades of service behind them are expected to remain in service another 25 years or more.¹³ In this new paradigm, the life of an individual aircraft or even a fleet of aircraft is no longer determined by a set number of years or a prescribed number of flight hours. Life is now generally thought of as “economic life” and tends to be determined more by an aircraft’s inherent operational capability and maintenance costs required for its continual operation.¹⁴ In fact,

the whole concept of what constitutes “failure” is being rethought. As Gallagher⁷ states:

Today, with a downward trend in the number of catastrophic airframe failures, structural failures are viewed by Leadership as the sudden increase in high structural maintenance costs and as unplanned structural maintenance efforts that impact availability and operational tempo. The new types of structural failure (as defined by Leadership) are largely the result of operating an aging fleet, which results in new classes of structural integrity issues.

1.3 Research Project Outline

1.3.1 Project Overview

The A-10 Thunderbolt II, shown in Fig. 1, is a twin-engine, close-air-support aircraft in service with the United States Air Force since 1975. The A-10 was designed and produced by Fairchild Republic, which discontinued aircraft production in 1984. The A-10 is a valuable asset to the United States Air Force and Army because of its unique capabilities. It can deliver precision-guided weapons at high altitudes, as well as surgical close-air support at low altitudes. It's also the only aircraft equipped with the GAU-8 30mm cannon, capable of firing 65 rounds a second of High-Explosive Incendiary (HEI) or Armor Piercing Incendiary (API) rounds. Furthermore, the sturdy airframe design enables the A-10 to operate from austere airfields and take battle damage without degrading capability. Examples of its survivability include self-sealing fuel cells protected by foam, manual flight control systems that back up hydraulic controls, armor and a ballistic tub surrounding the cockpit.

The original service requirement for the A-10 was 6,000 hours requiring periodic inspection, maintenance, and repairs. This was later upgraded to 8,000



Fig. 1 A-10 Thunderbolt II aircraft.¹⁵

hours after rework and retrofit of existing wings. The new requirement of 16,000 hours coupled with other system enhancements and a goal to increase availability resulted in a desire to reevaluate the total life and inspection requirements of Fatigue Critical Locations (FCLs) throughout the aircraft. Refined analyses of FCLs will reduce the inspection actions required thus reducing the overall cost of ownership and improving the aircraft availability. In regards to life extension analysis of aging structures, Grandt¹² stated:

The new analyses should employ the latest calculation methods and software, reflect the most recent assessment of structural condition, account for potential modifications or repairs, and consider projected usage. Since the updated analysis will, in most cases, be conducted with more sophisticated software and incorporate more accurate input data than available for the original design calculations, it is possible that some overly conservative assumptions and large safety factors may be relaxed, and there may, in fact, be more life remaining than originally calculated.

Just such a damage tolerance reassessment to update all FCLs for the A-10 was completed in 2006.¹⁶ This report was a collaborative effort between the USAF, Northrop Grumman Corporation, and Southwest Research Institute®. The Air Force, like many other entities, prefers to have standardized calculation procedures for fatigue life, crack growth and residual strength. In order to ensure consistency in the report a set of ground rules was created regarding the application of damage tolerance principles and the use of crack growth software codes. These ground rules establish initial crack sizes, retardation parameters, fracture toughness values, etc.

Having standardized procedures are useful, but such procedures can imply a considerable risk of unconservative or over-conservative results.¹¹ For instance, in the A-10 procedures, failure for any structure where a primary crack was growing from a hole toward a free edge was defined as the failure of that ligament. However, in the case of wing spar webs, significant residual strength and stable crack growth life still exists after the failure of this ligament. Where a double row of fasteners attach the spar web to the spar caps, a secondary crack will most likely form between the holes, and a continuing damage crack will grow upward toward the beam neutral axis as shown in Fig. 2.

There is a desire within the Air Force to develop a continuing damage model and methodology whereby this remaining life can be utilized. This research program is one step along that path. This work is the continuation of an effort begun in the A-10 analysis group wherein this project was recommended¹⁷.

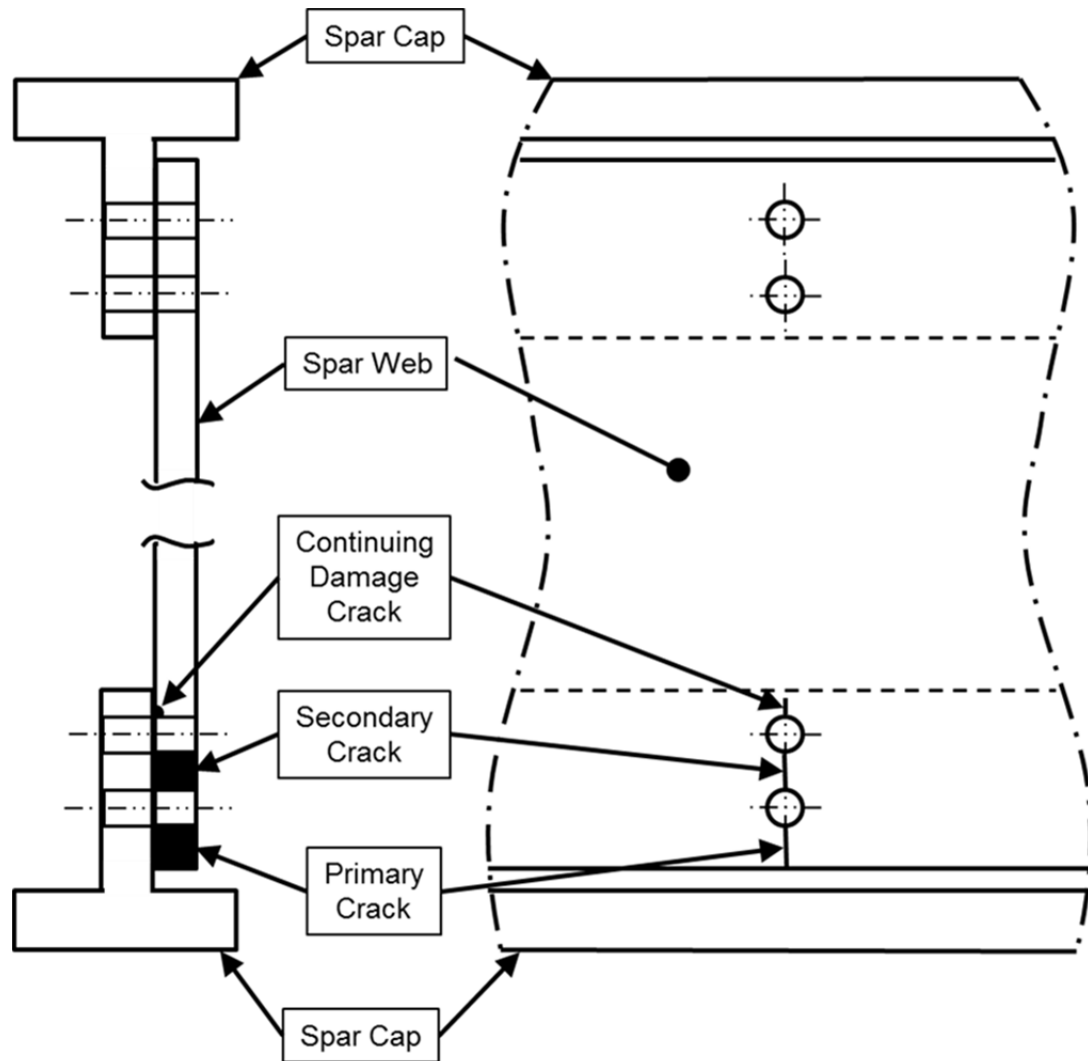


Fig. 2 Spar web crack identification.

This test program is also intended to validate the analysis assumptions utilized therein.

The plan for development of this methodology is to use a building-block approach through testing and analysis. In a building-block approach, simple tests with fewer variables are completed first and analysis is performed. Tests of increasing complexity are performed only after acceptable characterization and correlation to simpler tests are complete.¹⁸ In this program, components are first

tested using constant amplitude loading, and analysis is performed to validate the software tools and methods. Two elementary loading conditions are considered: pure tension and bending with vertical shear (3-point bending). This is the scope of this research effort. Once constant amplitude crack growth can successfully be modeled, variable-amplitude loading tests will be performed using the A-10's Reconfigured Post-Desert Storm (RPDS) Severe spectrum.¹⁹

Variable- amplitude loading is necessary to accurately predict the life of spar web components in the A-10.⁸ Spectrum-specific retardation parameters must be developed and applied to the analytical models. Finally, structural non-linearity must be considered. The forward and aft spars in the center wing panel are Intermediate Diagonal Tension (IDT) beams. The mid spar is shear resistant. The effectiveness of this method in non-linear structural behavior under variable-amplitude loading represents the top of the building-block pyramid. The decision to pursue these follow-on efforts relies on the results of this study.

1.3.2 Component Fatigue Tests

Component test articles were fabricated simulating typical A-10 wing spar geometry and construction.²⁰ Materials, material form, temper were all typical of A-10 center wing panel spar construction. These spars were constructed from extruded 2024-T3511 aluminum end caps riveted to stiffened 7075-T6 sheet metal aluminum webs. The cap-to-web attachment consisted of a double row of MS20470D8 protruding head solid rivets. Stiffener spacing in the test articles were typical of that used in the wing, and functioned primarily to prevent shear buckling in the web. Stiffeners were attached using single rows of MS20470D8

rivets. Test article webs were designed (for the bending specimen) to be shear-resistant. That is, no elastic buckling was expected up to and including the maximum applied shear load. As previously mentioned, the center spar is shear-resistant, and the forward and aft spars are IDT beams. In the outer wing panel, all three spars are IDT beams. Therefore, this test represents typical structure in the mid spar of the center wing panel.

Each test specimen had a 0.020 x 0.020 inch razor-cut induced flaw in one of the rivet holes from which to nucleate cracks as shown in Fig. 3. The procedure was to notch an undersized hole, then precrack the specimen at a stress of 22 kips per square inch (ksi) and a stress ratio of 0.05 until a fatigue crack formed. This crack was grown with the goal of having a 0.05 inch x 0.05 inch flaw once the hole was drilled-up to its final 0.253 inch to 0.256 inch diameter. The rivets installed in these holes were not bucked or otherwise expanded in the holes. The intent was to provide support to the hole and prevent deformation during loading while allowing easy access for crack measurements.

Upon completion of precracking, the stress was lowered to 15 ksi with a stress ratio of 0.05. Cycling commenced, and crack measurements were taken periodically and recorded until specimen failure. Complete test setup and testing requirements were detailed in a test planning document.²¹ Test results were documented in a final test report.²²

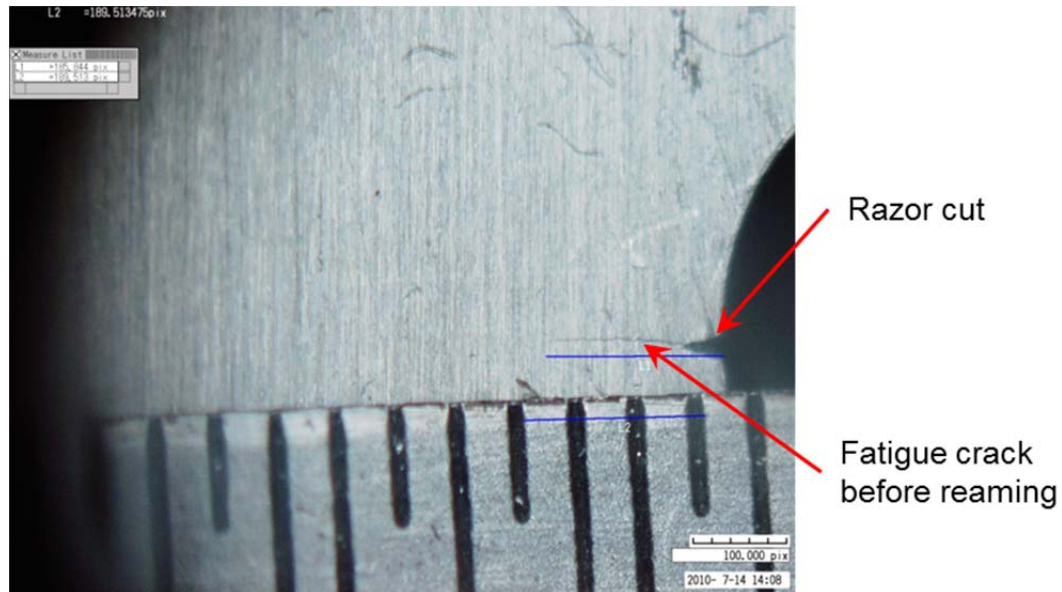


Fig. 3 Typical razor-cut and pre-crack.

1.3.3 StressCheck® Two-Dimensional (2D)

Crack Path Model Predictions

StressCheck® is a p-version Finite Element Analysis (FEA) software code created by Engineering Software Research & Development, Inc. (ESRD) of St. Louis, MO. A p-element FEA code utilizes polynomial elements in place of linear elements used in h-element FEA codes. The advantage of using p-elements is that traditional mesh refinement is not required in areas of high stress gradient. Instead, successive runs are made with increasing polynomial order to capture these gradients and converge on a solution. Energy methods are used to check for model convergence. StressCheck® version 9.2 was used for this project.

One of the unique features of the software is its ability to allow the user to model crack elements in the mesh and progressively grow those cracks into the structure at user-defined increments. Because it is a 2D planar model,

StressCheck[®] computes through-crack stress intensity factors for mode I and mode II along a predicted crack propagation path.²³ The trajectory of the crack is determined by a relationship between mode I and mode II stress intensity factors K_I and K_{II} , and is valid for two-dimensional planar analysis. StressCheck[®] does not compute the rate at which cracks will grow, merely the path they will take and the driving force for crack extension. In structures with multiple cracks growing, some accounting for crack interaction can be modeled by selecting different crack growth increments for each crack. The automesh tool in StressCheck[®] automatically re-meshes the geometry after each run with six-node triangular elements. For the crack path functionality it is recommended by ESRD to run the software at a p-level of 4. For crack growth rate predictions, the software code AFGROW is used.

1.3.4 AFGROW Crack Growth Predictions

AFGROW is a fatigue crack growth code, originally developed by the Air Force Research Laboratory, which allows users to input model-specific parameters and predict the life of metallic structures. AFGROW calculates cycle-by-cycle crack growth using one of five material models (Forman Equation, Walker Equation, Tabular Lookup, Harter-T method, and NASGRO Equation) and one of five load interaction (retardation) models (Closure, FASTRAN, Hsu, Wheeler, and Generalized Willenborg) for spectrum loading.

Stress intensity, K , is calculated according to Equation 1, where σ is the

$$K = \sigma \sqrt{\pi * a} * \beta \quad (1)$$

stress, 'a' is the crack length, and β is the correction factor that accounts for the effect of boundaries, loading, etc. The individual effects of boundaries are typically found in handbooks and their composite effect is obtained by compounding, or the multiplication of the individual effects.²⁴ For example, Equation 2 describes a compound beta solution comprised of n individual effects.

$$\beta = \beta_1 * \beta_2 * \beta_3 * ... * \beta_n \quad (2)$$

One particularly useful feature in AFGROW is the ability to enter user-defined beta values or beta corrections (beta multipliers) to adjust the stress fields, adjust for geometry, etc. Beta corrections are equivalent to the factors β_1 , β_2 , etc. above, whereas a user-defined beta is equivalent to the total beta solution β . This is where the tabular K (stress intensity) outputs from the StressCheck[®] models are integrated into AFGROW. With data regarding K versus crack length inputted into AFGROW, life predictions can be calculated and compared to test-derived crack growth data. AFGROW version 5.1.5.16 was used for this project.

1.4 Research Project Objective

Listed are the objectives for this research project:

1. Coordinate testing and documentation of two simulated spar specimens, one in pure tension and one in three-point bending (testing performed by Northrop Grumman Corporation, Bethpage, New York).
2. Assess the ability of StressCheck[®] to predict crack paths in simulated spar webs as compared to the testing performed in task 1.
3. Assess the ability of AFGROW to utilize the stress intensity solutions from StressCheck[®] to accurately predict crack growth lives in simulated spar webs under constant amplitude loading.

4. Determine from tasks 2 and 3 above if enough promise exists in this methodology to recommend that the Air Force proceed with the next phase of testing, that of variable-amplitude loading.

2 FATIGUE TESTING OF SIMULATED SPARS

2.1 Tension Specimen

2.1.1 Tension Test Setup and Cycling

The tension specimen represented the most elementary loading condition, pure tension undergoing constant-amplitude cycling. Previous analyses of web details used a pure tension loading assumption. The specimen was mounted in a servo-hydraulic test frame as shown in Fig. 4. Precracking was completed as described previously. Following pre-cracking and reaming the hole to final size, a maximum load of 56 kips was applied in the longitudinal direction, resulting in a gross section stress of 15 ksi. The stress ratio of 0.05 was used throughout testing.

Constant-amplitude cycling was performed and crack measurements taken periodically. The full crack growth history from starting notch to failure was recorded.²²

2.1.2 Tension Specimen Results

From the initial flaw, the lower ligament of the tension specimen failed in 22,378 cycles. Cycling continued and at 31,000 cycles, a 0.020 inch x 0.020 inch razor-cut notch was introduced at the upper edge of the lower hole to help nucleate a crack. At 38,000 cycles, the notch was increased in size to 0.070 inch

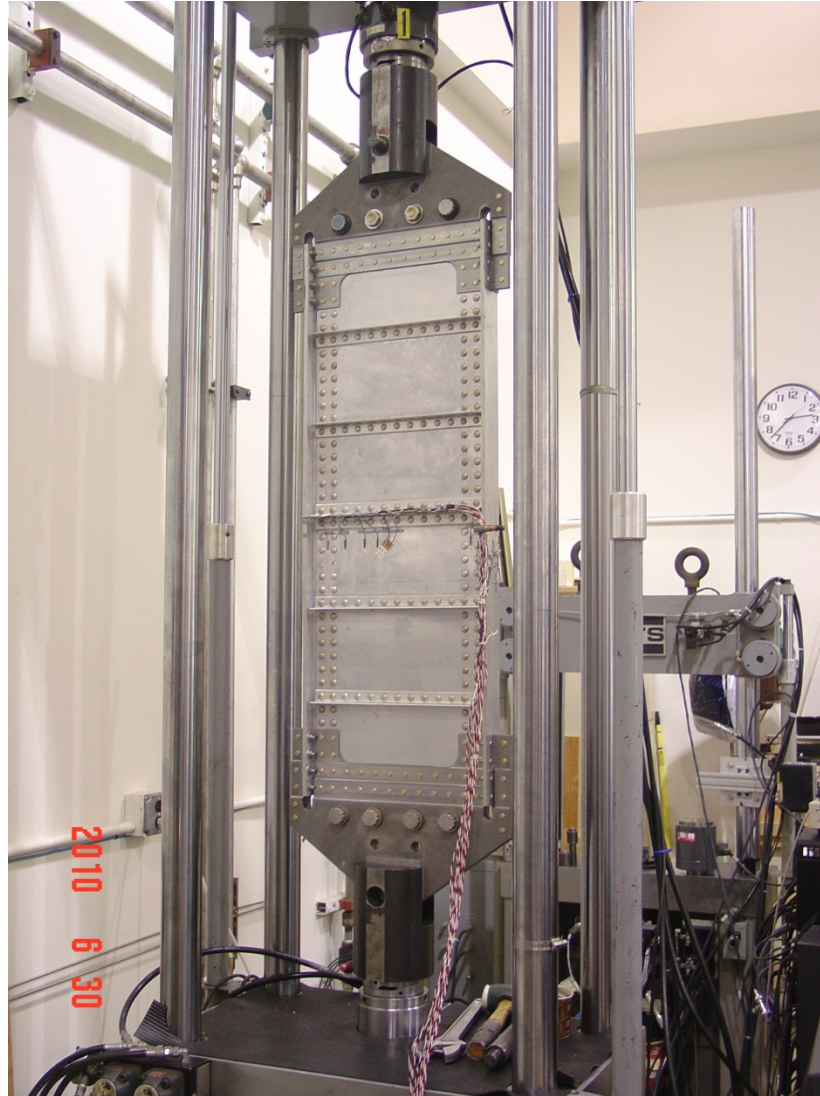


Fig. 4 Tension specimen test setup.

x 0.060 inch, with the 0.070 inch length measured along the face, and the 0.060 inch length measured along the bore of the hole. The crack between the lower and upper holes failed at 47,650 cycles, 25,272 cycles after the failure of the lower ligament and 9,650 cycles after the last razor-cut was introduced. Cycling continued and at 52,000 cycles, a 0.040 inch x 0.040 inch razor-cut notch was introduced at the upper edge of the upper hole to help nucleate a crack. By 64,400 cycles, the crack had grown to 6.4 inches long. In the next 24 cycles the

crack grew approximately another 3.9 inches. Total crack growth life of this third crack was 16,776 cycles after the crack grew to the upper hole. Therefore the total crack growth life was 63,954 cycles as shown in Fig. 5. The failed specimen is shown in Fig. 6. Additional photographs of the failed specimen, including magnified views of the fracture surfaces, can be found in Appendix A.

2.1.3 Tension Test Anomalies

At 13,672 cycles, a 6.56 inch-long anomalous crack was detected approximately 6 inches from the outer edge of the test specimen as shown in Fig. 7. The crack was stop-drilled and repaired with doubler plates, and an identical repair was installed on the opposite end of the test specimen as a precautionary measure as shown in Fig. 8. Although this crack was repaired and strain survey readings showed it to be effective, the presence of this crack affected the crack path of the continuing damage crack. This effect is discussed in greater detail in Section 3.

2.2 Bending Specimen

2.2.1 Bending Test Setup and Cycling

The three-point bending specimen (bending plus shear) most closely approximates the load case to which A-10 spars are subjected. The bending specimen was pre-cracked in a similar manner as the tension specimen. It was then mounted to a loading fixture²⁵ and placed into the servo-hydraulic test frame as shown in Fig. 9. Following pre-cracking and reaming the hole to final size, a maximum load of 24 kips was applied in the vertical direction, resulting in a tensile stress of 15 ksi at the edge of the web combined with a shear stress of 8

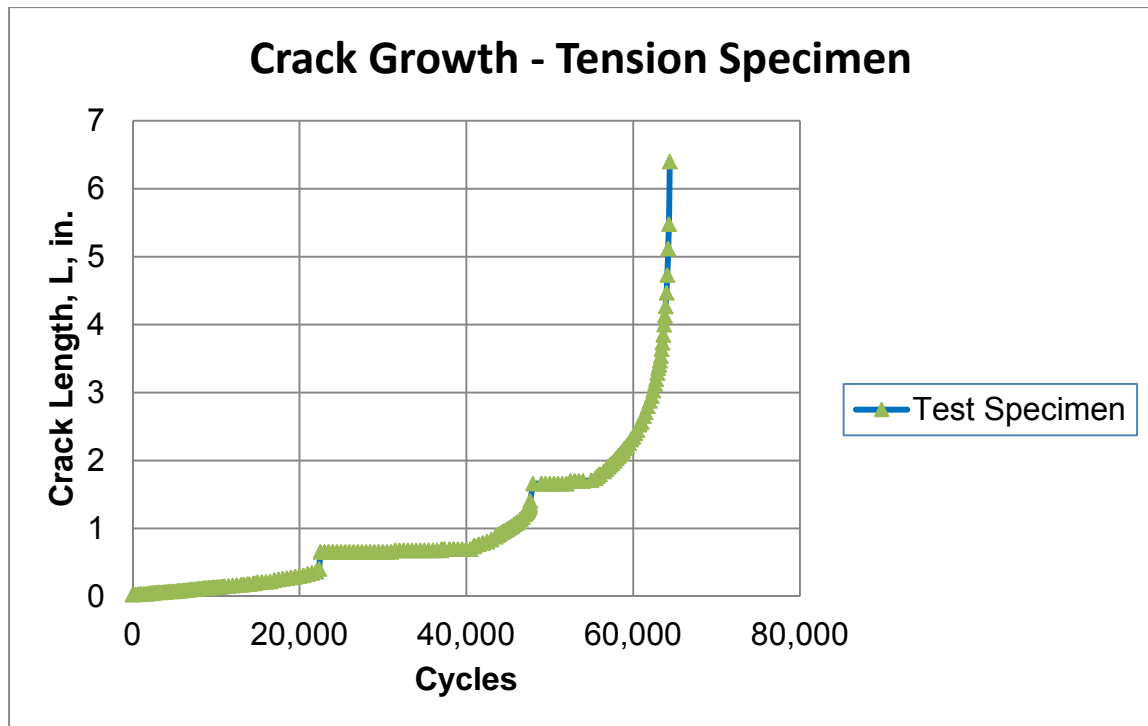


Fig. 5 Tension specimen crack growth curve.

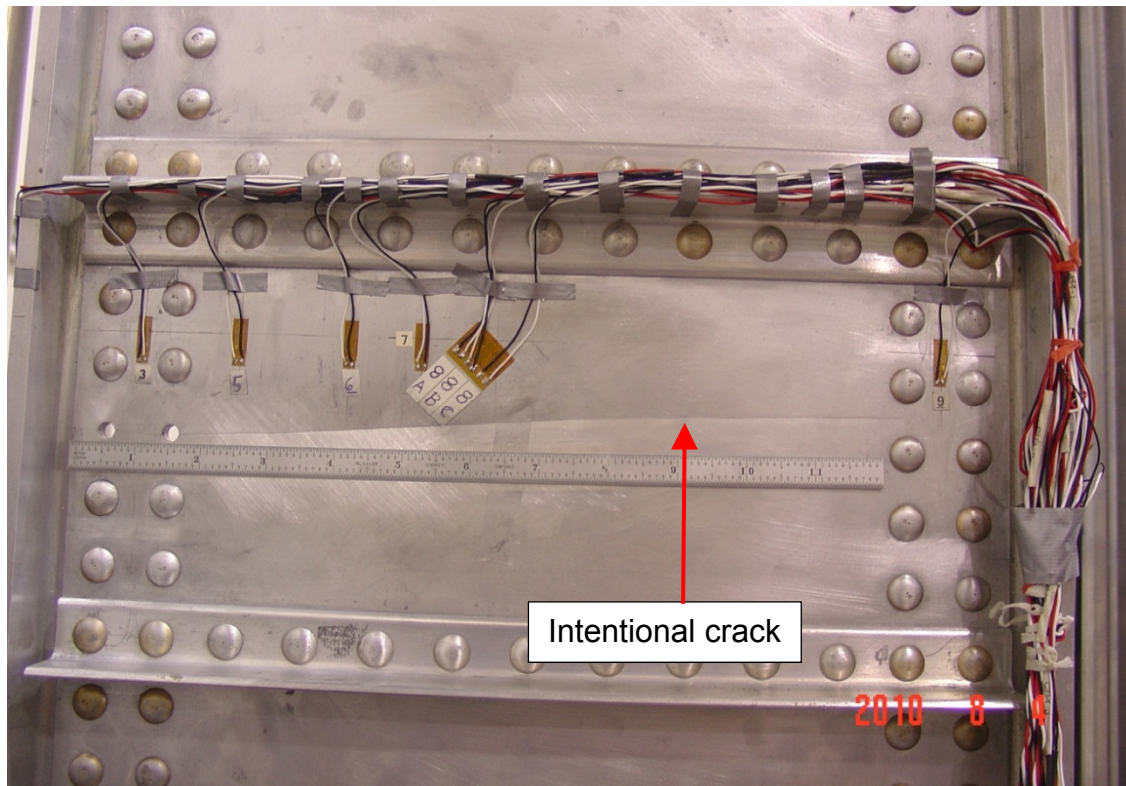


Fig. 6 Tension specimen failure.

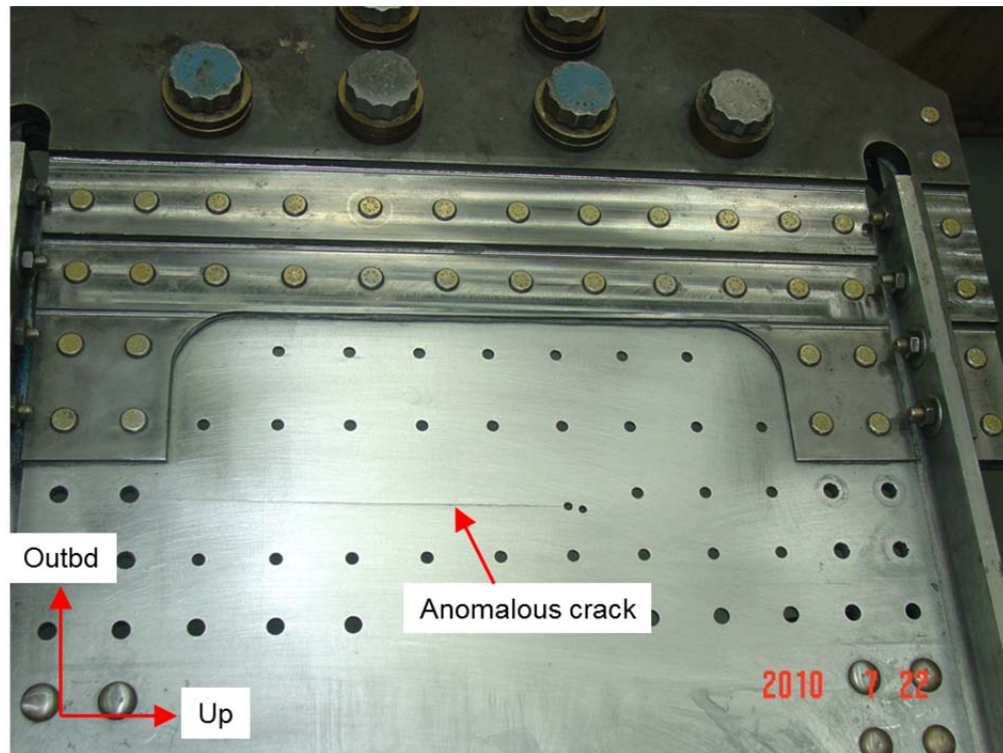


Fig. 7 Anomalous Crack in tension specimen at 13,762 cycles.

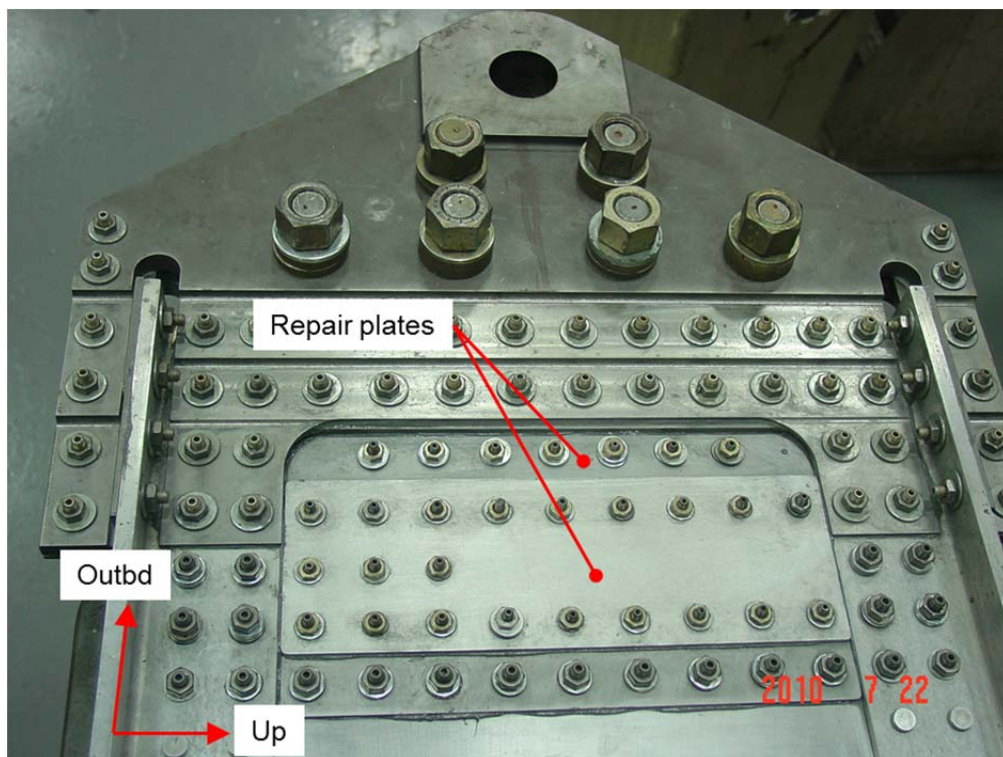


Fig. 8 Tension specimen repair for anomalous crack.

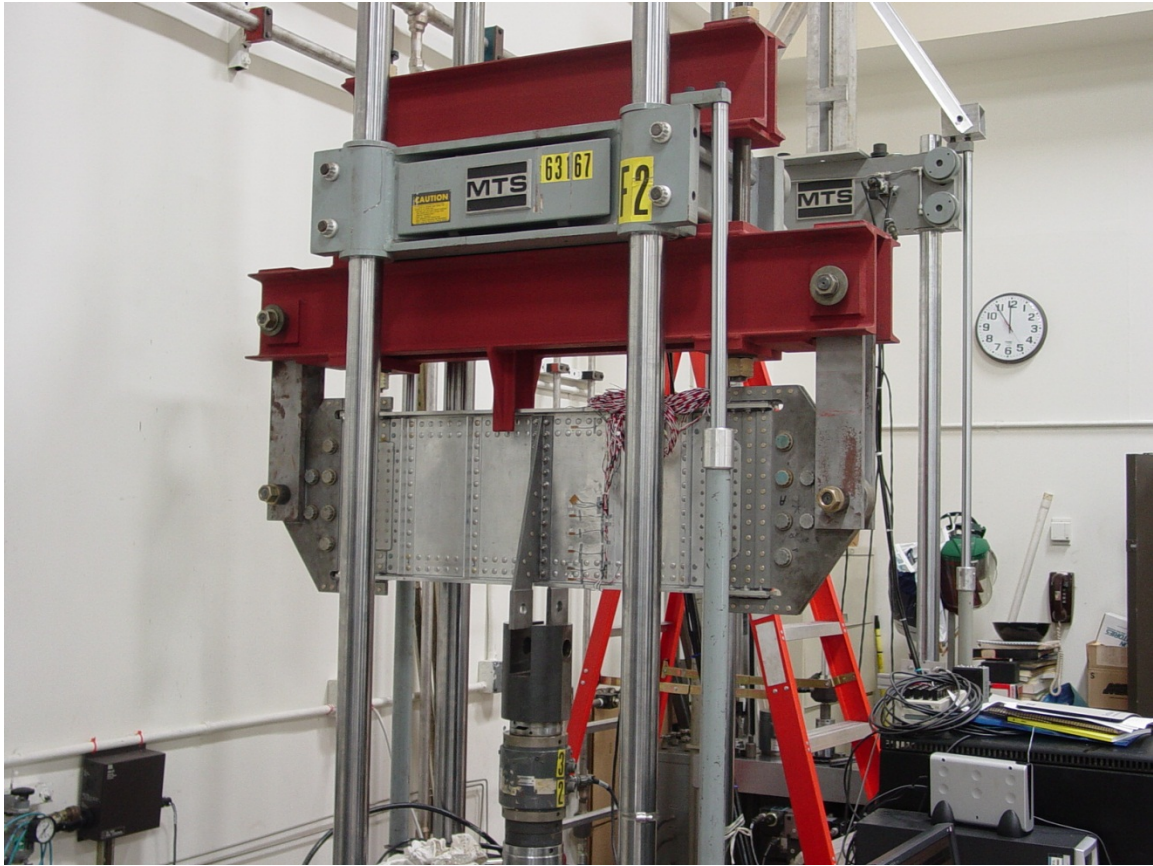


Fig. 9 Bending specimen test setup.

ksi. The stress ratio used was 0.05.

Constant-amplitude cycling was performed and crack measurements taken periodically. The full crack growth history from starting notch to failure was recorded.²²

2.2.2 Bending Specimen Results

From the initial flaw, the lower ligament of the bending specimen failed in 47,369 cycles. Cycling continued and at 60,000 cycles, a 0.030 inch x 0.030 inch razor-cut notch was introduced at the upper edge of the lower hole to help nucleate a crack. At 115,250 cycles the maximum applied load was increased to

26 kips (8.3% increase). At 116,000 cycles, the notch was increased in size to 0.040 inch x 0.060 inch, with the 0.040 inch length measured along the face, and the 0.060 inch length measured along the bore of the hole. Measurable crack growth occurred starting at 131,000 cycles. The crack growing up from the lower hole grew at an angle to the vertical, thus it never grew into the upper hole. A crack nucleated and began propagating up from the upper hole at 133,000 cycles. This crack grew up at an angle similar to the crack growing up from the lower hole. At 212,000 cycles, the crack growing up from the upper hole grew underneath the loading strap, and periodic measurements were no longer possible. The specimen failed outside of the test section, near the grips, at 336,293 cycles as shown in Fig. 10. The crack growth curve is presented in Fig. 11. A close-up view of the failed specimen is shown with cracks highlighted by marker in Fig. 12. At the time of failure, the crack growing up from the upper hole had grown to a vertical length of approximately 4.69 inches up measured from the bottom of the web. It grew into the sixth hole up from the bottom of the web, and no crack indications were found exiting the hole on the opposite side.

2.2.3 Bending Test Anomalies

Cracks were grown from the wrong fastener row as shown in Fig. 13; the holes that were notched, pre-cracked, and from where the primary cracks were grown were one row inboard (closer to test article centerline) than were prescribed from the test article drawings. Since the moment arm in the test article increased toward the fastener centerline, the moment, and thus the longitudinal load at the notch, were increased by approximately 3.7%. Since vertical shear was constant

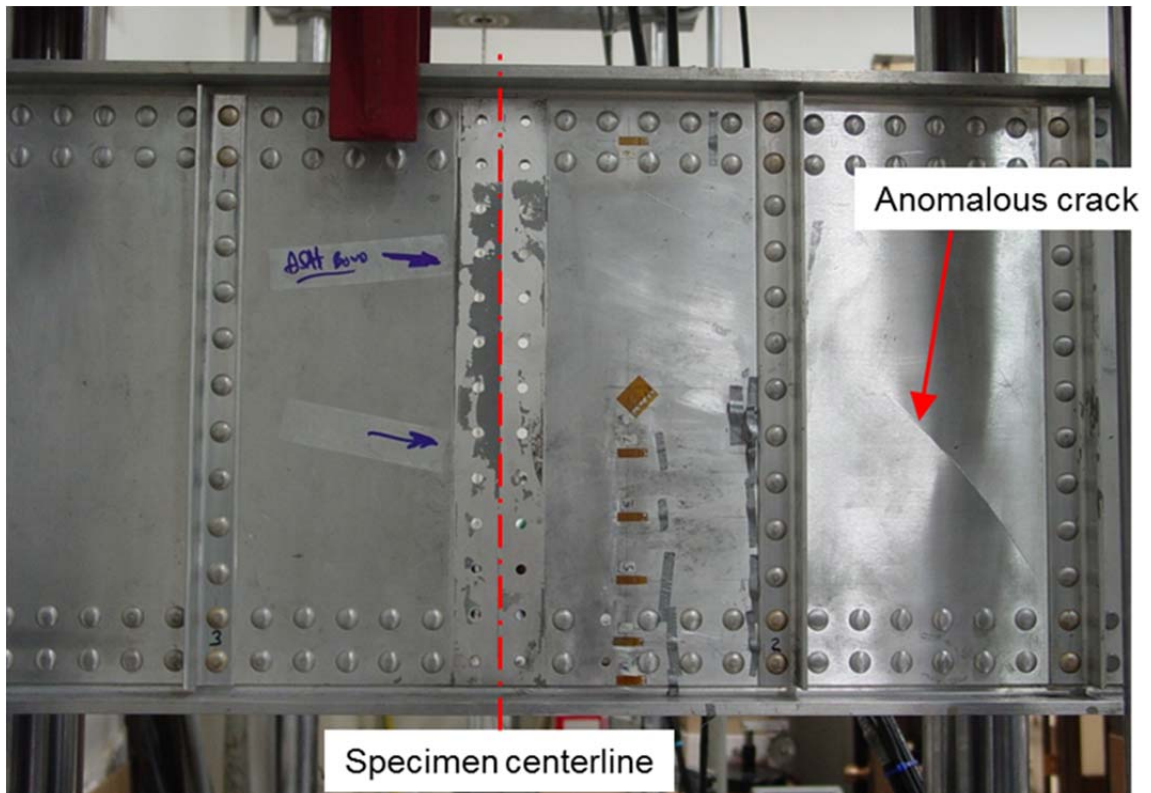


Fig. 10 Bending specimen at failure.

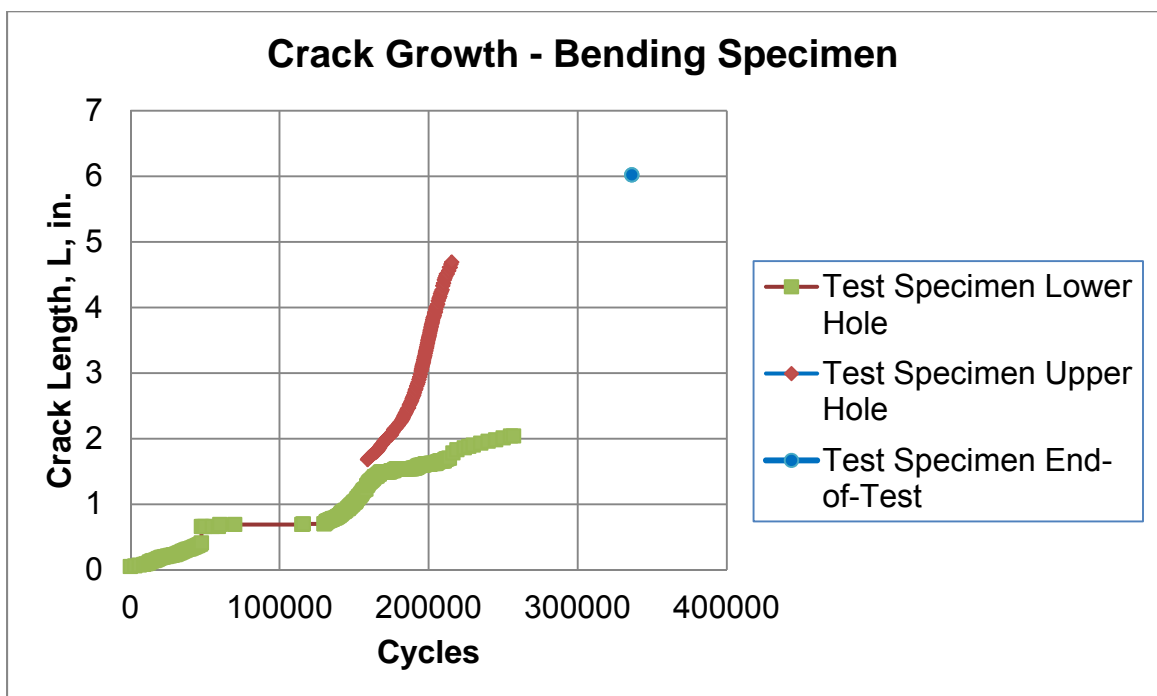


Fig. 11 Bending specimen crack growth curve.

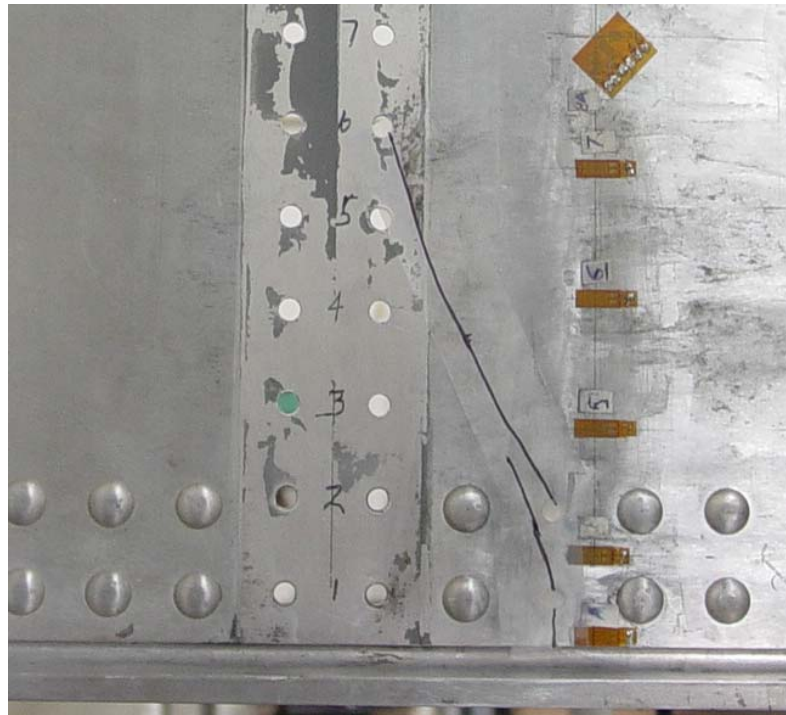


Fig. 12 Intentional cracks in bending specimen.

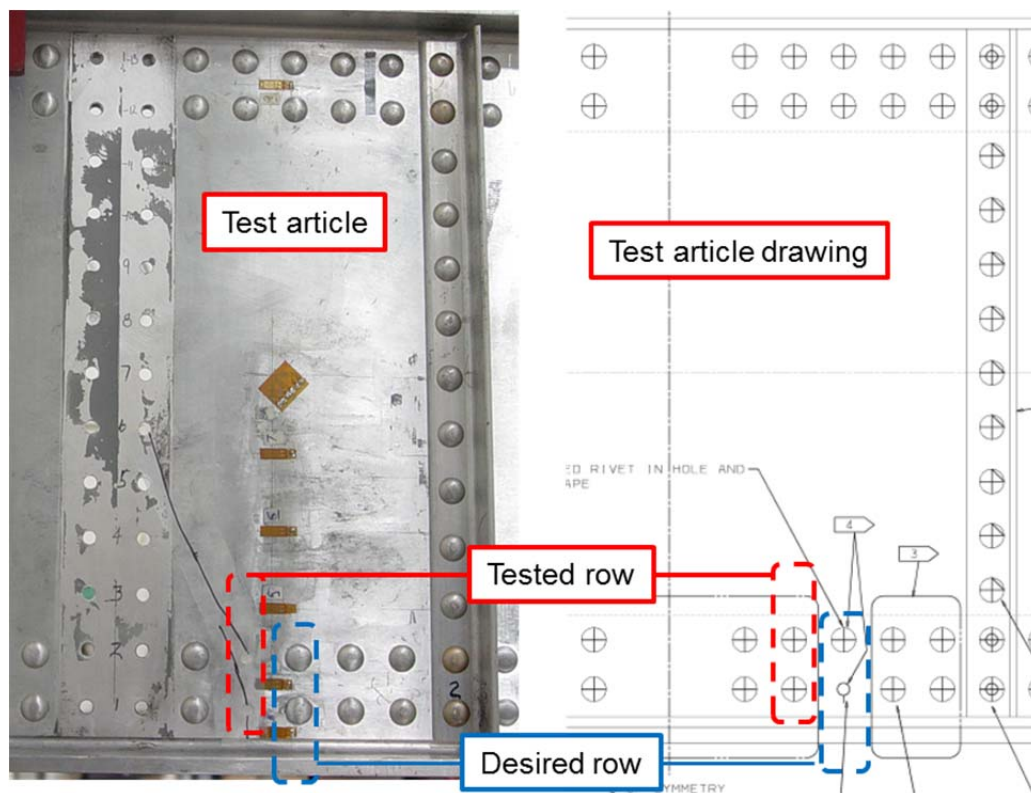


Fig. 13 Bending test article tested incorrect hole.

throughout the test section, shear was unaffected by the error. Also, because the primary cracks started growing closer to the center loading angles, less crack growth data was recorded before the crack grew underneath the angles. Thus, much of the data on crack rate as the crack grew closer to the neutral axis was lost.

During precracking, a 1 inch long crack was detected near the end of the specimen common to the last fastener in the grips, similar to the cracking seen in the tension specimen as shown in Fig. 14. The repair developed for the tension specimen was applied at both ends of the bending specimen to preclude further cracking.

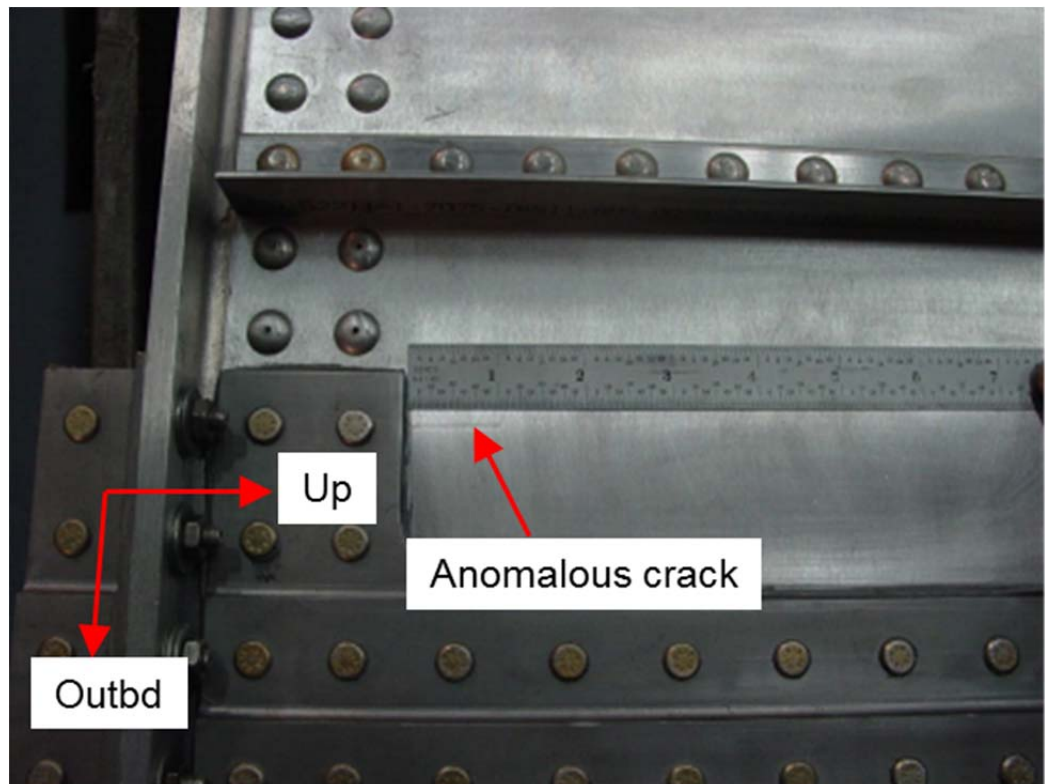


Fig. 14 Anomalous crack in bending specimen.

An additional crack not documented in the test report grew down and outboard from the upper hole. No data exists to document the cycle count at which this crack nucleated, nor is there any crack growth history. For this reason, it is difficult to model the interaction of this crack with the documented cracks.

Finally, there is no crack growth history recorded for the large anomalous crack near the outboard end whose failure ultimately caused the end of the bending test. Because no crack growth history exists for this crack, it was difficult to determine the influence it may have had on the growth and crack path on the primary cracks.

3 STRESSCHECK® 2D CRACK PATH PREDICTIONS

3.1 StressCheck® Crack Path Procedure

3.1.1 Structure Idealization and Model Definition

Since StressCheck® only has the ability to grow cracks in a 2D planar model, the three-dimensional built-up structure must be idealized in a 2D environment. This was accomplished by modeling the built-up beam as a unitized I-beam with properties approximating those of the as-tested structure as shown in Fig. 15. Properties of the built-up structure were calculated using MechaTools Technologies' Shape Designer SaaS software. Shape Designer SaaS is a beam section properties and stress analysis software package. Using this tool, geometric dimensions of the idealized beam's cross-section were manipulated until the section properties of the idealized beam most closely matched those of the built-up test specimen. The web geometry was unchanged, as was the overall height of the beam. The final cap dimensions were 0.53 inches thick and 2.0213 inches wide. With these dimensions, the idealized beam matched the area and second moment of inertia of the built-up beam within 1.6% and 0.3%, respectively.

Only a single material property can be used for the unitized beam, so the properties of the web were chosen since this was the focus of the research effort. The stiffness of the caps and webs differ by approximately 5% (the caps are

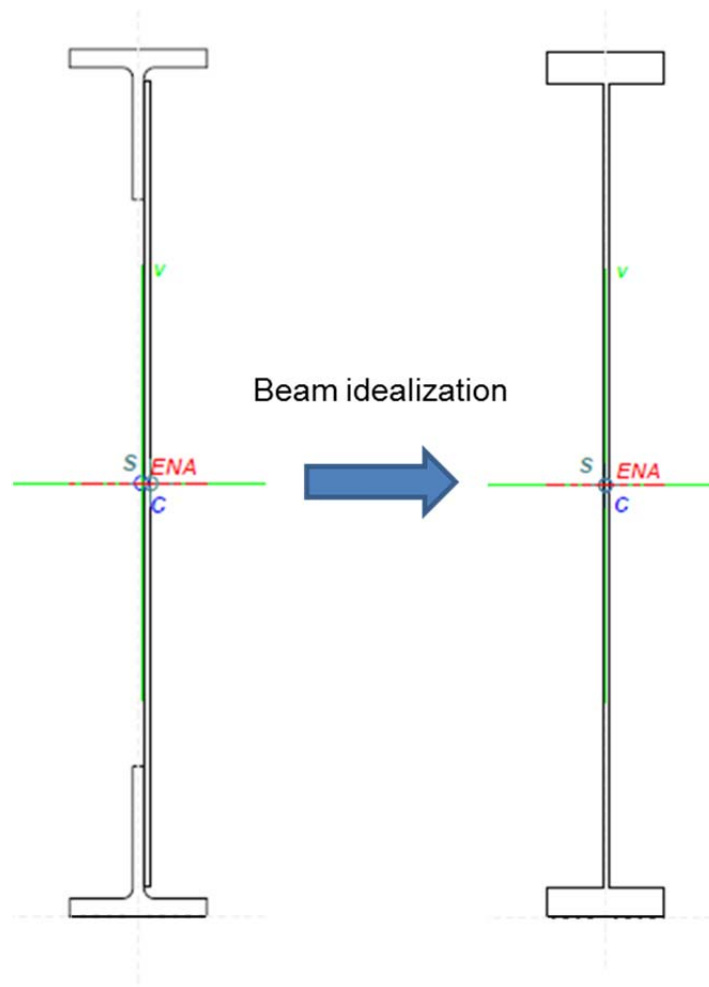


Fig. 15 Beam idealization for StressCheck® models.

stiffer) so by essentially softening the caps in the idealized model, a larger portion of the load will be reacted by the webs. This will give a conservative result in regards to stress intensities, and thus crack growth, in the web.

The StressCheck® tension model propagated three cracks: the primary ligament crack, the secondary crack between the fasteners growing upward from the lower hole, and the continuing damage crack growing upward from the upper hole as seen in Fig. 16. The tension model setup with cracks inserted can be seen in Fig. 17.

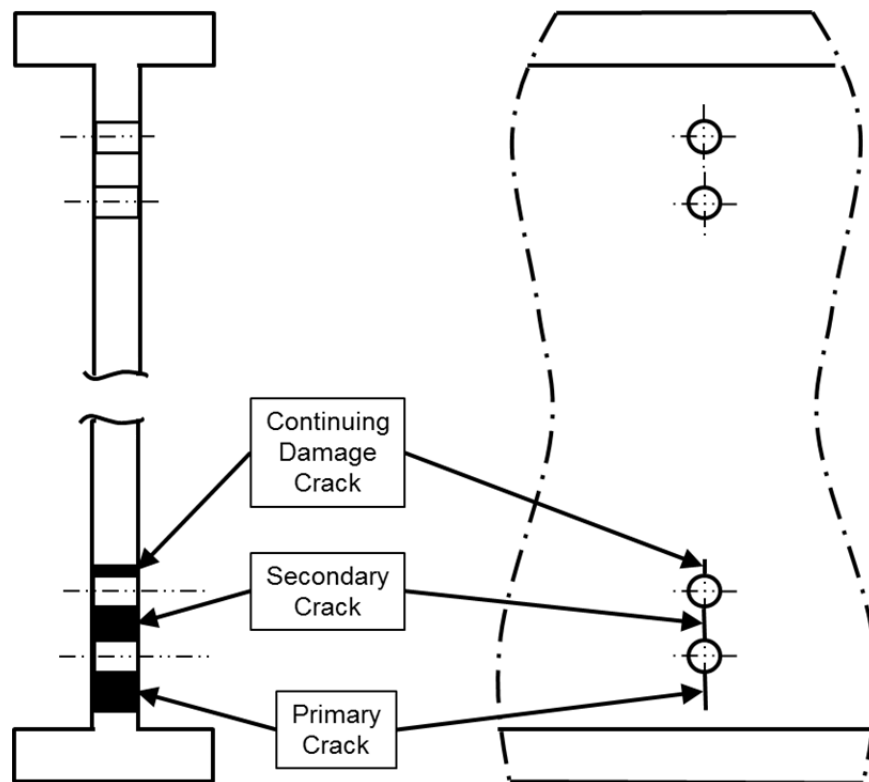


Fig. 16 Crack definition in idealized StressCheck® model.

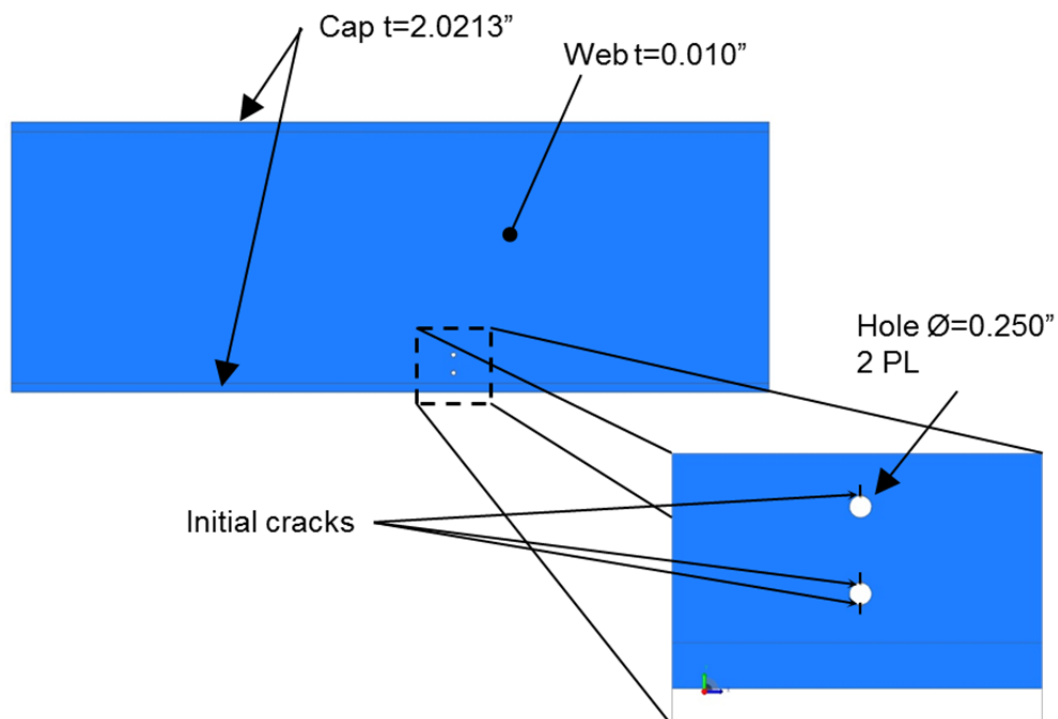


Fig. 17 Tension model geometry.

3.1.2 Model Loading and Constraint

The end plates that held the test specimens were designed to uniformly load both the caps and the webs. Any minor variations in loading due to construction variability, fastener hole fill, etc. was dissipated by the time the load reached the test section. Strain surveys performed before the start of cyclic loading confirmed the uniformity of the load across the test section. Therefore, the end plates were not modeled and the tension specimen model was loaded with a constant traction of 15 ksi along one edge. The specimen had a fixed displacement constraint on the edge opposite the load as seen in Fig. 18.

The bending test specimen was loaded in 3-point bending via load introduction angles attached at the specimen centerline. The specimen was allowed to pivot at the bolt in the outboard end plates. This was modeled by extending the idealized beam geometry out until the length matched the overall test specimen's length as seen in Fig. 19. The hole for the pivot point was included directly into the web as seen in Fig. 20. Since this model was only for use in determining stress intensities and crack paths near the center of the beam this simplification was acceptable. Load was introduced via bearing in the holes common to the loading angles as seen in Fig. 21. Vertical displacements were constrained at the pivot holes but rotation and horizontal translation were unconstrained, similar to the tested specimen. The complete bending model is shown in Fig. 22.

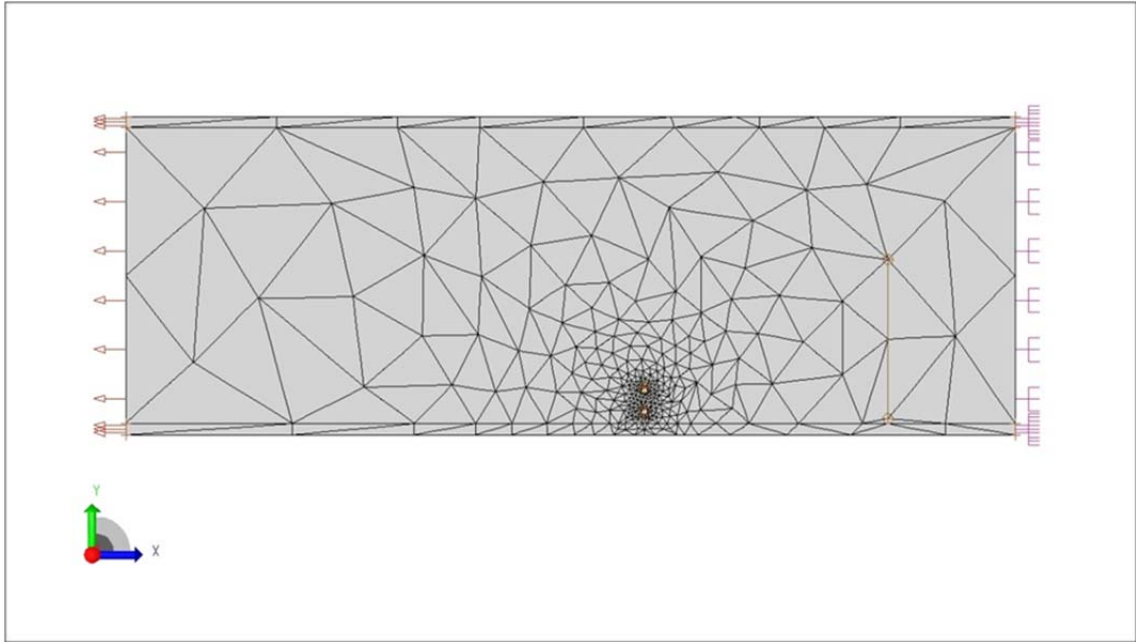


Fig. 18 StressCheck® tension model.

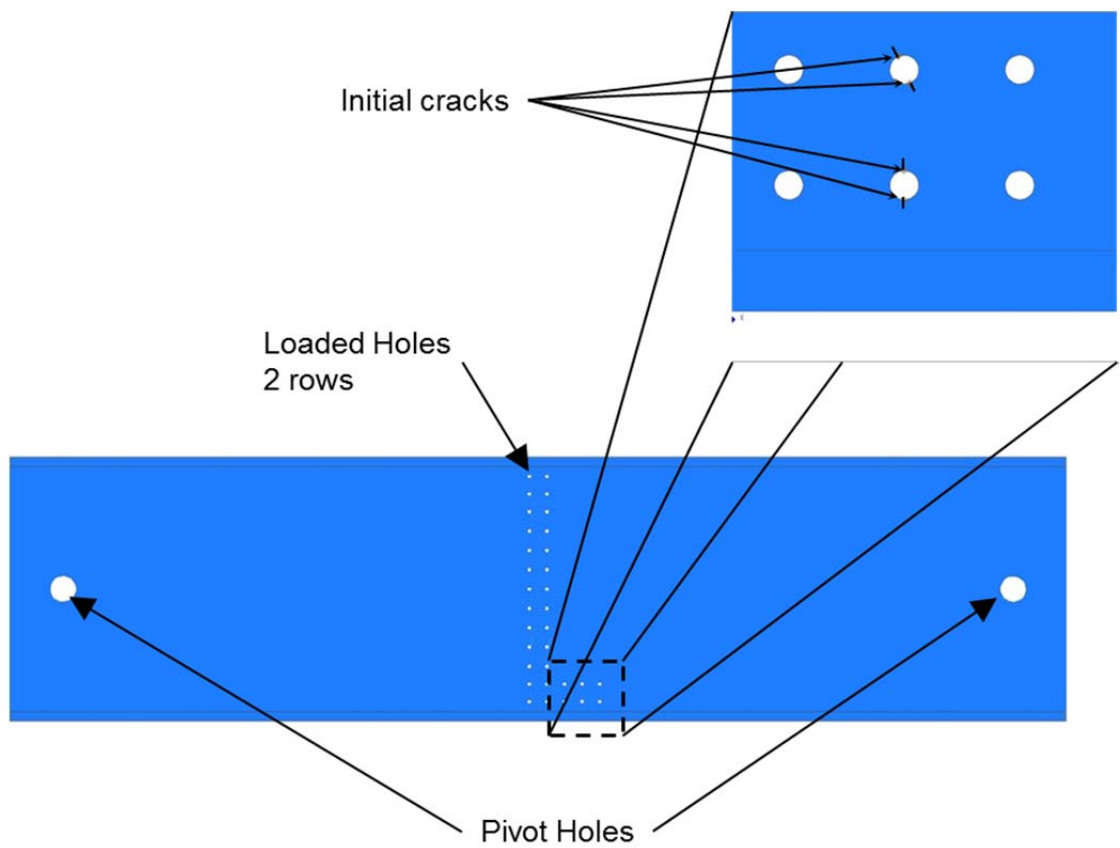


Fig. 19 Bending model geometry.

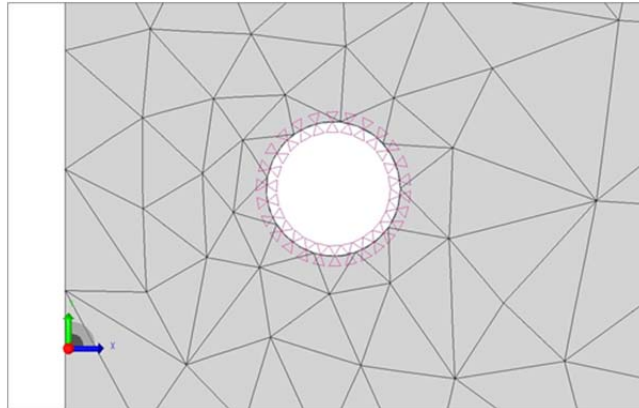


Fig. 20 Normal constraint at pivot holes in bending model

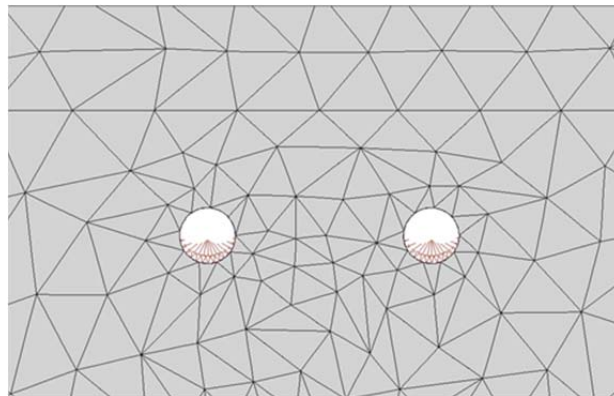


Fig. 21 Typical bearing load in holes of bending model.

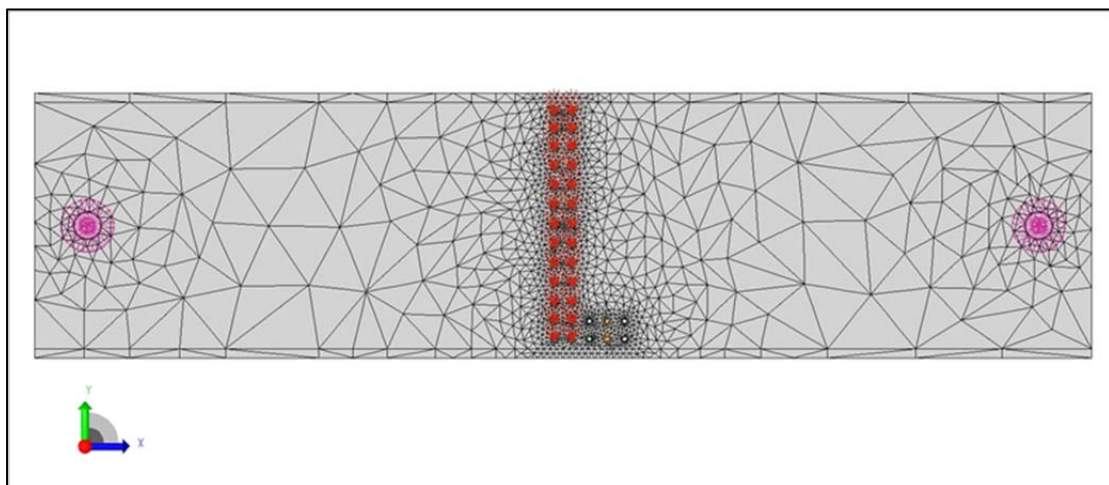


Fig. 22 StressCheck® bending model.

3.2 StressCheck® Crack Path Model Results

3.2.1 Tension Model Results

The StressCheck® model was run with three cracks growing: the primary ligament crack, the secondary crack between the fasteners growing upward from the lower hole, and the continuing damage crack growing upward from the upper hole. As expected, the lower ligament crack propagated downward at very nearly -90 degrees with respect to the horizontal. The secondary crack propagated up and into the upper hole at an angle of almost exactly 90 degrees. The continuing damage crack also propagated through the web at close to 90 degrees as seen in Fig. 23. However, this did not match the crack growth experienced in the test article as seen in Fig. 24.

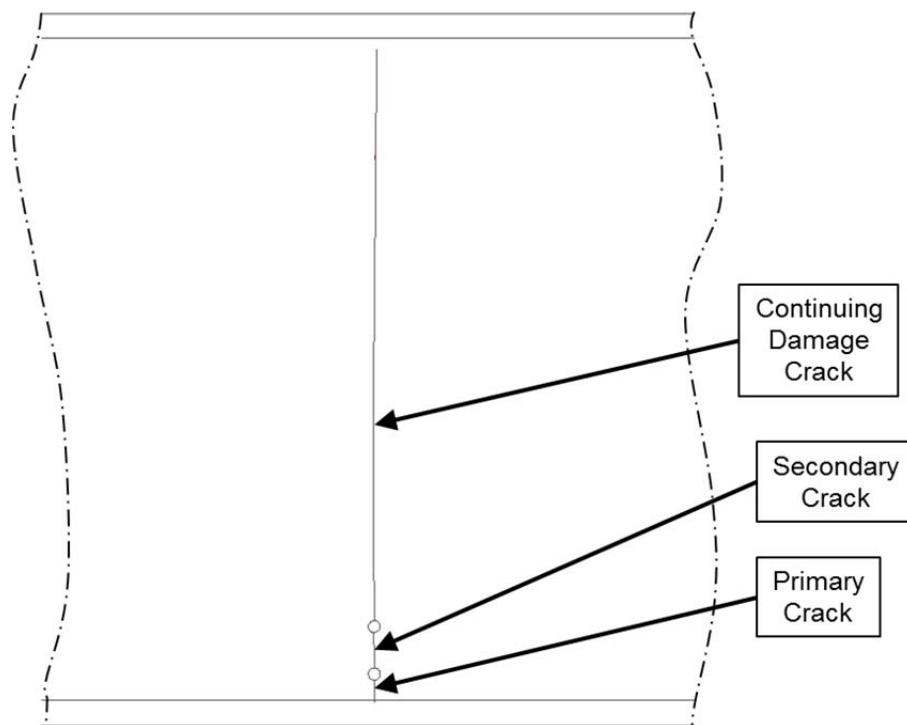


Fig. 23 Baseline crack path prediction in tension specimen.

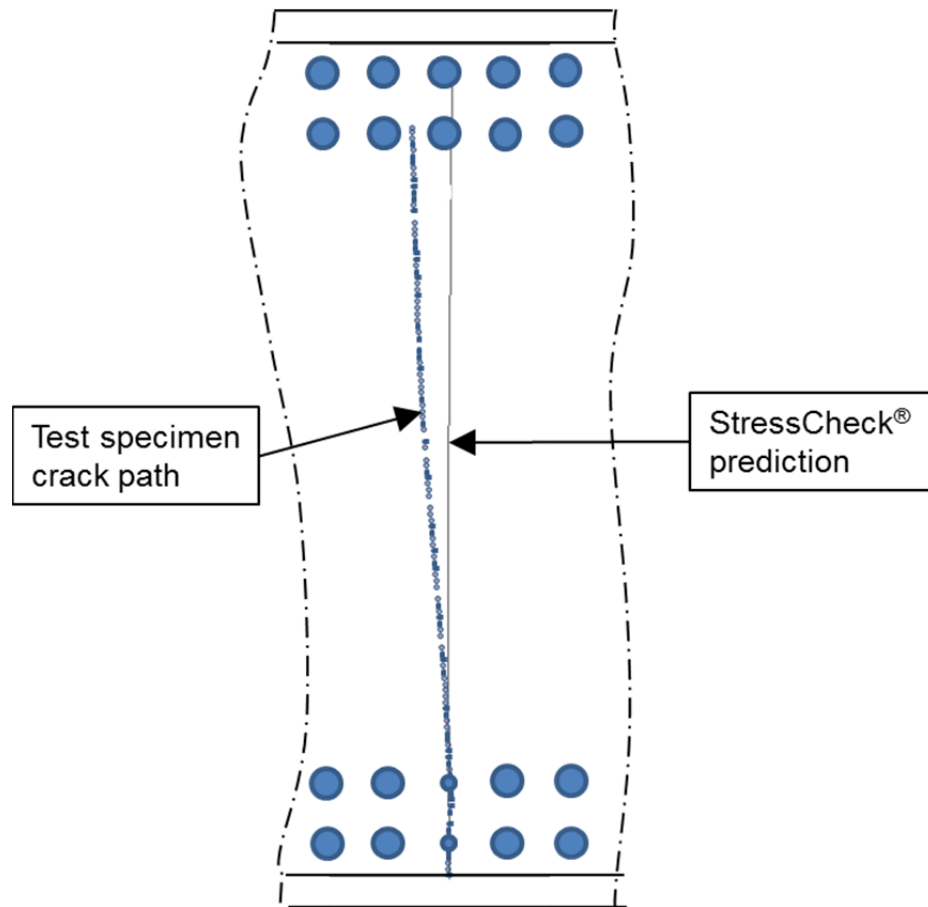


Fig. 24 Crack path prediction compared to tension specimen crack.

However, as noted previously a 6.56 inch-long crack was repaired near the outboard end of the test specimen at 13,672 cycles, before the continuing damage crack nucleated. The influence of this anomalous crack on the path of the continuing damage crack was investigated through the creation of a second StressCheck® tension model as seen in Fig. 25. This second model included a fourth crack, the anomalous crack, which was grown in the model at a rate one-half that of the continuing damage crack's rate. The improved correlation of the second model's crack path prediction with the tested specimen as seen in Fig. 26 suggests that perhaps the repair installed on the test article was not fully

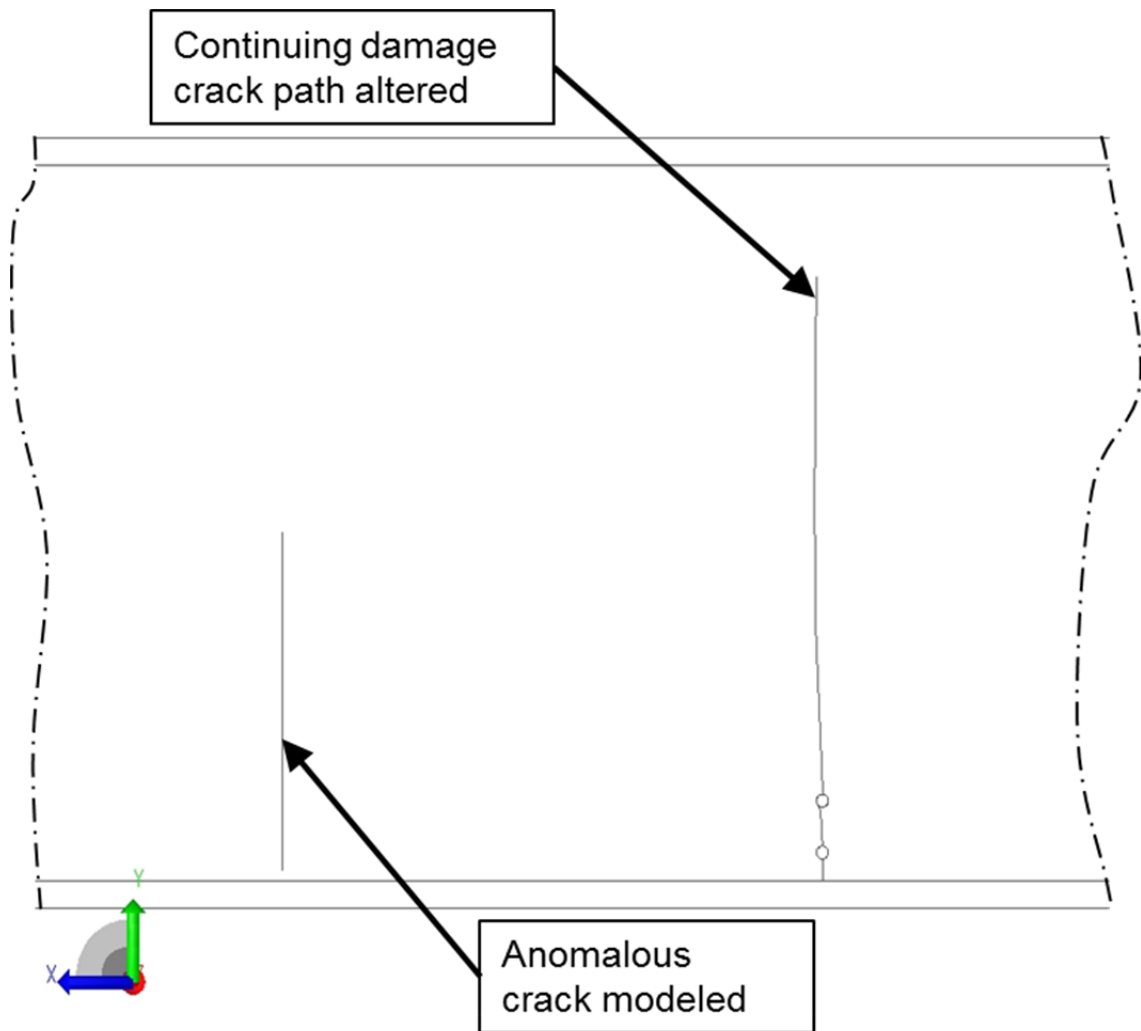


Fig. 25 Second tension model with anomalous crack included.

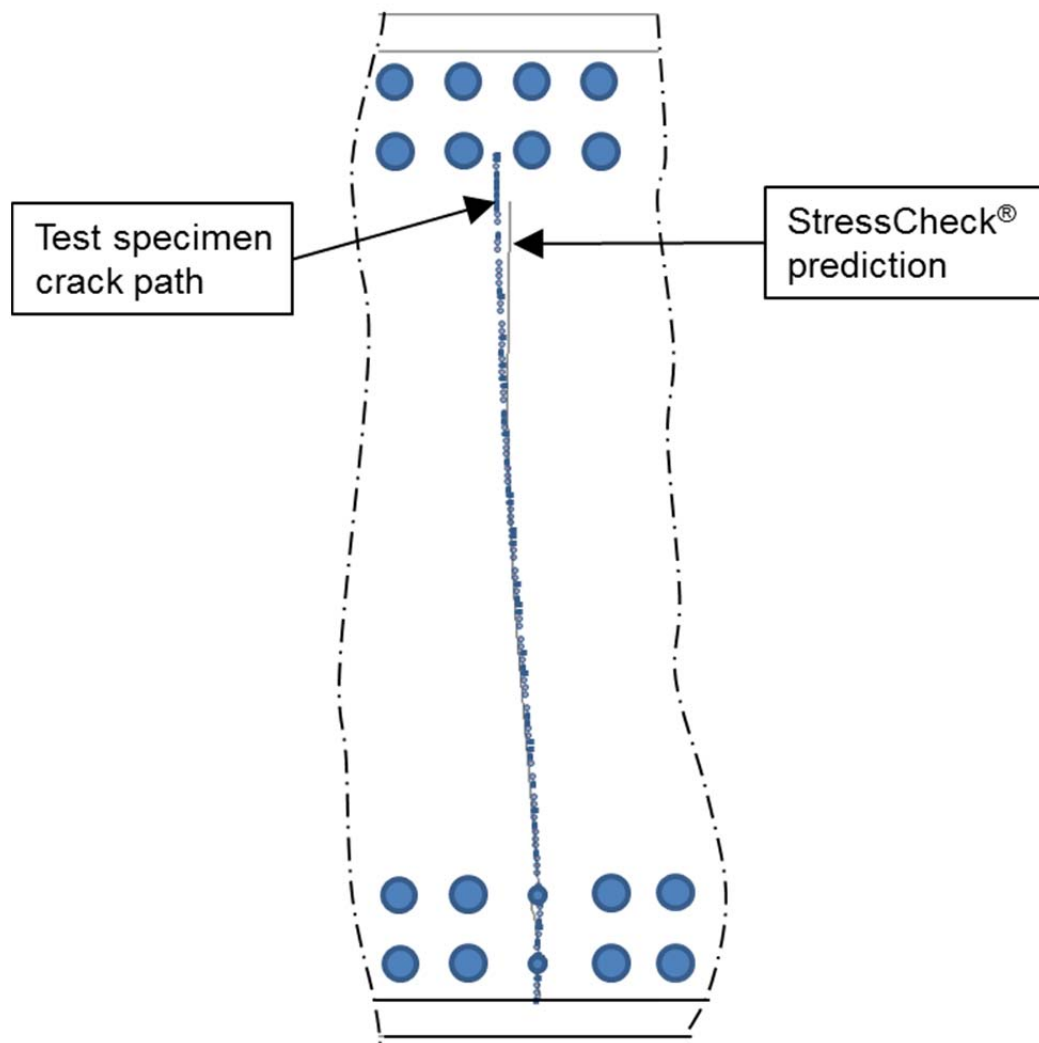


Fig. 26 Improved correlation to test when anomalous crack is modeled

effective in replacing the stiffness lost from the crack. No data we recorded to indicate whether or not the repair plates applied over this anomalous crack were removed after test completion to determine whether there was any crack growth after application of the repair.

The stress intensity values were recorded from the output file. These stress intensities were then used in the AFGROW crack growth predictions as outlined in Section 4.

3.2.2 Bending Model Results

Based on the results of the bending test, the bending model contained four initial cracks: the three cracks analogous to the ones in the tension model, plus an additional crack growing downward from the upper hole as seen in Fig. 19. This crack, although not an intentional crack as outlined in the original test plan, formed naturally nonetheless and exerted influence upon the other cracks. Since no crack growth history was recorded for this crack, it was assumed to nucleate and grow in parallel with the other cracks in the model. The orientation of the crack elements common to the upper hole were at 112 degrees and 292 degrees, approximating the nucleation points of the naturally-occurring cracks found in the test specimen. The cracks were programmed to grow simultaneously, and the length of each crack was limited to the final length of the cracks as documented in the test specimen. The final results of the predicted crack path versus the tested cracks is shown in Fig. 27. The stress intensity values were recorded from the output file. These stress intensities were then used in the AFGROW crack growth predictions as outlined in Section 4.

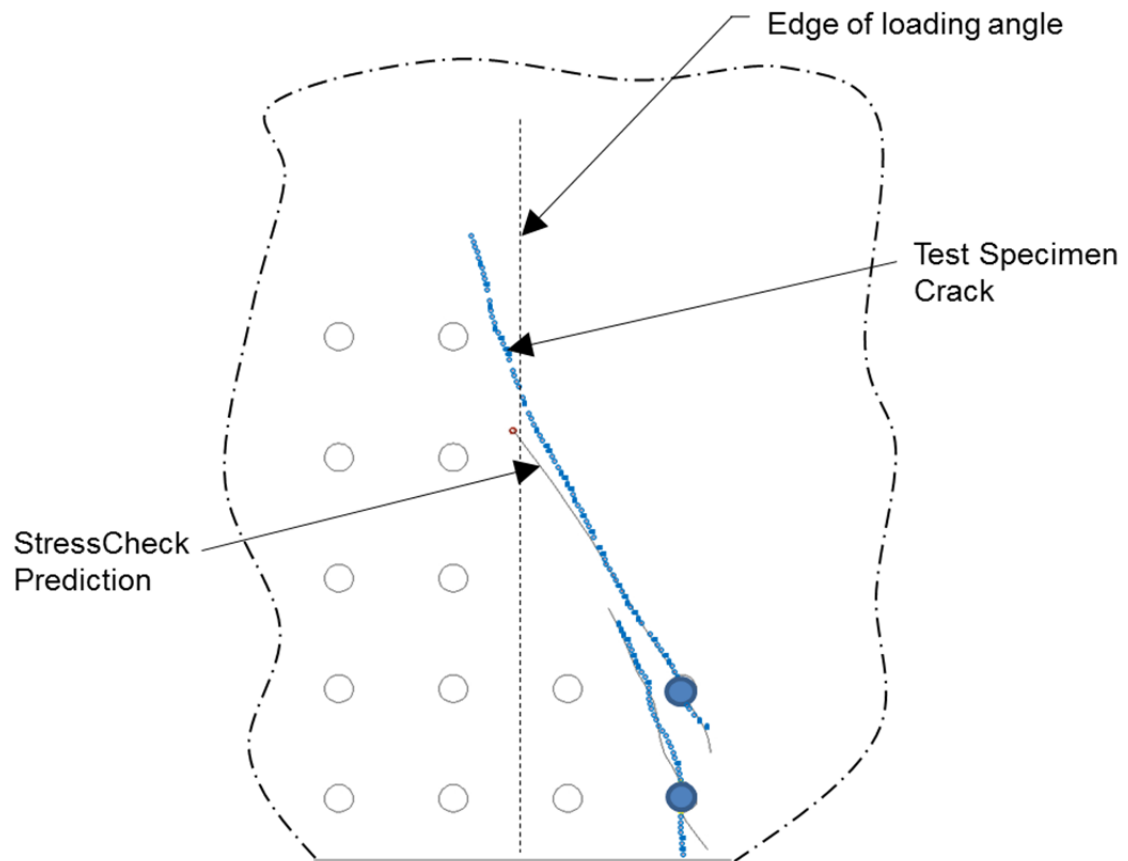


Fig. 27 Crack path prediction compared to bending specimen crack.

4 AFGROW CRACK GROWTH PREDICTIONS

4.1 A-10 DTA Ground Rules and Program Inputs

The DTA ground rules adopted by the A-10 analysis group are a combination of directives specified by the Air Force and program-specific procedures and inputs developed collaboratively between the A-10 analysis group and the Air Force's contractor support team. A copy of the current ground rules is contained in Appendix D. An example of an Air Force directive is the Initial Flaw Size (IFS) requirement. Air Force guidance documents direct the IFS for various structural configurations.⁹ In the case of continuing damage, it is required that the IFS of the continuing damage crack be 0.005 inch radius corner flaw + Δa (amount of growth which occurs prior to primary element failure) on the diametrically opposite side of the hole where the flaw growth terminated. However, recent guidance has suggested that this procedure lacks sufficient conservatism, and directs that this initial flaw should increase from 0.005 inch to 0.010 inch.²⁶

An example of a program-specific analysis input is the crack retardation parameter, or Shutoff Overload Ratio (SOLR). SOLR is the parameter that characterizes the amount of retardation used in the Willenborg Retardation model. It is the ratio of overload maximum stress to the subsequent maximum stress required to arrest crack growth. The Generalized Willenborg retardation model is a commonly used model based on fracture mechanics work performed

at Wright-Patterson Air Force Base, Ohio. It uses an effective stress intensity factor based on the size of the yield zone in front of the crack tip. SOLR testing has been performed under the direction of the A-10 analysis group for specific combinations of material and load spectrum used on the A-10. Since SOLR values are specific to variable-amplitude loading, they were not required during this phase of the project, but will be important in subsequent phases.

All AFGROW inputs were in accordance with the A-10 DTA ground rules. Material input files were from the built-in NASGRO database as shown in Fig. 28, and geometry and load inputs reflected the as-built geometry of the test specimens. Three crack growth life predictions were made for each specimen: the baseline prediction using all standard models and methods as used in the Air Force today, a second prediction using a beta correction based off of a geometric net-section correction, and lastly a user-defined beta based off of the stress intensity solutions produced from the StressCheck[®] models.

The second prediction (with the geometrically-derived beta correction) was investigated to determine the additional crack growth life that might be realized by allowing load from the web to redistribute to the spar caps as the web cracks grew, without specific knowledge of the crack path. The standard AFGROW model in use today does not reflect that reality. It assumes that all of the load that begins in a component must stay in that component as the crack propagates. The model is also unaware of any redundant load paths. The assumption in these models is that all of the load capability lost in the web is absorbed by the caps. This keeps the net section stress constant as the cracks

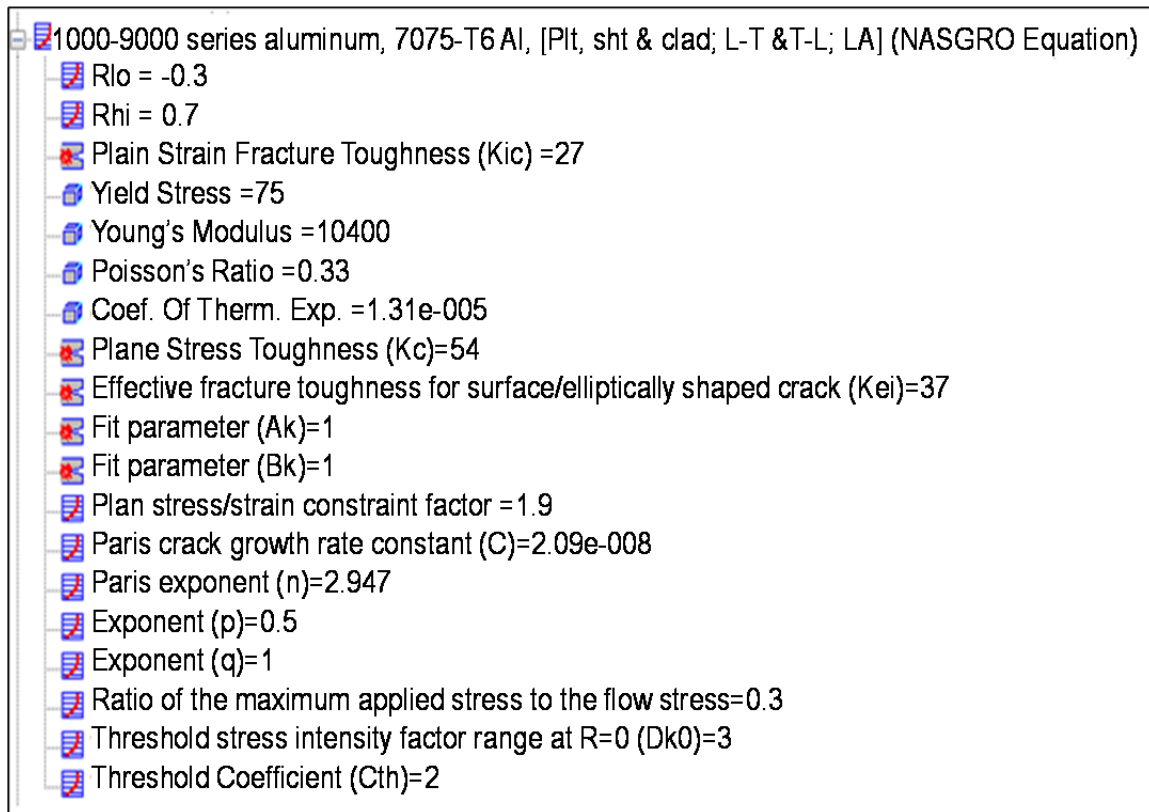


Fig. 28 NASGRO material file inputs for 7075-T6 aluminum.

grow. In this case, cracks are assumed to grow in a constant plane. That is, they grow straight through that part and do not turn.

The third prediction (with the StressCheck[®] user-defined beta) utilizes the stress intensity solutions from the StressCheck[®] models to compute beta solutions. Knowing the stress intensities as a function of crack length, beta values were computed at each crack growth increment and input into AFGROW. In the user-defined beta option in AFGROW, the values input by the user are used in place of the beta values computed by a standard model. AFGROW allows up to 25 user-defined data pairs (crack length and beta). Therefore, for each model, engineering judgment was used to down-select the 25 pairs when more than 25 pairs were generated by StressCheck[®]. In general, an attempt was

made to concentrate length-data pairs in regions where the beta gradient was high, and to use less data where the gradient was low. Since AFGROW interpolates between successive data points when a crack is at an intermediate length, it was desirable to have the maximum resolution in areas where the beta gradient was high. The stress intensity values calculated by StressCheck[®] (and the resulting beta values) reflect the changing stress field experienced by the crack along its natural path. The use of these beta values in AFGROW corrects for the effects of crack path in what is otherwise assumed to be a straight crack.

No load transfer is assumed in any of the models (i.e., the tension stress fraction is 1 and the bearing stress fraction is 0). This is because the web cannot carry load across a crack, and the hole-fill experienced by the web with an expanded rivet is lost as soon as a crack begins to propagate. Additionally, the two test specimens had unexpanded rivets in the notched holes so that they could be removed for crack measurements resulting in a diametrical clearance of 0.003 inch to 0.006 inch based on assembly drawing tolerances. Therefore, the unfilled hole assumption most closely approximates the conditions seen in the tests.

4.2 Tension Model Crack Growth Predictions

The total AFGROW-predicted life is composed of the sum of three individual models (one for each crack), with a fourth required to determine the growth of the assumed damage on the opposite side of the hole from which the primary ligament crack is growing to be used as the IFS of the secondary crack.

The first model for the primary ligament crack is based off of AFGROW's standard model for a single quarter-circular crack at a hole as shown in Fig. 29. The second model, to determine the secondary crack's IFS, uses the same basic model, but grows the crack toward the middle of the part rather than toward the edge of part. The third model, for the secondary crack between the two holes, uses an advanced model within AFGROW as shown in Fig. 30. The initial flaw in this model is a quarter-circular crack, the dimensions of which are taken from the second model. The fourth model, for the continuing damage crack, also uses an advanced model. In this model, the web is assumed to be cracked (modeled as a slot) all the way through to the top of the upper hole as shown in Fig. 31. A 0.005 inch x 0.005 inch quarter-circular flaw is used to grow the continuing damage crack.

The second set of predictions, those with the geometric beta corrections, utilized the same model templates, but included the beta correction capability within AFGROW. The beta correction allows the user to add a multiplication factor to the standard stress intensity solution. This is helpful in situations not explicitly covered by the basic models. In this case, the beta correction is used to account for the fact that the longitudinal stress in the part, the primary driving force for the crack for short crack lengths, is diminishing as a linear function of crack length as shown in Fig. 32. Data used for beta corrections are contained in Table 1.

The third set of predictions for the tension specimen utilized the user-defined beta option within AFGROW. The user-defined beta option replaces the

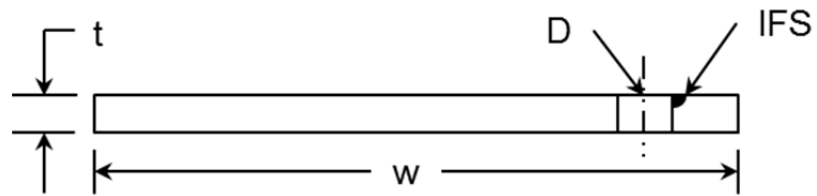


Fig. 29 AFGROW model for primary ligament crack – baseline condition.

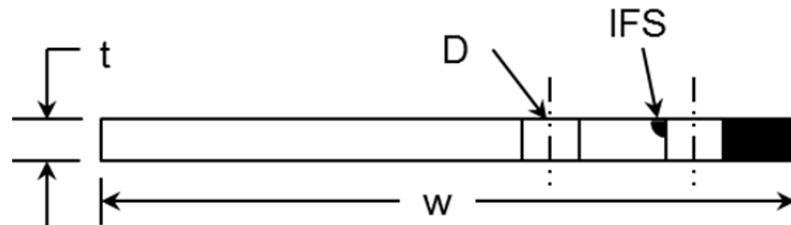


Fig. 30 AFGROW model for secondary crack – baseline condition.

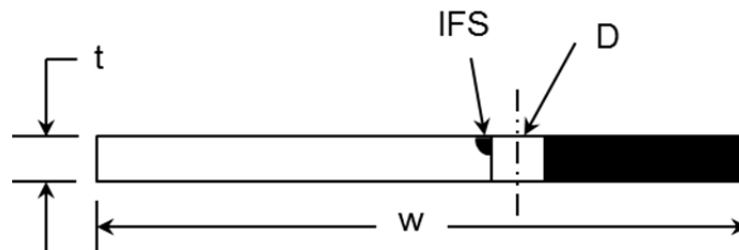


Fig. 31 AFGROW model for continuing damage crack – baseline condition.

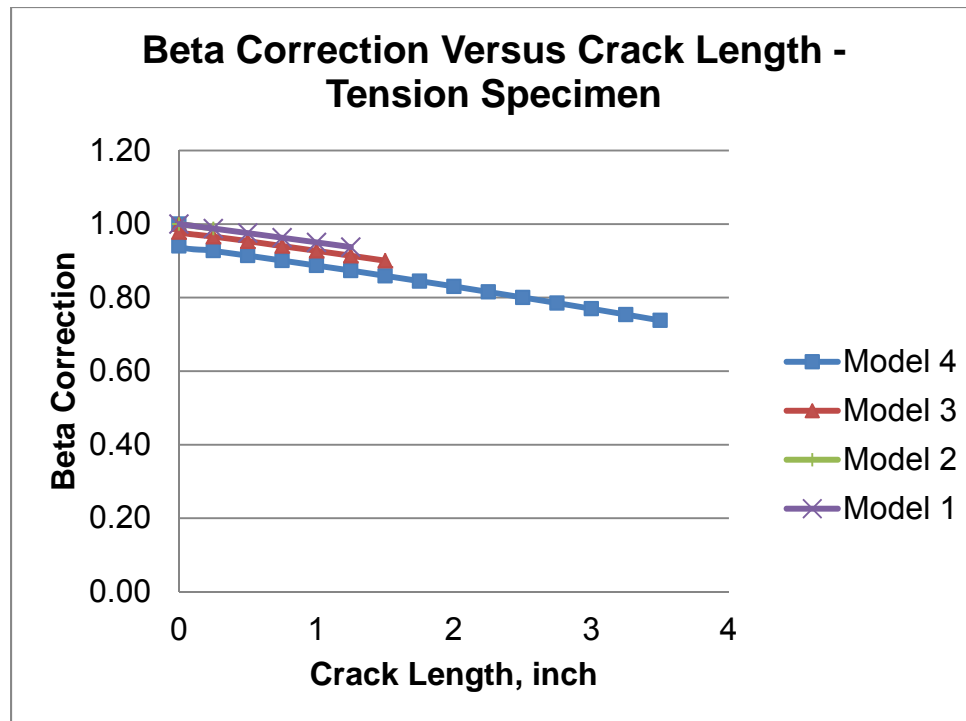


Fig. 32 Beta correction versus crack length for tension specimen.

Table 1 Beta corrections for tension model

Model 1		Model 2		Model 3		Model 4	
a	β	a	β	a	β	a	β
0.00	1.0000	0.00	1.0000	0.0000	1.0000	0	1.0000
0.25	0.9878	0.25	0.9878	0.00001	0.9783	0.00001	0.9406
0.50	0.9755			0.25	0.9658	0.25	0.9276
0.75	0.9629			0.50	0.9532	0.5	0.9143
1.00	0.9502			0.75	0.9403	0.75	0.9009
1.25	0.9373			1.00	0.9272	1	0.8872
				1.25	0.914	1.25	0.8733
				1.50	0.9005	1.5	0.8592
						1.75	0.8449
						2	0.8303
						2.25	0.8155
						2.5	0.8005
						2.75	0.7852
						3	0.7697
						3.25	0.7539
						3.5	0.7379

beta from the AFGROW solution, rather than multiplying it by a factor like the beta correction option. Thus, the user-defined beta values are a direct reflection of the through-crack stress intensities developed by the StressCheck[®] models as shown in Fig. 33. Data for the user-defined betas are summarized in Table 2.

Because StressCheck[®] uses a through-crack, the first and fourth models used in AFGROW were adjusted accordingly. The second and third models retained the quarter-circular initial flaw to be consistent with the continuing damage guidance from the Air Force. The through-crack model for the user-defined beta is shown in Fig. 34. The crack growth curves generated by AFGROW for all three sets of data are summarized in Fig. 35. A breakdown of the life of each crack compared to the test specimen is summarized in Fig. 36.

4.3 Bending Model Crack Growth Predictions

The models for the bending condition were, for the most part, analogous to the ones for the tension condition. One difference, however, was the initial flaw size for the first model. Since the tested specimen started with a 0.05 inch through crack instead of a corner crack, the first AFGROW model for the primary ligament crack reflected this as seen in Fig. 37. Beta corrections for the second set of predictions were generated analogously to the ones for the tension case and are shown in Fig. 38. Note that for the first model the beta correction grows as a function of crack length and becomes greater than 1.0. This reflects the fact that the longitudinal stress from bending increases as the crack goes toward the extreme fiber, and this influence overrides the geometric correction for load transfer to the caps. For the other cracks, the beta correction drops as a function

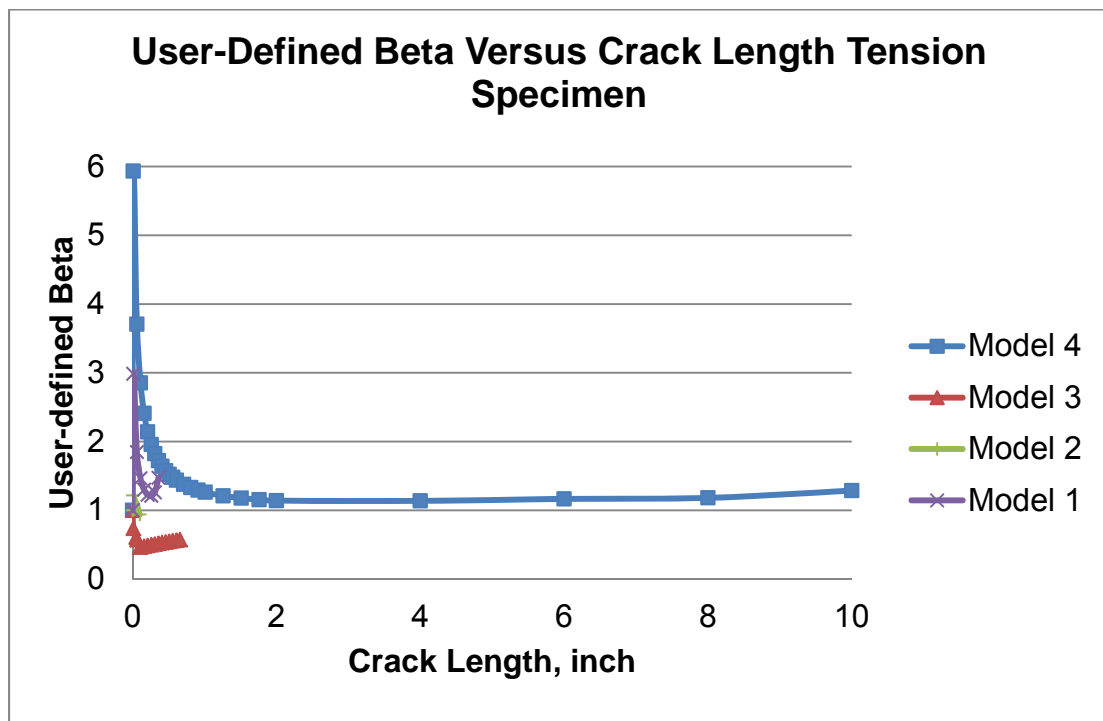


Fig. 33 User-defined beta versus crack length for tension specimen.

Table 2 User-defined beta values for tension model

Model 1		Model 2		Model 3		Model 4	
a	β	a	β	a	β	a	β
0.00	1.000	0.00	1.000	0.000	1.000	0.00	1.000
0.01	2.986	0.005	1.217	0.01	0.738	0.01	5.934
0.06	1.848	0.10	0.940	0.05	0.609	0.06	3.706
0.11	1.467			0.06	0.572	0.11	2.853
0.16	1.300			0.10	0.466	0.16	2.412
0.21	1.226			0.11	0.467	0.21	2.141
0.26	1.212			0.16	0.480	0.26	1.957
0.31	1.262			0.21	0.489	0.31	1.824
0.36	1.472			0.26	0.500	0.36	1.722
				0.31	0.510	0.41	1.641
				0.36	0.520	0.46	1.576
				0.41	0.530	0.51	1.523
				0.46	0.539	0.56	1.479
				0.51	0.548	0.61	1.439
				0.56	0.557	0.71	1.377
				0.61	0.565	0.81	1.330
				0.66	0.576	0.91	1.293
						1.01	1.263
						1.26	1.210
						1.51	1.177
						1.76	1.155
						2.00	1.140
						4.00	1.137
						6.00	1.165
						8.00	1.181
						10.00	1.286

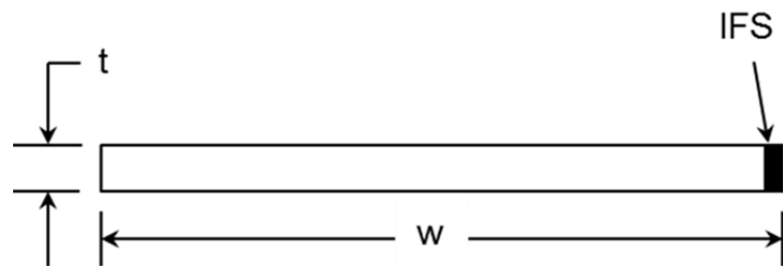


Fig. 34 AFGROW model for user-defined beta

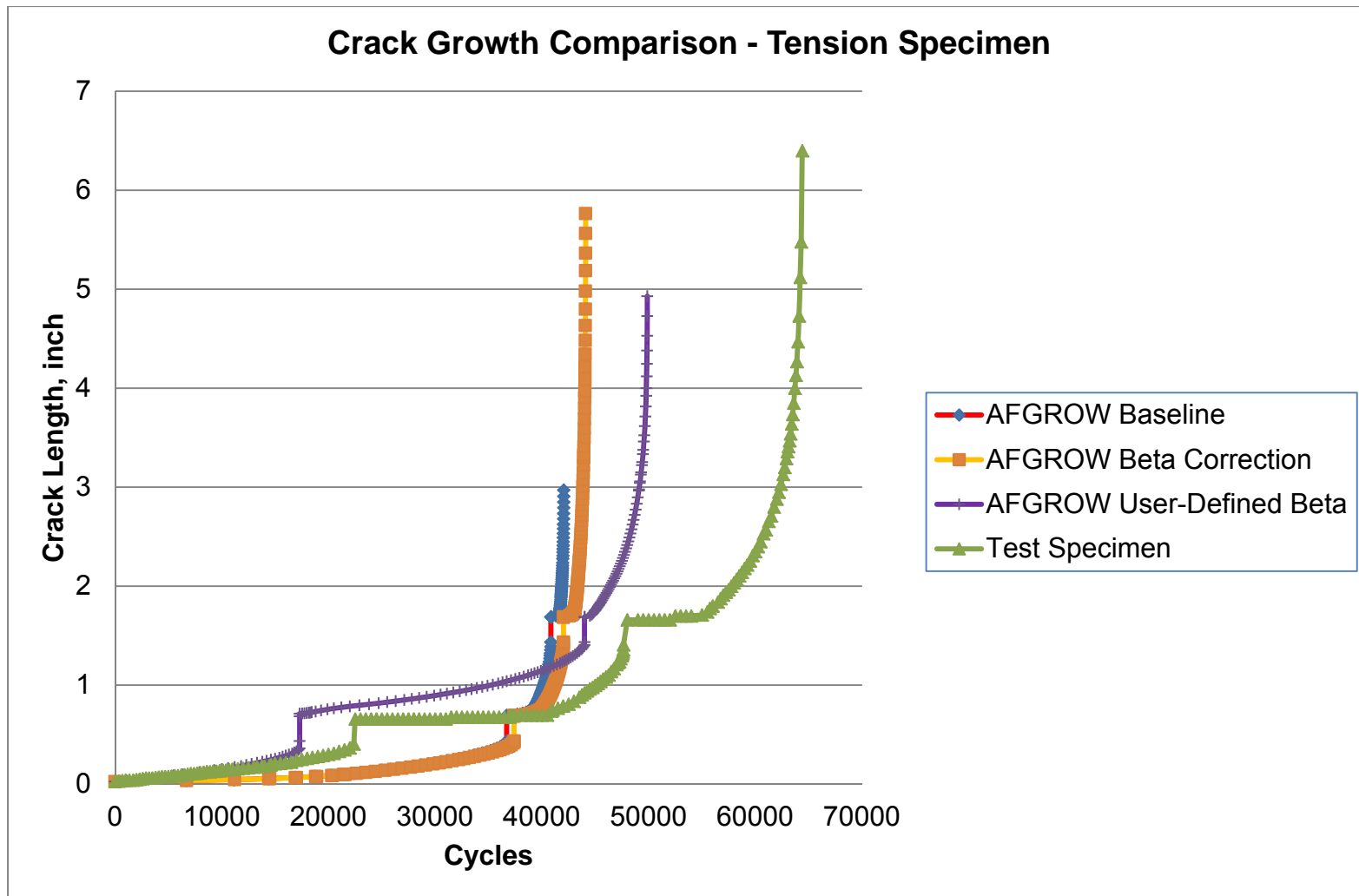


Fig. 35 Crack growth comparison - tension specimen.

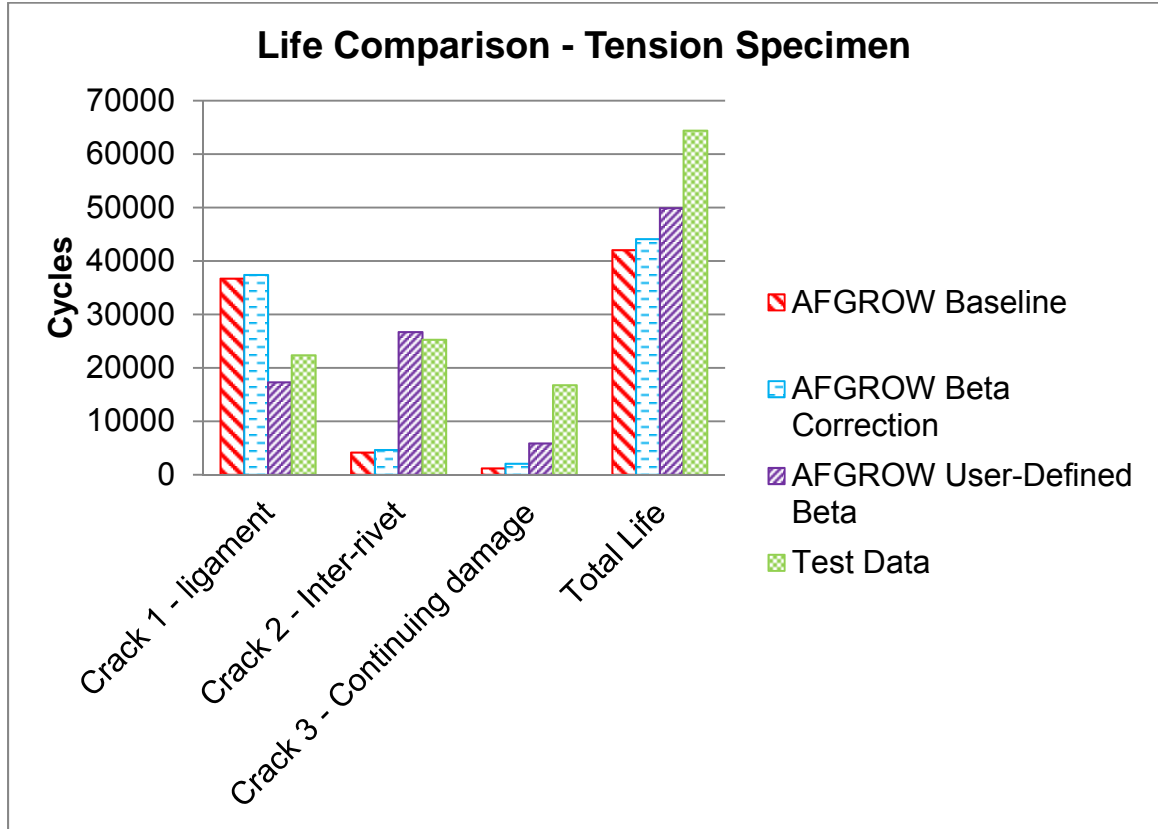


Fig. 36 Crack life comparison - tension specimen.

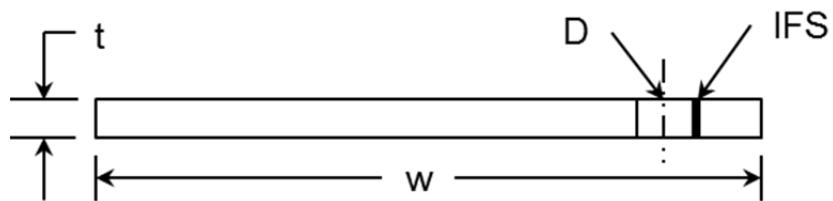


Fig. 37 AFGROW model for through crack at a hole.

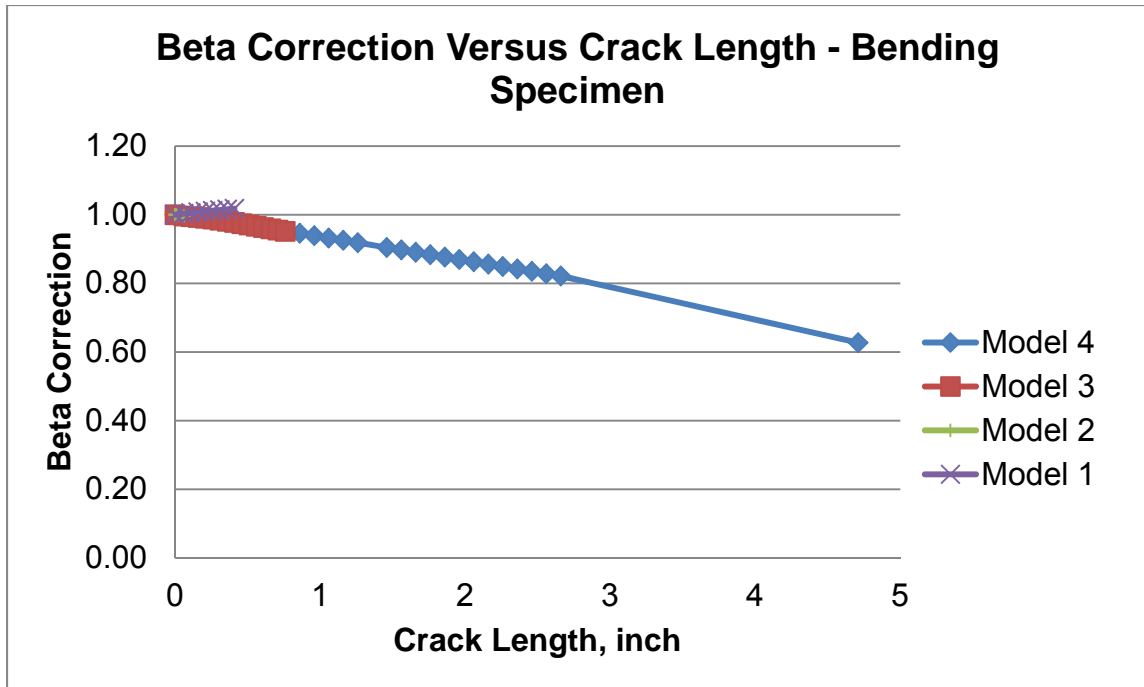


Fig. 38 Beta correction versus crack length for bending specimen.

of crack length, as expected. The user-defined beta values were calculated in the same manner as for the tension case, and can be seen in Fig. 39. Data for user-defined betas are summarized in Table 3 and Table 4. The crack growth comparison for all models to the test data is shown in Fig. 40. The relative lives of each crack can be seen in Fig. 41.

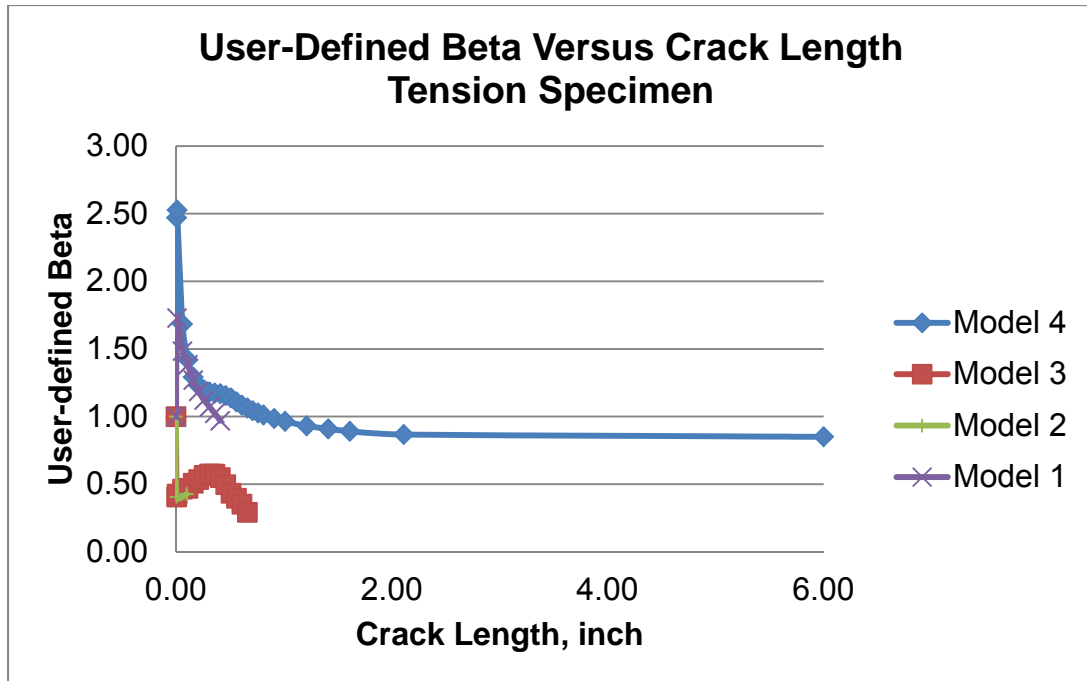


Fig. 39 User-defined beta versus crack length for bending specimen.

Table 3 Beta corrections for bending model.

Model 1		Model 2		Model 3		Model 4	
a	β	a	β	a	β	a	β
0.00	1.000	0.00	1.000	0.00	1.000	0.00	1.000
0.06	1.003	0.01	1.000	0.06	0.997	0.06	0.997
0.11	1.005	0.06	0.996	0.11	0.994	0.26	0.985
0.16	1.008			0.16	0.992	0.46	0.973
0.21	1.010			0.21	0.990	0.56	0.966
0.26	1.012			0.26	0.987	0.66	0.960
0.31	1.014			0.31	0.984	0.76	0.953
0.36	1.016			0.36	0.981	0.86	0.946
0.41	1.018			0.41	0.978	0.96	0.939
				0.46	0.974	1.06	0.932
				0.51	0.970	1.16	0.925
				0.56	0.967	1.26	0.918
				0.61	0.963	1.46	0.905
				0.66	0.959	1.56	0.898
				0.71	0.955	1.66	0.891
				0.76	0.952	1.76	0.884
						1.86	0.877
						1.96	0.870
						2.06	0.863
						2.16	0.856
						2.26	0.849
						2.36	0.842
						2.46	0.835
						2.56	0.828
						2.66	0.821
						4.71	0.627

Table 4 User-defined beta values for bending model

Model 1		Model 2		Model 3		Model 4	
a	β	a	β	a	β	a	β
0.00	1.000	0.00	1.000	0.00	1.000	0.00	1.000
0.00	1.000	0.00	1.000	0.00	1.000	0.00	1.000
0.01	1.729	0.005	0.406	0.005	0.406	0.005	2.47
0.06	1.484	0.10	0.427	0.01	0.427	0.01	2.527
0.11	1.383			0.06	0.464	0.06	1.683
0.16	1.269			0.11	0.469	0.11	1.420
0.21	1.185			0.16	0.507	0.16	1.292
0.26	1.122			0.21	0.535	0.21	1.228
0.31	1.072			0.26	0.565	0.26	1.196
0.36	1.023			0.31	0.576	0.31	1.181
0.41	0.969			0.36	0.575	0.36	1.173
				0.41	0.549	0.41	1.169
				0.46	0.497	0.46	1.155
				0.51	0.433	0.51	1.138
				0.56	0.396	0.56	1.109
				0.61	0.352	0.61	1.084
				0.66	0.292	0.66	1.063
						0.71	1.043
						0.76	1.027
						0.81	1.011
						0.91	0.985
						1.01	0.964
						1.21	0.931
						1.41	0.909
						1.61	0.891
						2.11	0.867
						6.00	0.850

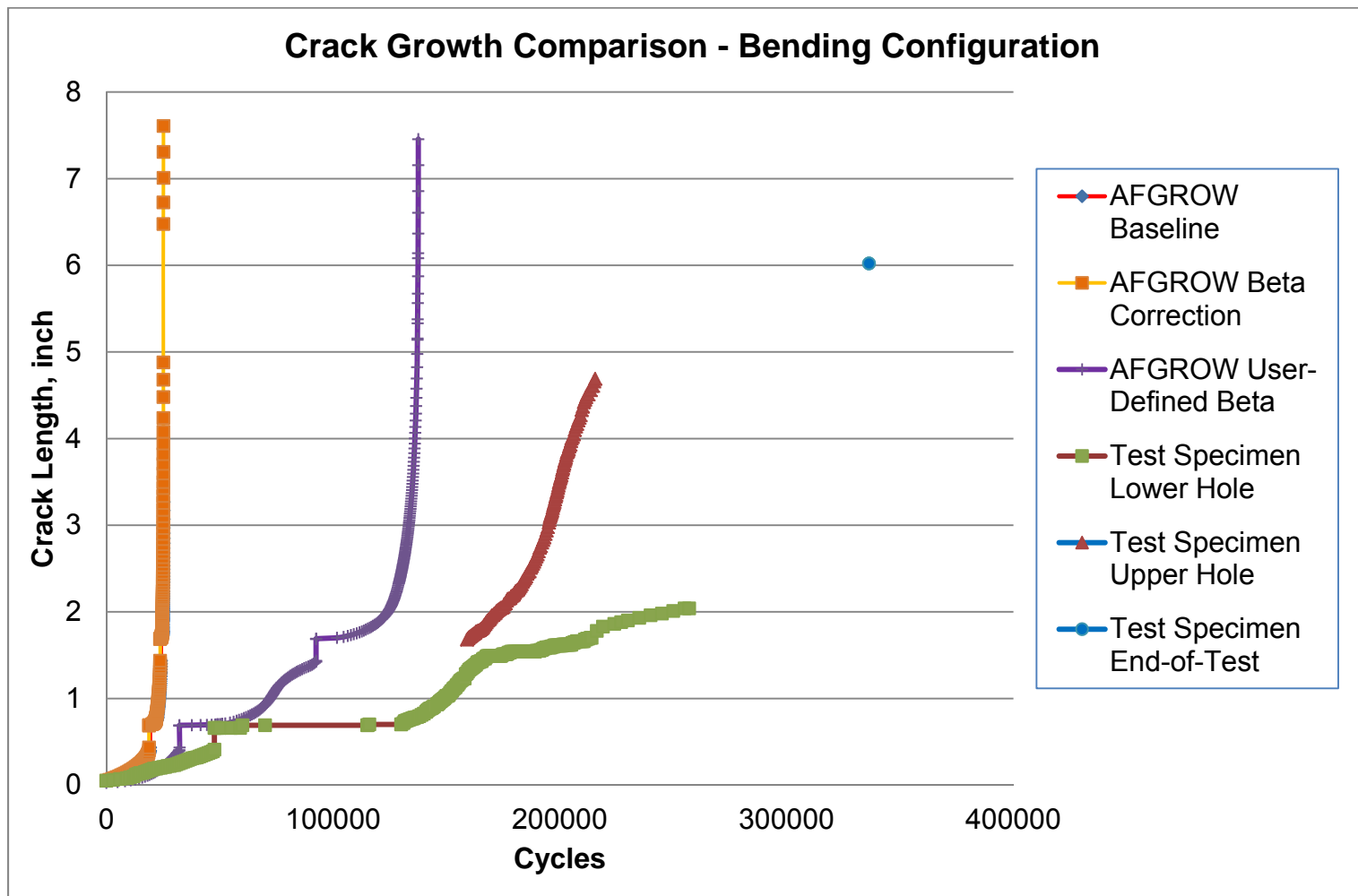


Fig. 40 Crack growth comparison - bending specimen.

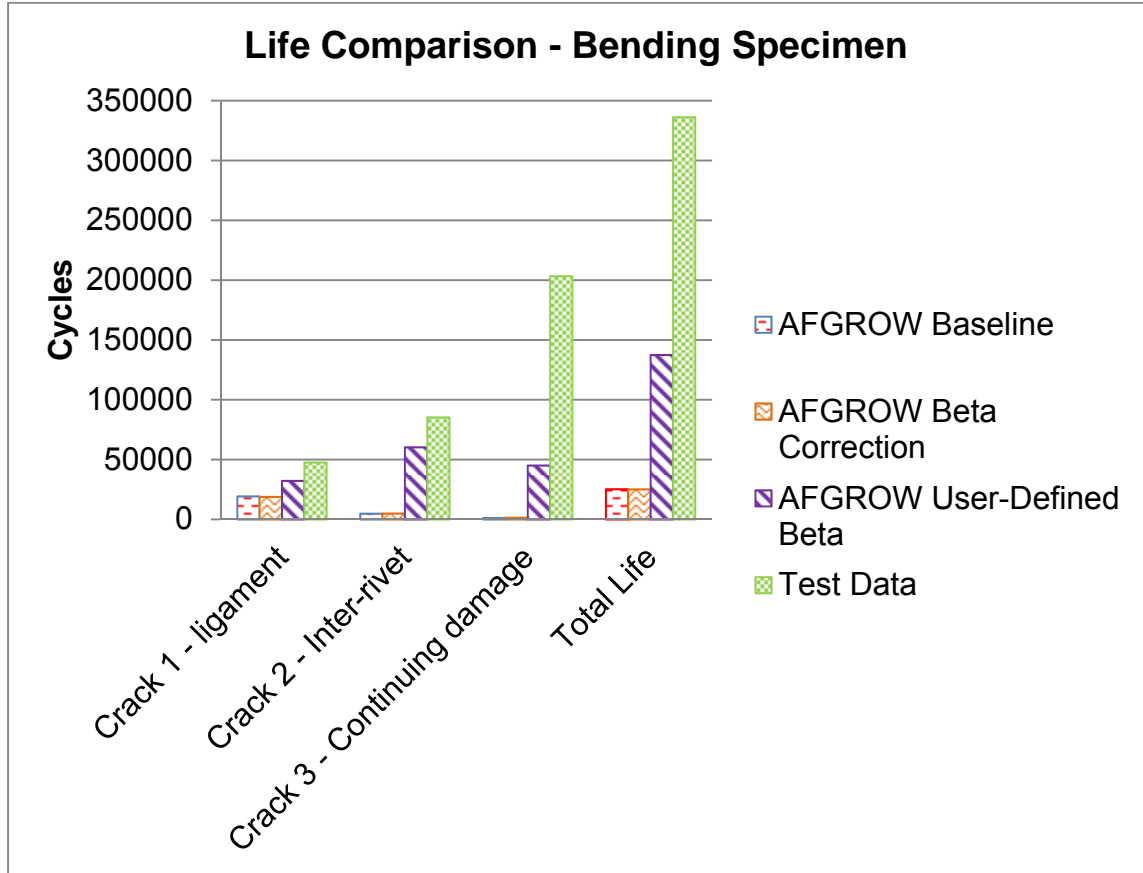


Fig. 41 Crack life comparison - bending specimen.

5 DISCUSSION

5.1 Fatigue Crack Growth Testing Observations

The building-block approach was chosen for this project so that the most basic load conditions could be tested and analytical models could be validated against that test data. However, various developments during the test program introduced some complexity and uncertainty in the process.

The presence of the numerous anomalous cracks significantly affected the tests and their results. During testing for the tension specimen, a large anomalous crack developed just inside of the test fixture, altering the path of the continuing damage crack. This anomalous crack was repaired with doubler plates that appeared to be less than fully effective at restoring the stiffness of the original load path. While an analytical model was developed that seemingly captured the effect of the anomalous crack, there is no direct evidence in the form of strain data that validates these assumptions.

Similarly, in the bending test, at least three anomalous cracks developed: one near the edge of the end plate, the large crack that ultimately stopped the test, and the crack growing downward from the upper hole. No data were recorded for any of these three cracks, so no investigation of these cracks' influence was possible. Having some crack history on the large test-ending crack may have explained the deviation in predicted continuing damage crack path near the end of its life.

Because the incorrect row was notched in the bending specimen, the crack had a shorter distance to travel before it grew underneath the loading angle. Potentially valuable data was unobtainable because the crack was obscured by the loading fixture. It is apparent from the crack growth curve that some crack slowing occurred, but the time it took for the continuing damage crack to propagate into the hole where it arrested is unknown.

For both specimens, additional notches were introduced at the holes and for the bending specimen, loads were increased part-way through the testing in order to accelerate the nucleation of cracks for the secondary and/or continuing damage cracks. These procedures were outside the scope of the test plan. Part of this project's goal was to compare the analytically-predicted life to naturally-occurring cracks, and to determine what conservatism exists in the analytical methods. By changing the nucleation mechanisms of the secondary and continuing damage cracks, the meaningfulness of this comparison was questioned. The analytical predictions are still conservative compared to the test, but the true magnitude of that margin cannot be known in light of the way the cracks were nucleated.

It is also possible that an increased plastic zone was introduced to the bending specimen by increasing the load by 8.3% for 16,250 cycles from 115,250 cycles until 131,500 cycles. This increased load would have the effect of slowing the crack until the crack grew through this plastic zone. The crack growth rate in that zone would differ from the rest of the specimen, possibly skewing the correlation with the analytical predictions from AFGROW.

Strain survey data were collected at several points during both tests. It was hoped that this data could be used to correlate stresses in the specimens as a function of crack length. However, for the tension test, no strain surveys were taken after the nucleation of the continuing damage crack. Data were only recorded at 0 cycles and 14,500 cycles. Only 10 of the 14 channels had data reported for both runs. This made a correlation impossible.

For the bending specimen, four strain surveys were taken: at 0 cycles, 47,639 cycles, 205,000 cycles, and 336,293 cycles. However, the first two surveys were run to a maximum load of 22 kips, and the last two were run to a load of 24 kips, making direct comparison more difficult. During the four bending surveys, only 8 of the 16 channels recorded data for all four runs. This made extracting useful data regarding load redistribution difficult.

5.2 StressCheck® Modeling Observations

StressCheck® offers a powerful capability to predict crack paths in structure. The primary challenge facing the analyst is the idealization of three-dimensional (3D) structure into a 2D environment. Typical structural assemblies consist of many different materials, thicknesses, or perhaps many different forms and tempers of the same material. Additionally, built-up structural assemblies, like the kind modeled for this project, contained fastened joints, the stiffness of which must be accounted for to accurately model the system. Other 3D components, loads, material nonlinearities, or structural instabilities will not be captured. StressCheck® calculates the stress state at the crack tip and grows the crack in the plane perpendicular to the direction of greatest tension. Any

simplifications or idealizations that alter stiffness (and thus load path) will affect the crack path calculation so great care must be taken in modeling the structure.

Significant flexibility exists within the program to grow cracks simultaneously or serially. The default Run Mode of *Automatic* will cause all cracks to grow simultaneously. This type of analysis could be very beneficial in a multisite damage scenario. Conversely, running cracks in a *Stepwise* mode will work best for cracks that grow consecutively, as in the continuing damage model.

For this project StressCheck[®]'s crack path predictions trended well with the test specimen's cracks. Addition of the anomalous cracking present in the tension test specimen improved this correlation. Output files of stress intensities were then available for processing as beta file inputs to AFGROW.

5.3 AFGROW Modeling Observations

AFGROW offers a large number of standard and advanced models in its library. The program allows customization of many of the model parameters important to the analyst. This provides for a great deal of flexibility in modeling unusual structural configurations. The program accepts many user-defined parameters that also contribute to its flexibility.

AFGROW crack life predictions were generally conservative compared to the test specimen's recorded life. The geometrically-derived beta correction method yielded very similar results to the standard AFGROW model in use today. When examining the crack growth life for each crack individually, the cracks grown using the user-defined beta option most closely matched the test data in every segment. However, the total predicted crack life for the bending

specimen is still very conservative compared to test. One reason for this is that, in the test specimen, the crack was growing at an angle, whereas AFGROW treats this as though the crack is growing straight through the cross section. Thus, for a given crack length, the net cross sectional area is higher in the test specimen than what AFGROW calculates. This results in higher apparent stresses in AFGROW, accelerating the crack growth relative to the test.

The crack growth predictions using the user-defined beta inputs show promise for being able to take credit for additional stable crack growth life in spar webs while still maintaining an acceptable margin of safety.

6 SUMMARY

6.1 Conclusions

This project set out to evaluate the feasibility of developing a new analysis method using StressCheck[®] and AFGROW, validated against test data, to extend stable crack growth life predictions for certain A-10 FCLs where a continuing damage model may be appropriate. These constant-amplitude testing and analyses were the first steps in a building-block approach to studying this issue. The following conclusions from this project are reported:

1. It was validated that crack growth predictions of this type of structure and loading using the current Air Force methodology are extremely conservative. Testing of the tension specimen yielded a total life approximately 50% longer than predicted. Testing of the bending specimen yielded a total life approximately 13 times as long as predicted.
2. The geometrically-based beta correction did not predict significantly longer lives than the baseline AFGROW models. Further investigation is not expected to change these results.
3. The crack growth predictions utilizing the user-defined beta inputs most closely matched the test data.
4. The 2D planar crack path functionality within StressCheck[®] is capable of predicting crack paths with sufficient accuracy for stress intensity extraction for use in AFGROW.
5. Cracks growing into a diminishing stress field, such as in the specimens tested for this project, decelerate as they grow toward the neutral axis. This deceleration is proportional to the decrease in the crack driving force.
6. Three-dimensional structure can successfully be idealized into a two-dimensional space for use in crack path analysis. The idealized beam's area and second moment of inertia are critical parameters that should be matched to that of the 3D structure as closely as possible.

7. Crack life predictions utilizing StressCheck[®]-derived beta values are still conservative compared to test. This conservatism is due in part to the planar crack growth assumption in AFGROW.

6.2 Recommendations

The following recommendations are made with regards to the testing phase of this project:

1. Testing on the last constant-amplitude test specimen (four-point bending) should proceed, but precautions should be taken to prevent the anomalous cracking seen in the first two specimens. Specifically, cold-expansion of all lower row rivet holes in the web outside of the test section is recommended.
2. Periodic visual inspections should be performed over the entire test article to detect the presence of any anomalous cracking before it has a chance to influence the crack paths of the intentional cracks. Crack growth data on all cracks should be captured.
3. Any structural repairs made to test specimens should be carefully designed to replace the stiffness of the original material, not just the static strength.
4. Perform strain surveys more frequently as cracks grow in order to capture load redistribution effects.
5. Ensure strain gages are in working order prior to all strain surveys. Repair or replace damaged gages as required.

The following recommendations are made in regards to the analysis phase of this project:

1. Great care should be exercised when creating the idealized 2D model in StressCheck[®]. The effect of material changes, stiffness changes, the presence of fasteners, etc. can have significant impact on results.
2. Include in the model, as appropriate, any anomalous cracks that are either unrepaired, or repaired with low-stiffness repairs.

The following general recommendations are made regarding the overall scope and purpose of this project:

1. The results of this project show sufficient promise that this method of analysis will extend short inspection intervals on relevant built-up beam structural details potentially resulting in significant cost savings to the Air Force. Recommend funding and pursuing further research along this path.
2. The building-block approach to this project is appropriate and future phases should continue to add complexity in loading and structural detail.
3. Variable-amplitude loading should be explored with the same loading conditions as tested herein.
4. As two of the three A-10 center wing panel spars and all three of the outer wing panel spars are IDT beams, testing and analysis should extend to spar webs that buckle elastically, and corresponding nonlinear analyses should be performed.

APPENDIX A TENSION SPECIMEN PHOTOGRAPHS

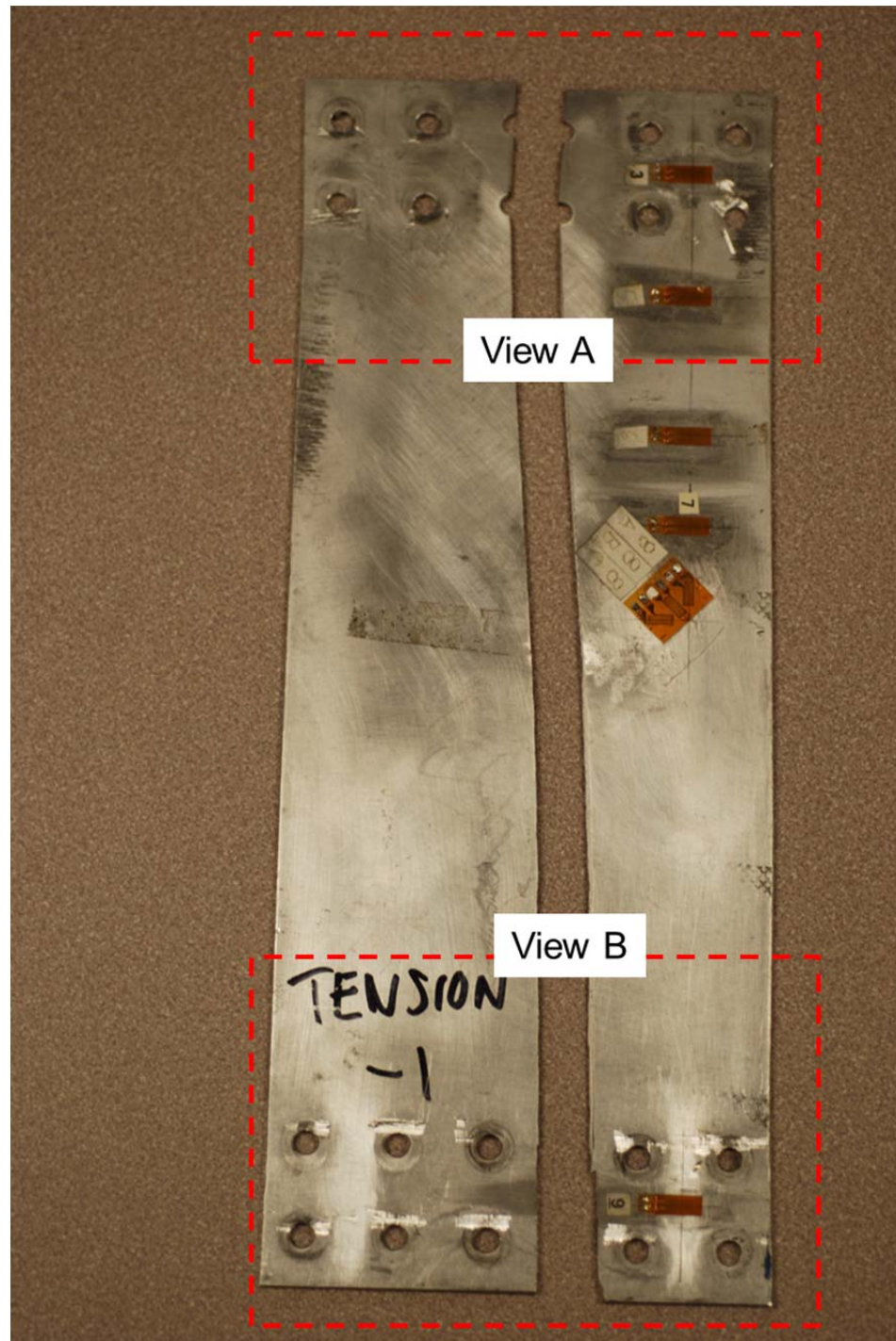


Fig. 42 Tension specimen failed web.

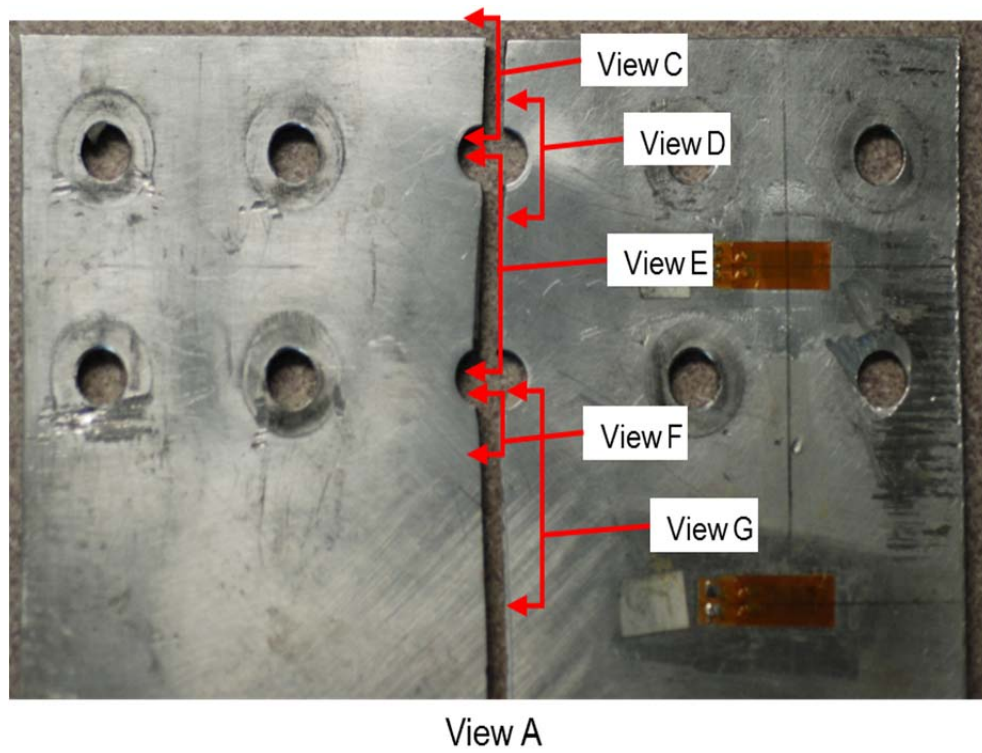


Fig. 43 View A tension specimen.

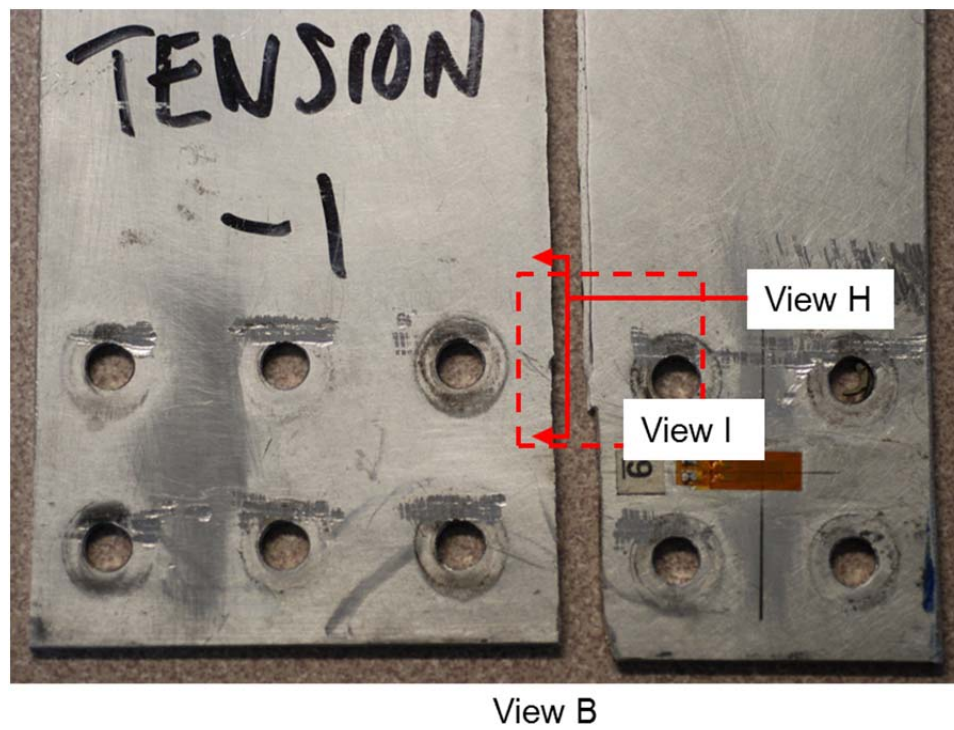


Fig. 44 View B tension specimen.

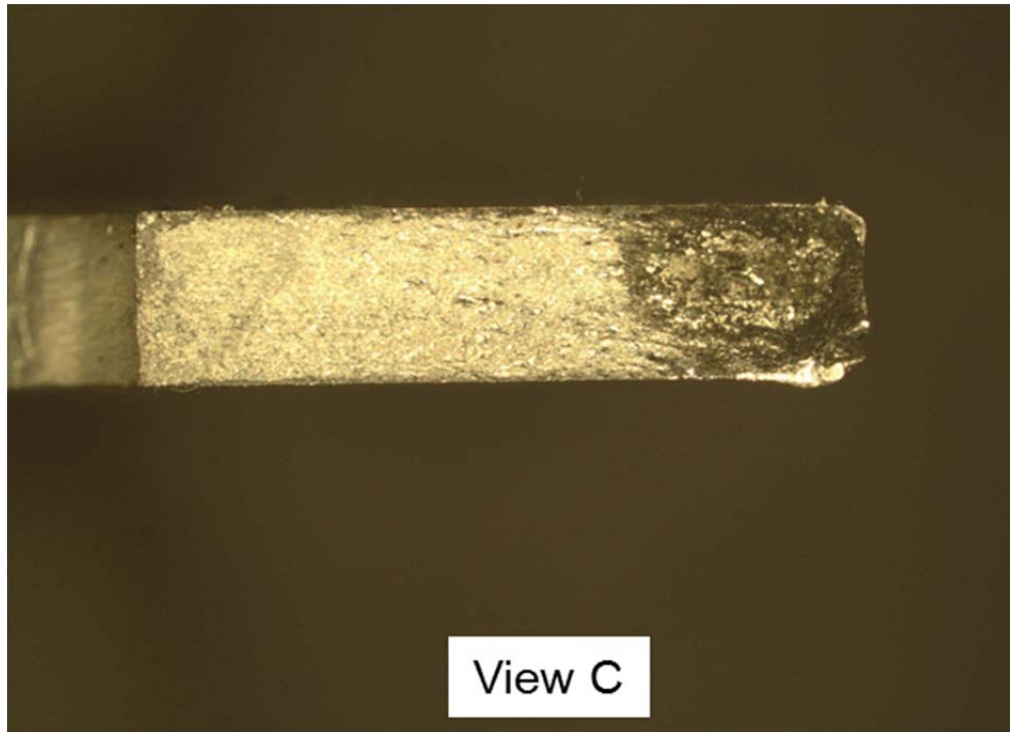


Fig. 45 View C tension specimen.

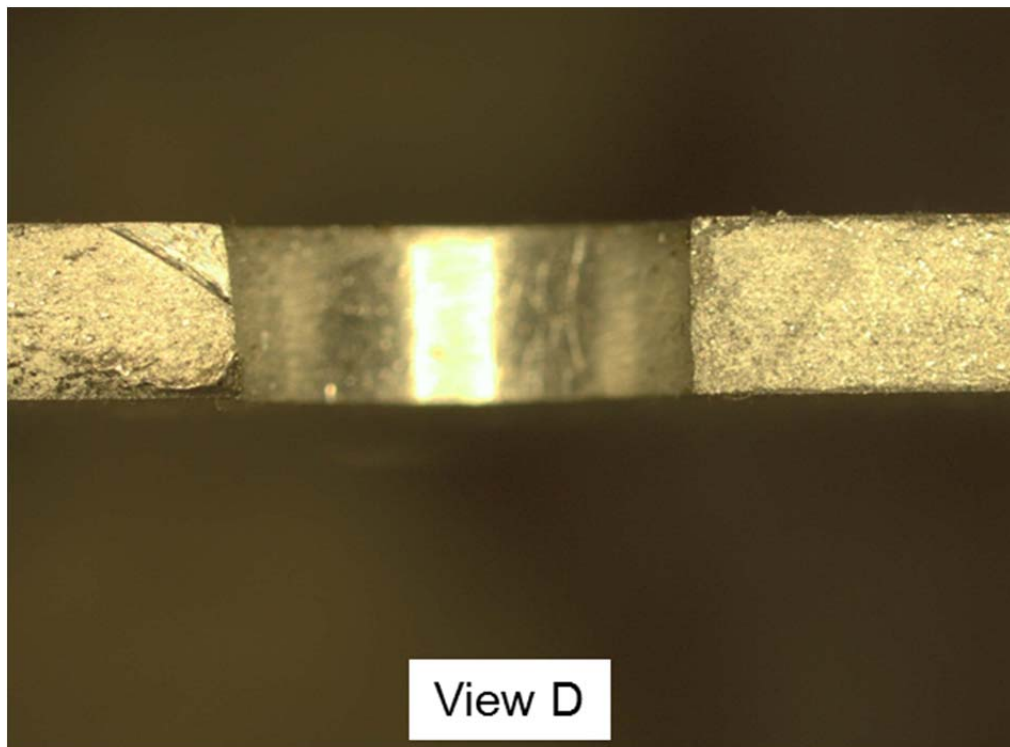


Fig. 46 View D tension specimen.

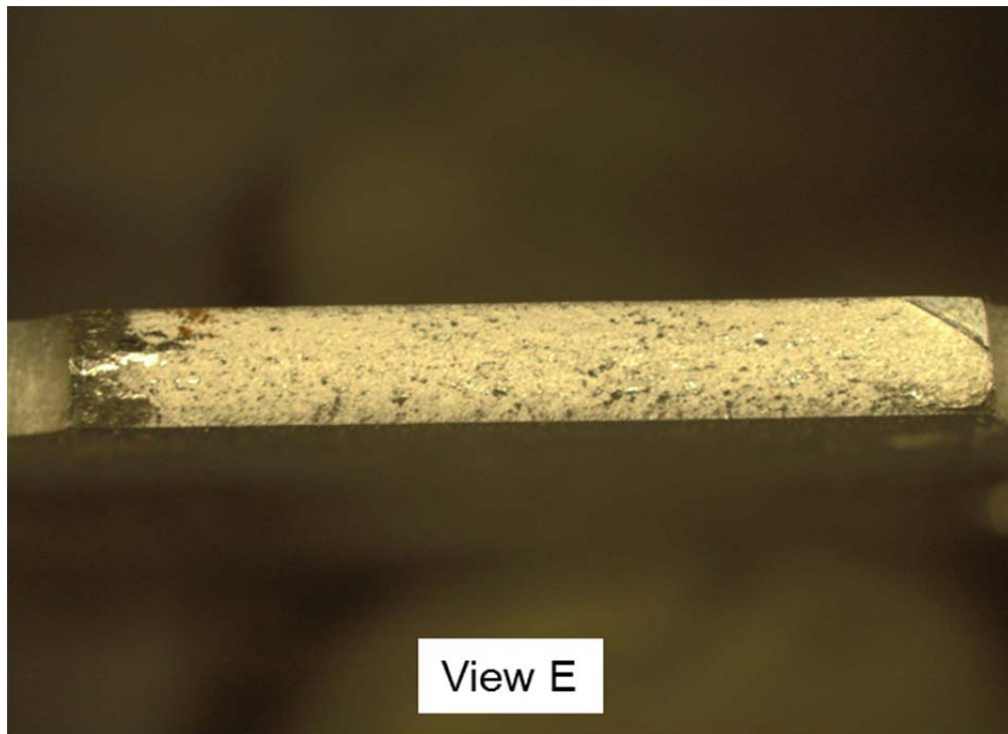


Fig. 47 View E tension specimen.

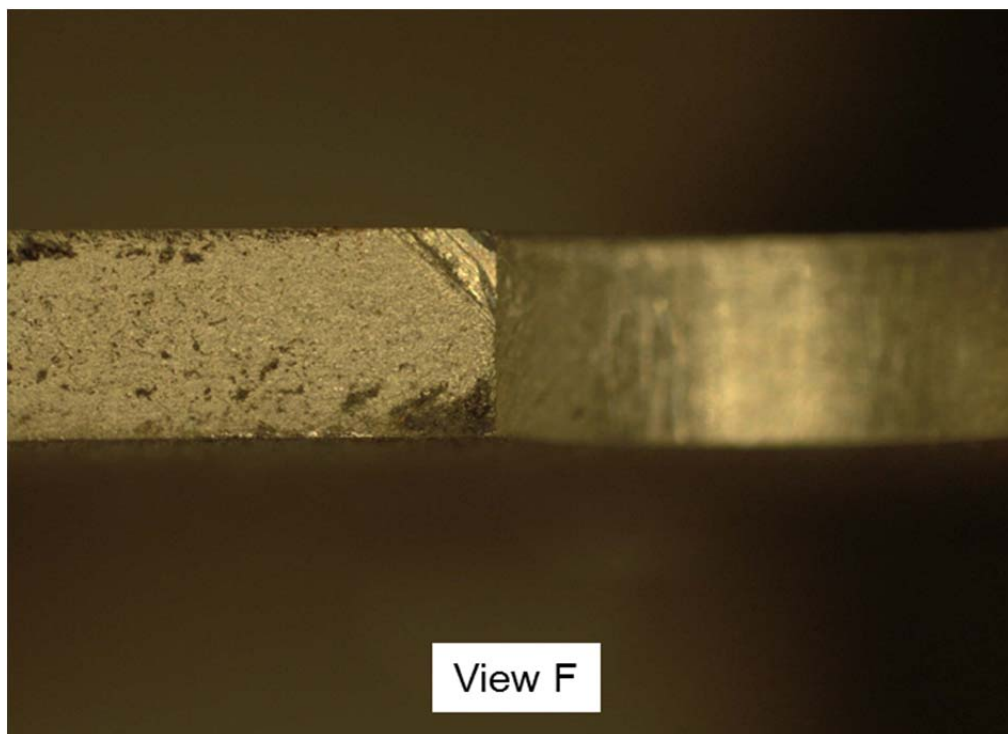


Fig. 48 View F tension specimen.

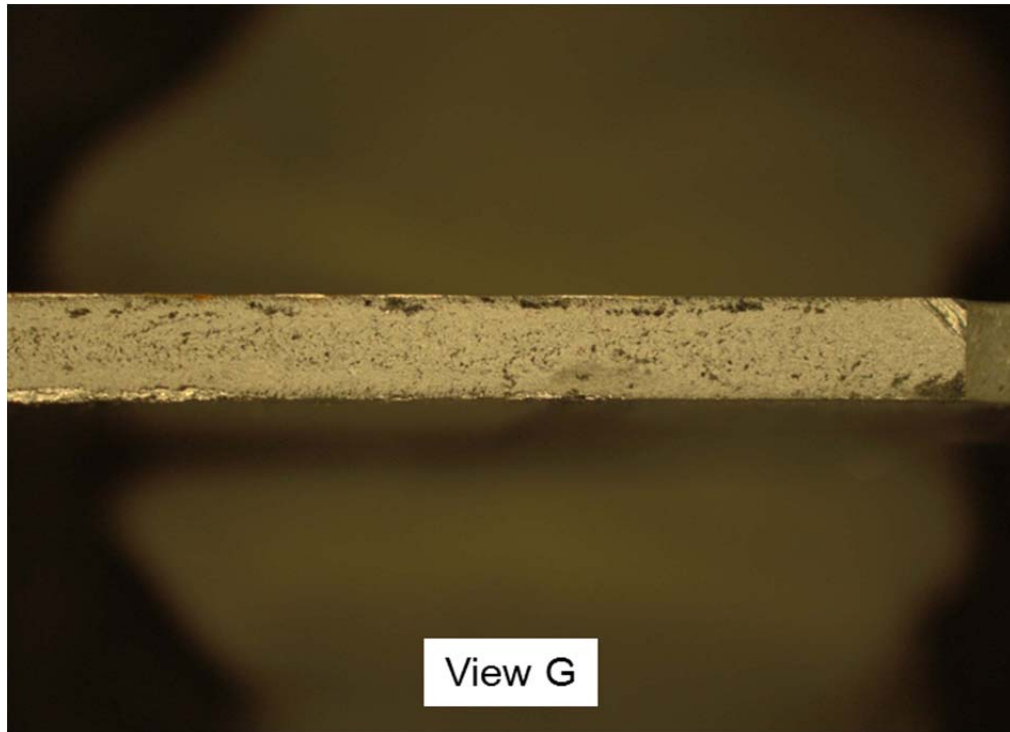


Fig. 49 View G tension specimen.

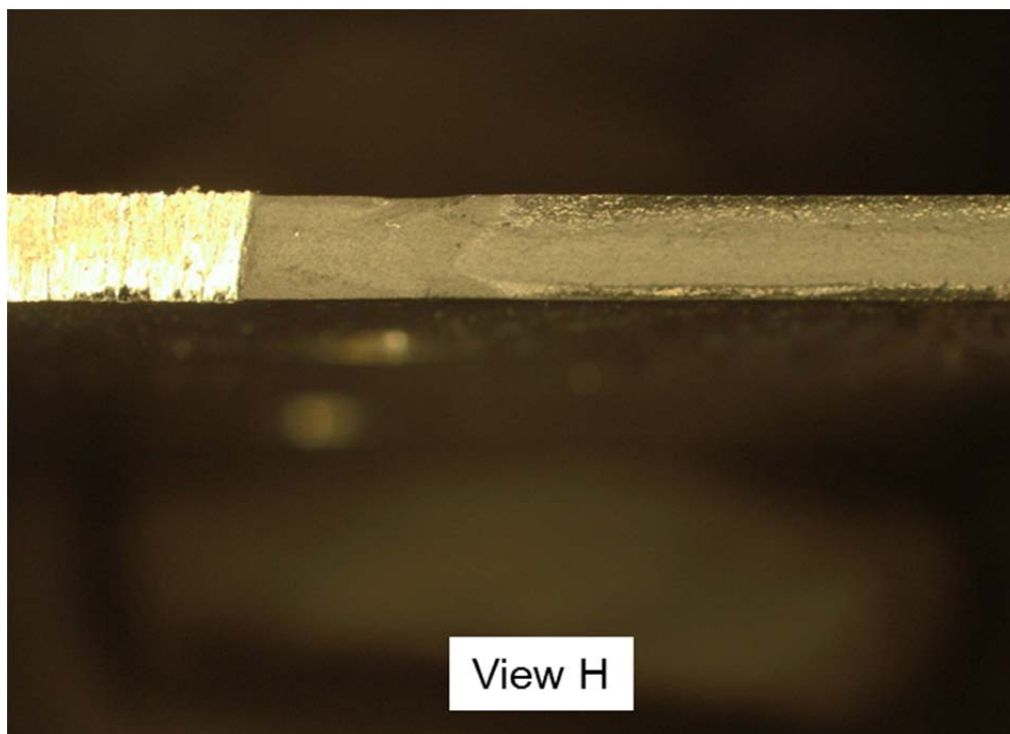


Fig. 50 View H tension specimen.

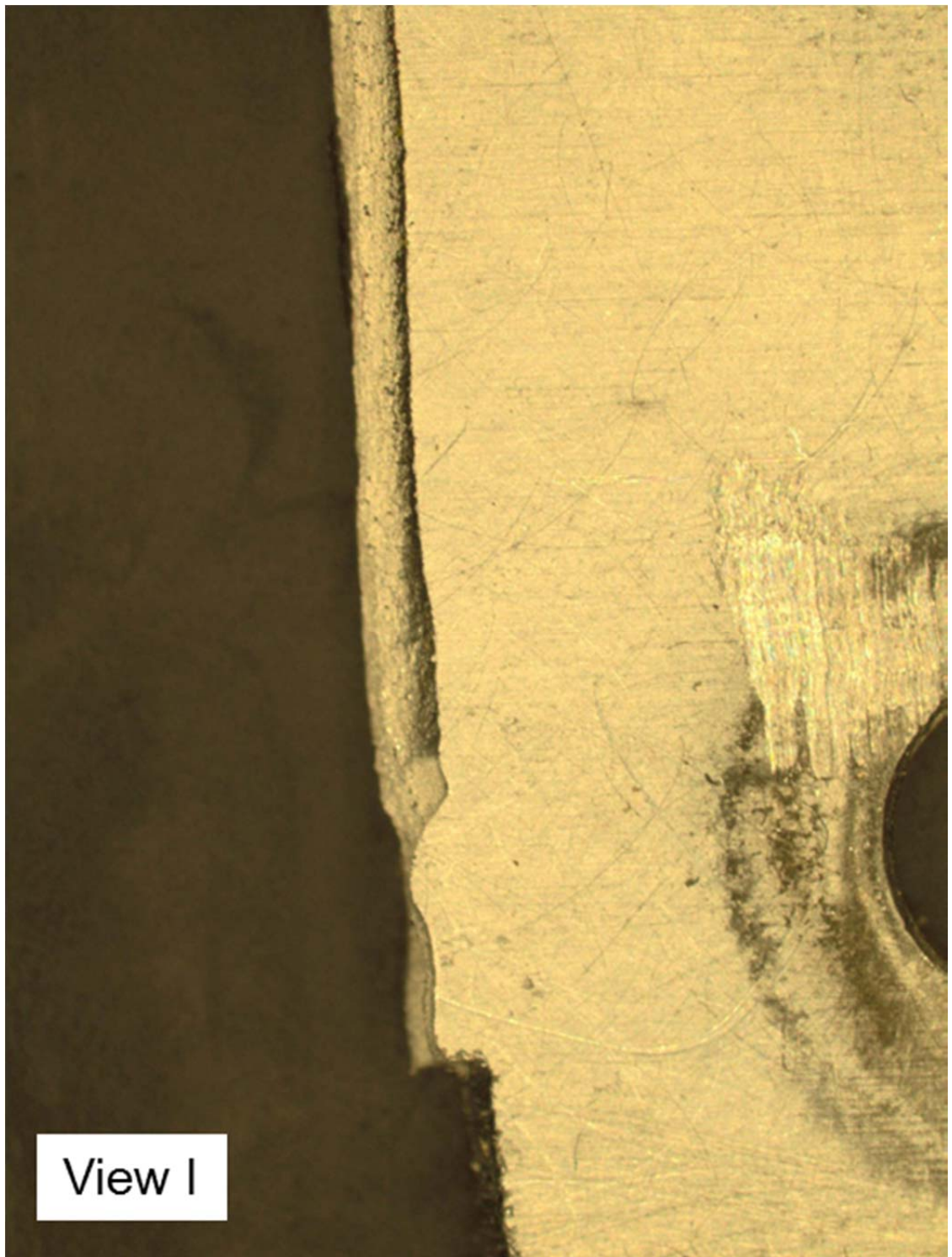


Fig. 51 View I tension specimen.

APPENDIX B BENDING SPECIMEN PHOTOGRAPHS

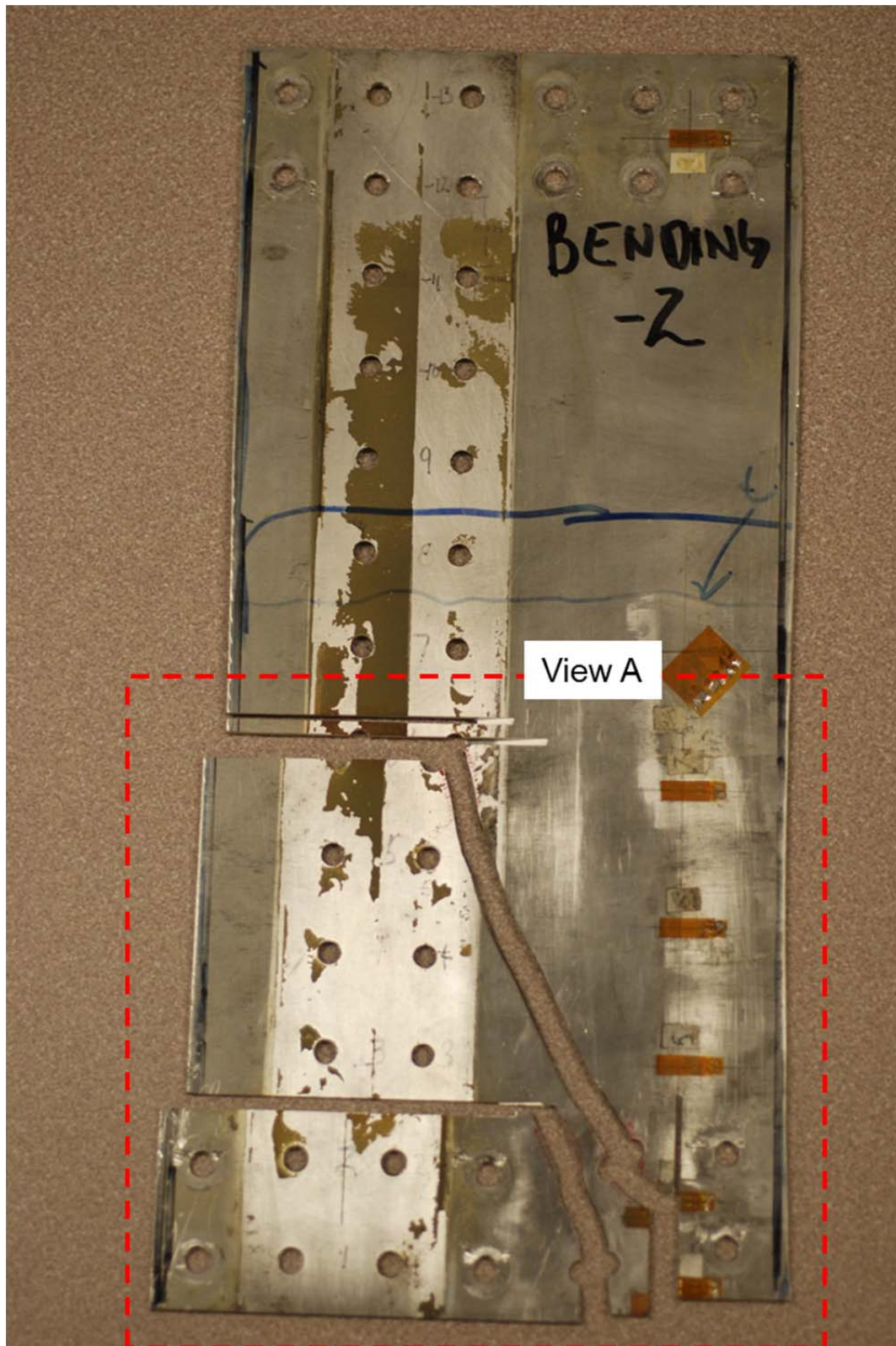


Fig. 52 Bending specimen failed web.

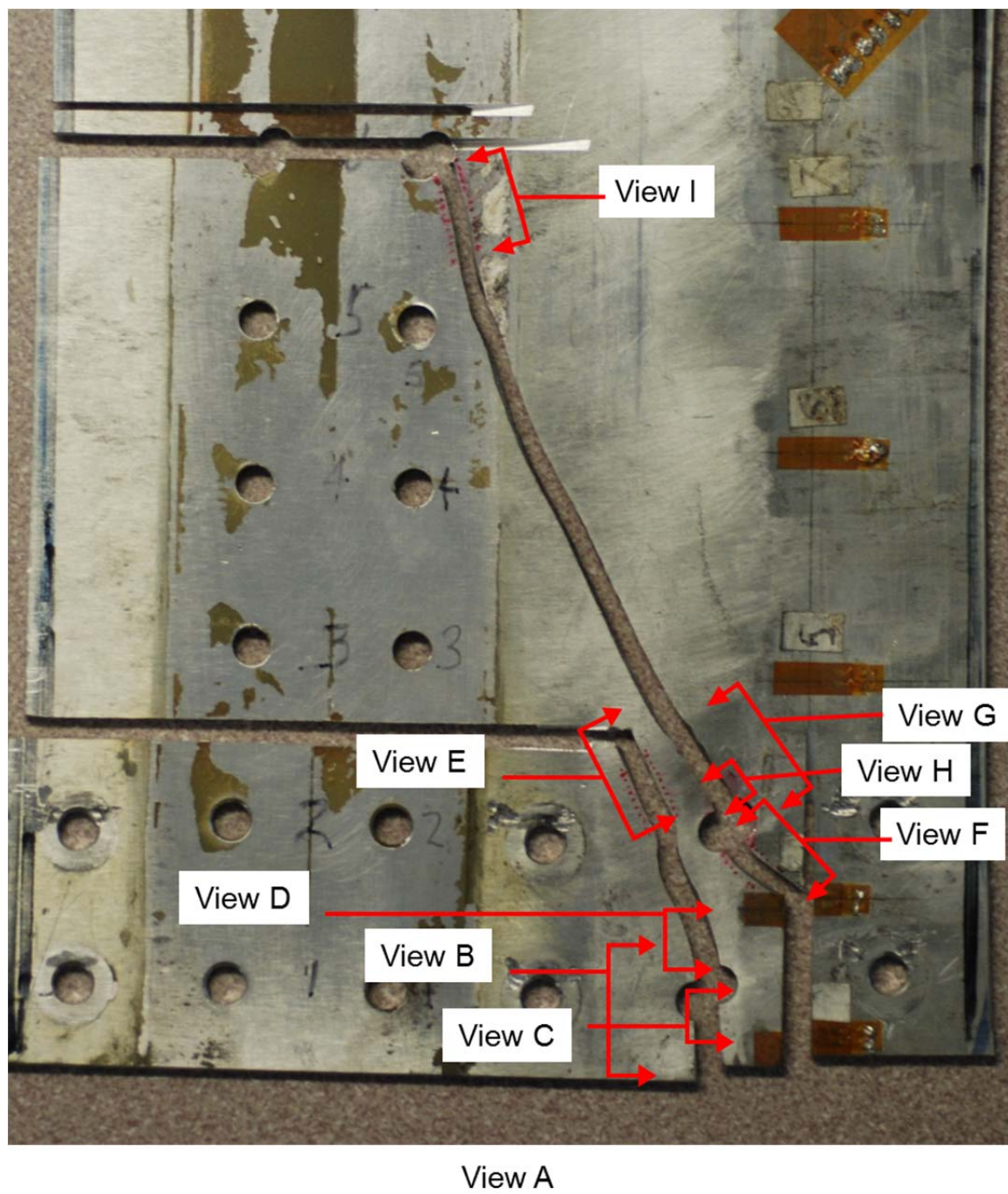


Fig. 53 View A bending specimen.

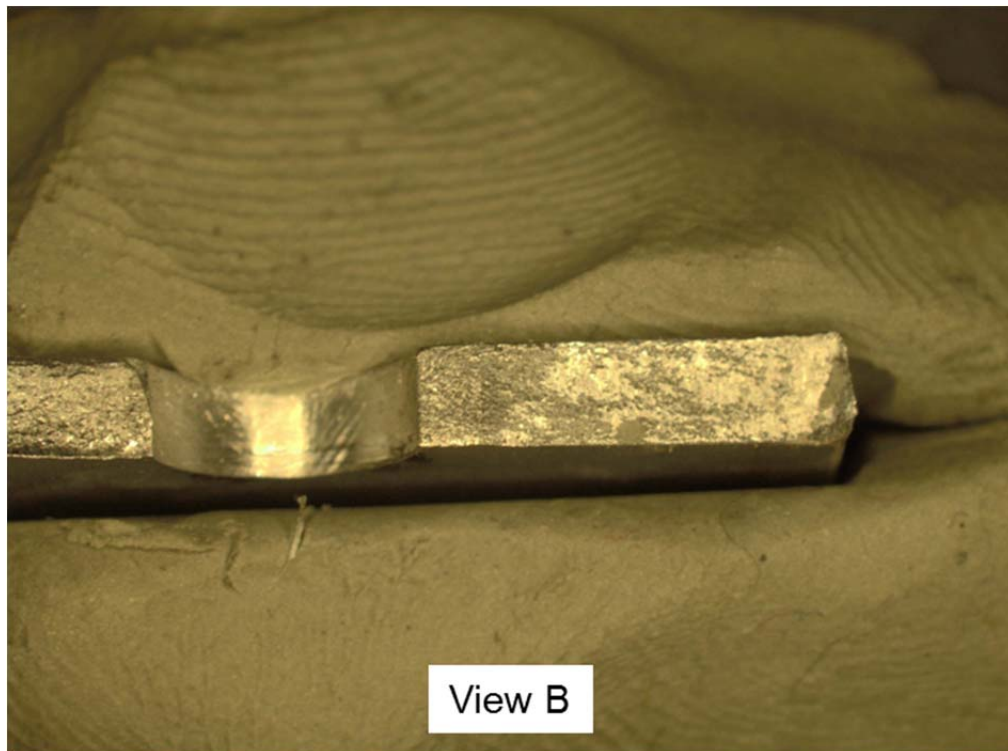


Fig. 54 View B bending specimen.

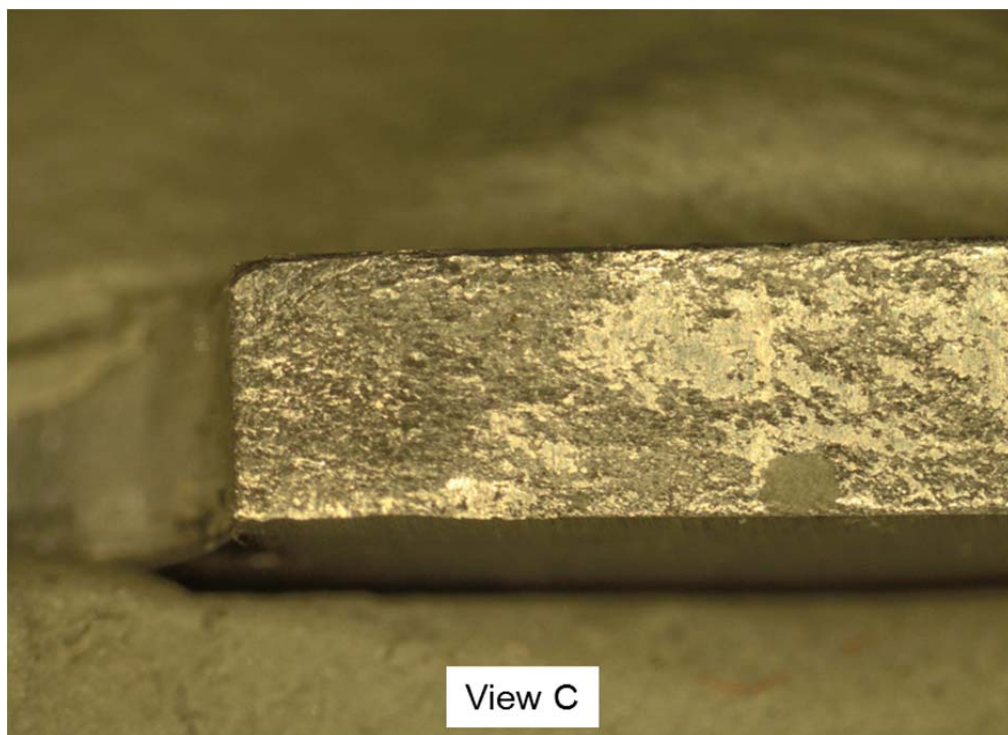


Fig. 55 View C bending specimen.

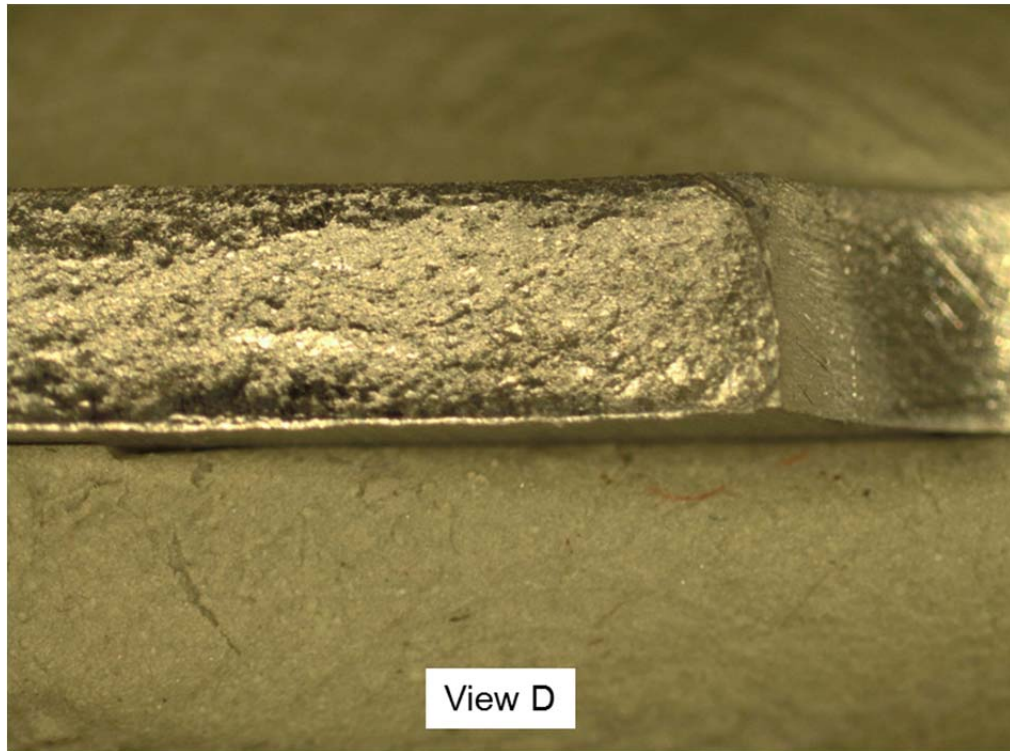


Fig. 56 View D bending specimen.

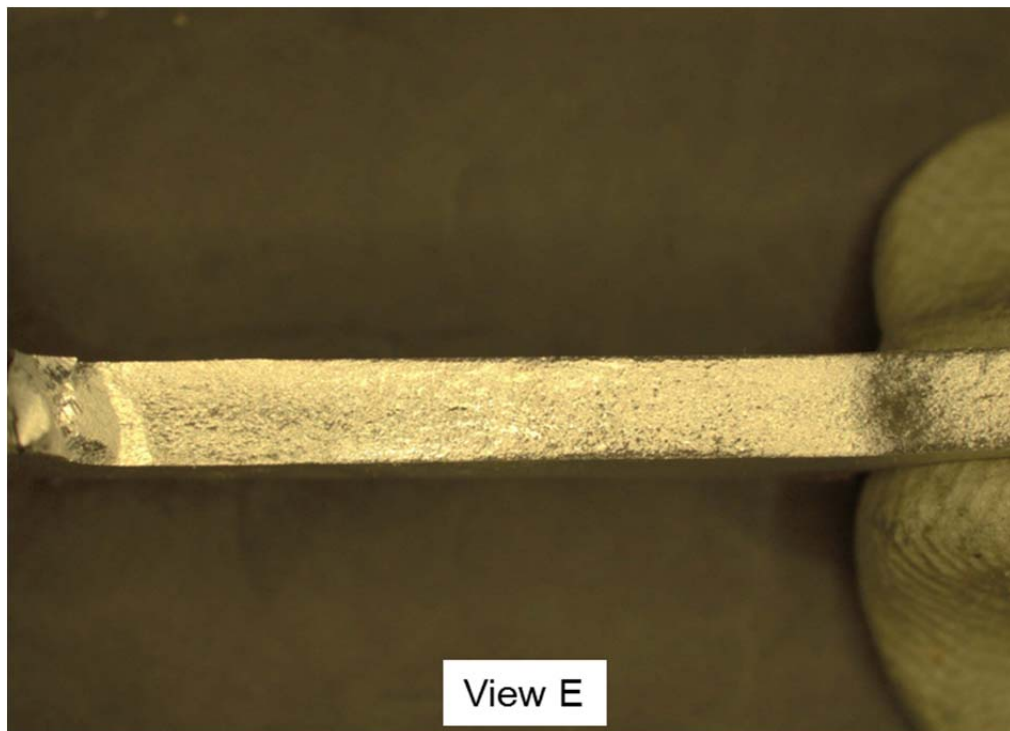


Fig. 57 View E bending specimen.

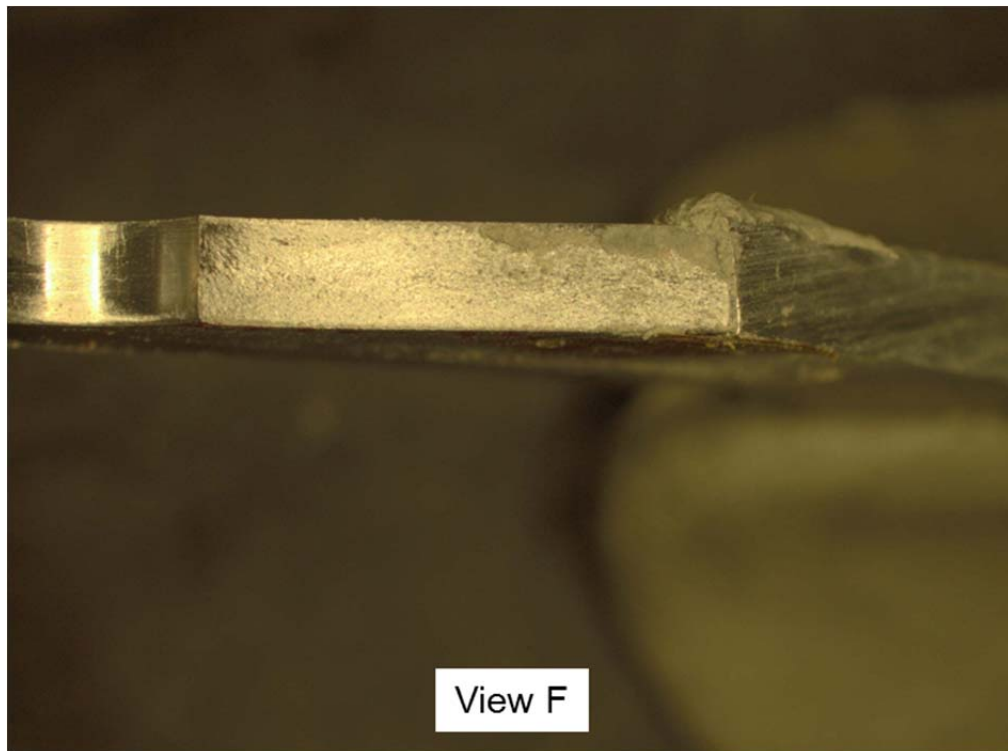


Fig. 58 View F bending specimen.

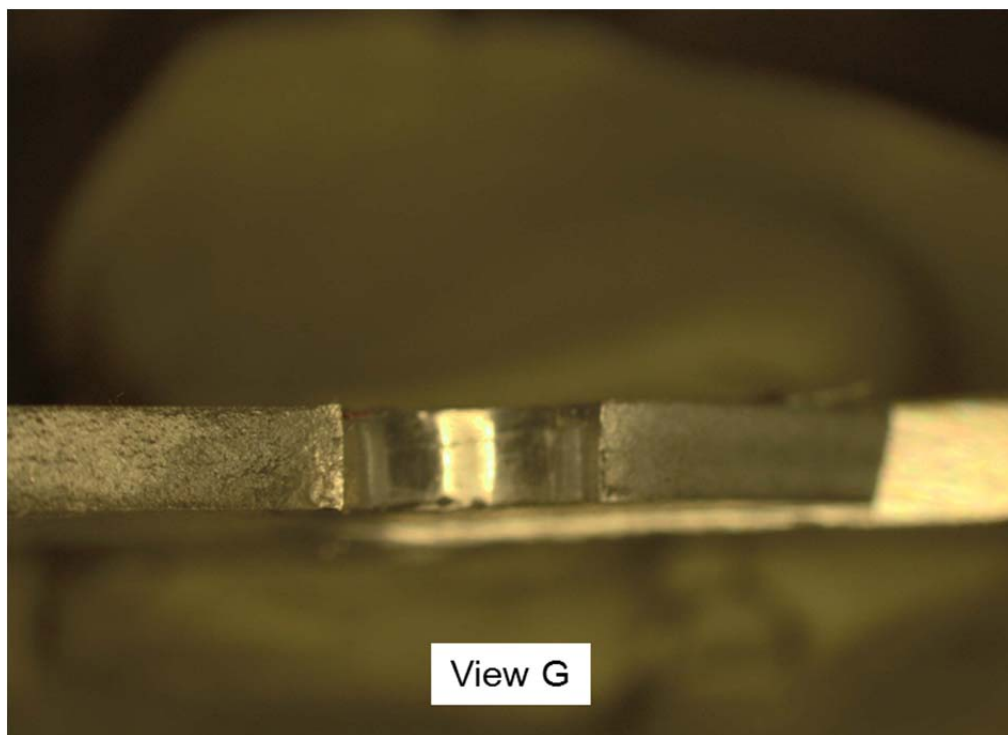


Fig. 59 View G bending specimen.

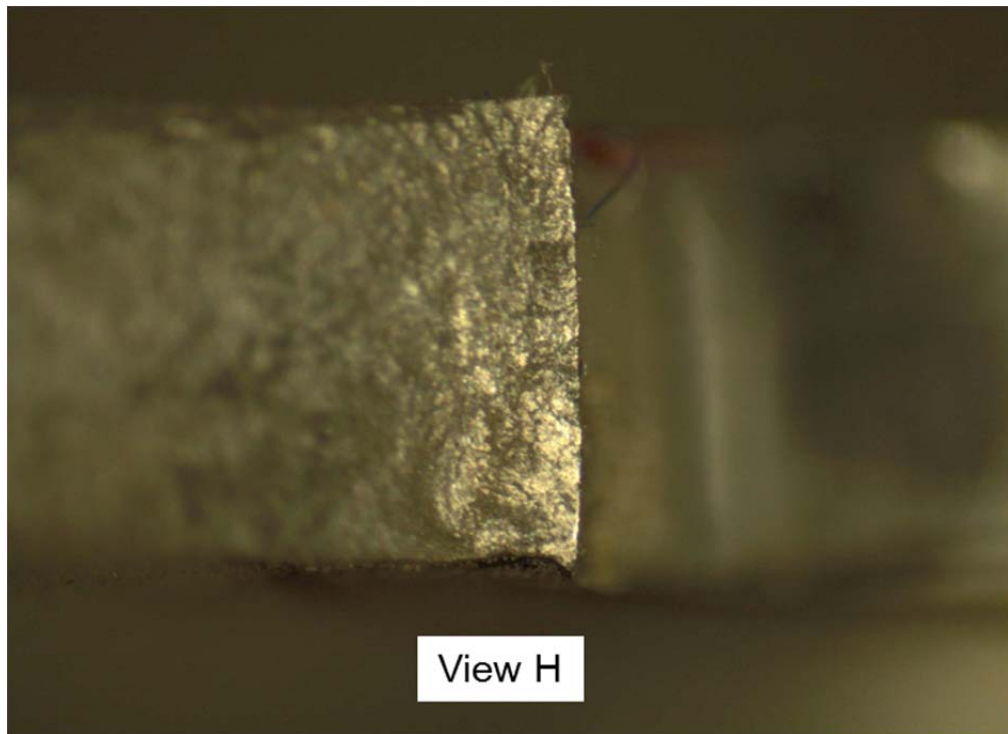


Fig. 60 View H bending specimen.

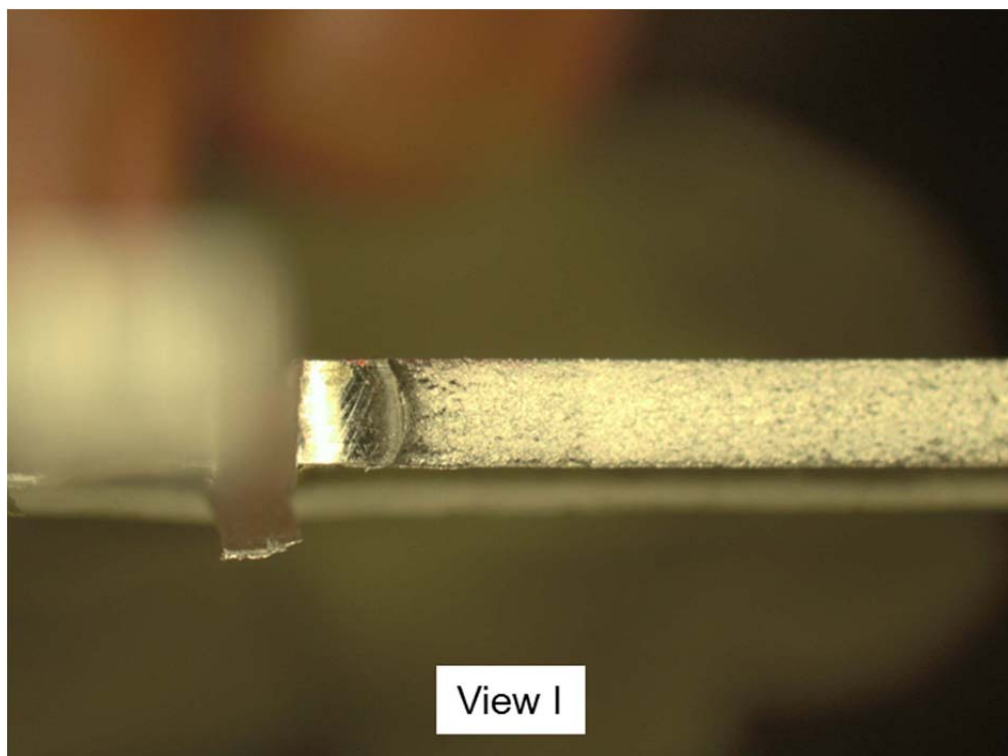


Fig. 61 View I bending specimen.

APPENDIX C SHAPE DESIGNER SECTION DATA

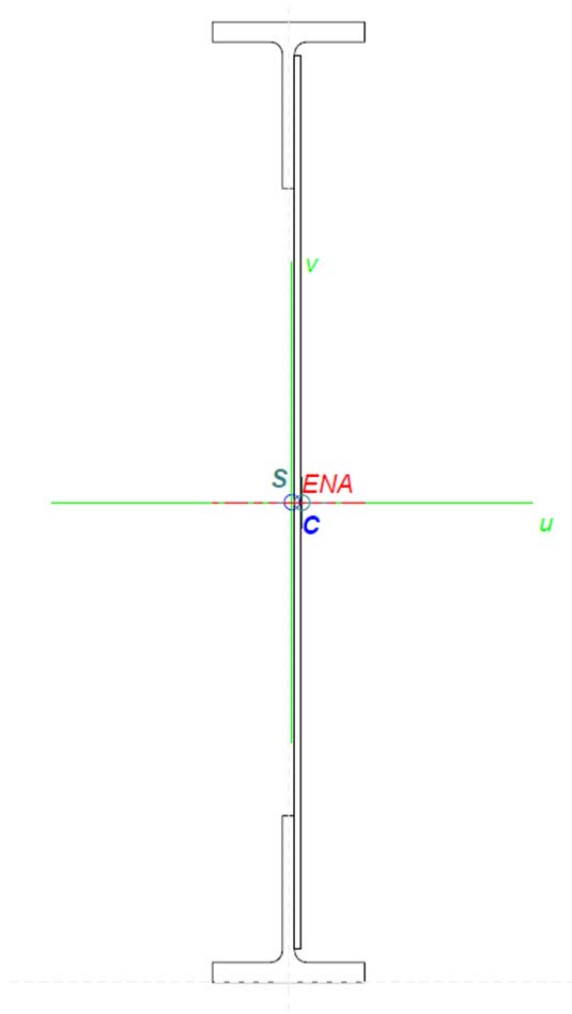
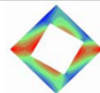


Fig. 62 Shape Designer SaaS beam geometry.




Section Design and Calculation Report

Approved by:

page 2/2

This Product is licensed to : Southwest Research Institute



	Axes X-Y	Centroidal Axes	Principal Axes
Ix (in^4)	+34.419E+01	+13.513E+01	+13.513E+01
Iy (in^4)	+72.879E-02	+71.874E-02	+71.874E-02
Ixy (in^4)	+14.493E-01	+18.865E-07	+18.865E-07
Io (in^4)	+34.492E+01	+13.585E+01	+13.585E+01
rx (in)	+96.221E-01	+60.290E-01	+60.290E-01
ry (in)	+44.276E-02	+43.970E-02	+43.970E-02
ro (in)	+96.322E-01	+60.450E-01	+60.450E-01
Y top (in)		+74.990E-01	+74.990E-01
Y bot (in)		+74.990E-01	+74.990E-01
Sx top (in^3)		+18.020E+00	+18.020E+00
Sx bot (in^3)		+18.020E+00	+18.020E+00
X right (in)		+11.355E-01	+11.355E-01
X left (in)		+12.395E-01	+12.395E-01
Sy right (in^3)		+63.296E-02	+63.296E-02
Sy left (in^3)		+57.987E-02	+57.987E-02
Zpx (in^3)		+21.175E+00	+21.175E+00
Zpy (in^3)		+10.405E-01	+10.405E-01
Max Mx (lb.in)		+91.275E+04	+91.275E+04
Max My (lb.in)		+26.188E+03	+26.188E+03
Mpx (lb.in)		+10.725E+05	+10.725E+05
Mpy (lb.in)		+46.992E+03	+46.992E+03
SFx		+11.751E-01	+11.751E-01
SFy		+17.944E-01	+17.944E-01
IMax (in^4)			+13.513E+01
IMin (in^4)			+71.874E-02
Theta (Deg)			+00.000E+00

Fig. 63 Shape Designer SaaS beam properties.

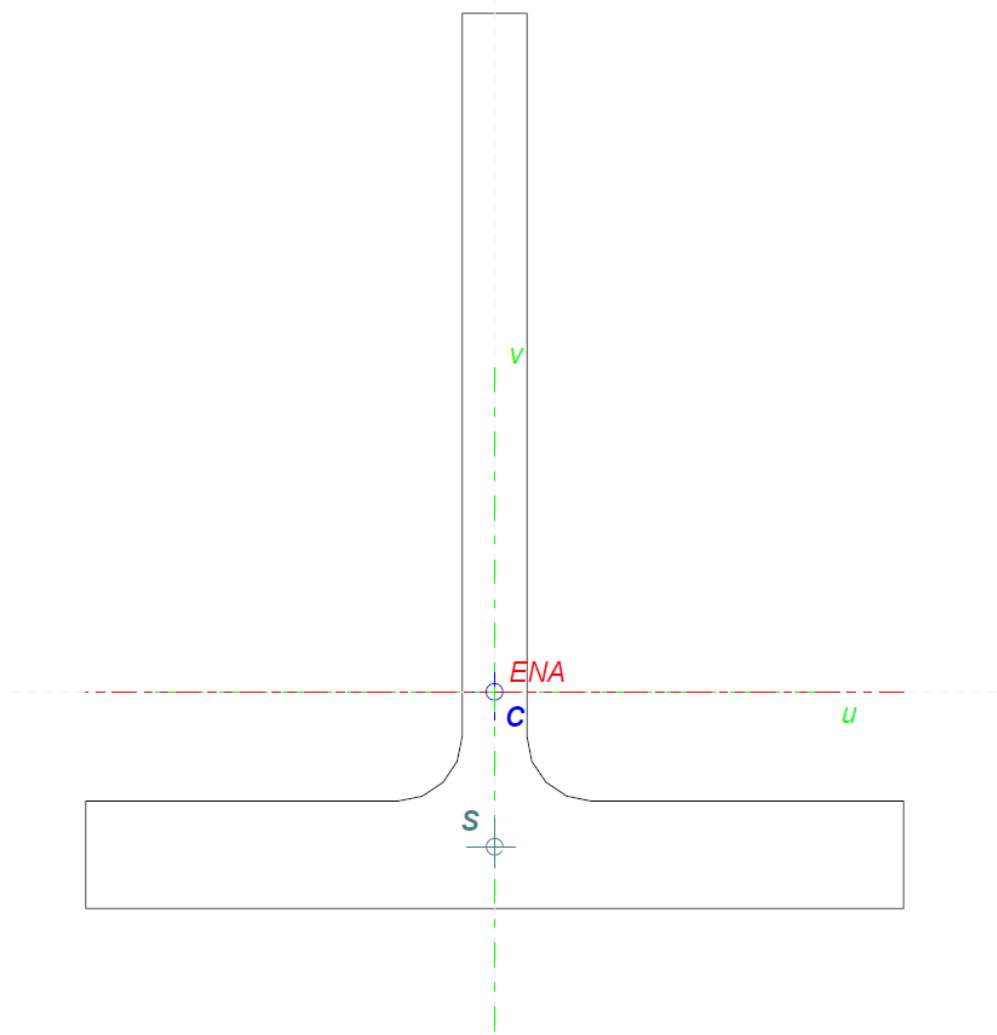


Fig. 64 Shape Designer SaaS cap geometry.



		Section Design and Calculation Report		This Product is licenced to: Southwest Research Institute	
Approved by:		page 2/2			
		V2011 - © MechaTools Technologies Inc. 2011. All rights reserved			
	Axes X-Y	Centroidal Axes	Principal Axes		
Ix (in ⁴)	+65.489E-02	+65.489E-02	+65.489E-02		
Iy (in ⁴)	+34.992E-02	+34.992E-02	+34.992E-02		
Ixy (in ⁴)	-38.123E-09	-38.123E-09	-38.123E-09		
Io (in ⁴)	+10.048E-01	+10.048E-01	+10.048E-01		
rx (in)	+74.255E-02	+74.255E-02	+74.255E-02		
ry (in)	+54.278E-02	+54.278E-02	+54.278E-02		
ro (in)	+91.978E-02	+91.978E-02	+91.978E-02		
Y top (in)		+19.704E-01	+19.704E-01		
Y bot (in)		+62.960E-02	+62.960E-02		
Sx top (in ³)		+33.236E-02	+33.236E-02		
Sx bot (in ³)		+10.402E-01	+10.402E-01		
X right (in)		+11.875E-01	+11.875E-01		
X left (in)		+11.875E-01	+11.875E-01		
Sy right (in ³)		+29.467E-02	+29.467E-02		
Sy left (in ³)		+29.467E-02	+29.467E-02		
Zpx (in ³)		+59.930E-02	+59.930E-02		
Zpy (in ³)		+46.248E-02	+46.248E-02		
Max Mx (lb.in)		+14.624E+03	+14.624E+03		
Max My (lb.in)		+12.965E+03	+12.965E+03		
Mpx (lb.in)		+26.369E+03	+26.369E+03		
Mpy (lb.in)		+20.349E+03	+20.349E+03		
SFx		+18.031E-01	+18.031E-01		
SFy		+15.695E-01	+15.695E-01		
IMax (in ⁴)			+65.489E-02		
IMin (in ⁴)			+34.992E-02		
Theta (Deg)			+00.000E+00		

Fig. 65 Shape Designer SaaS cap properties.

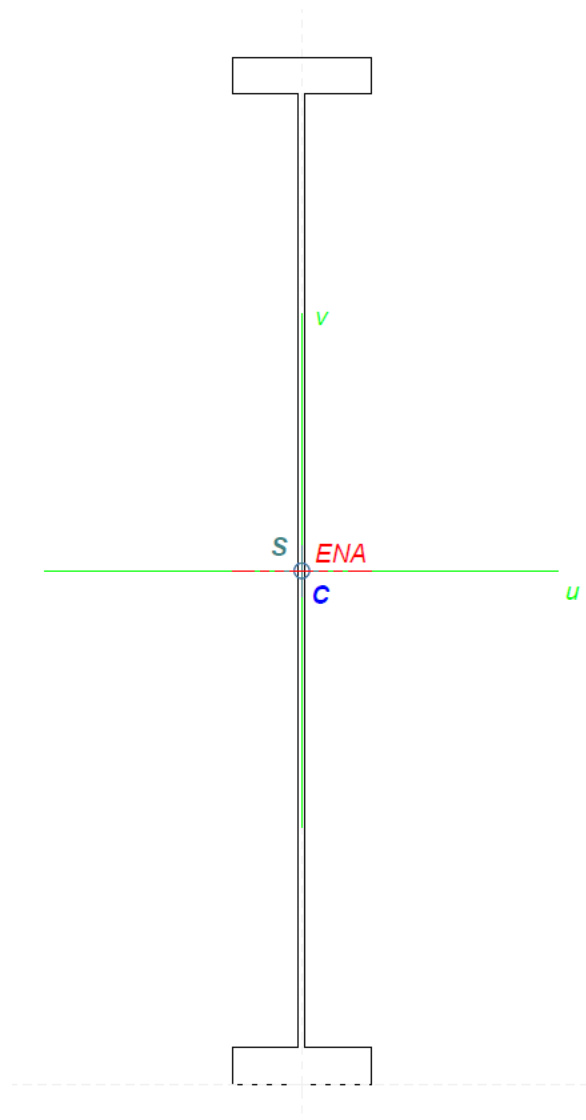


Fig. 66 Shape Designer SaaS idealized beam geometry



		Section Design and Calculation Report Approved by: _____ page 2/2		This Product is licenced to : Southwest Research Institute ShapeDesigner SaaS <small>V/2011 - © MechaTools Technologies Inc. 2011. All rights reserved</small> 
	Axes X-Y	Centroidal Axes	Principal Axes	
Ix (in ⁴)	+33.361E+01	+13.474E+01	+13.474E+01	
Iy (in ⁴)	+73.065E-02	+73.065E-02	+73.065E-02	
Ixy (in ⁴)	-19.588E-06	+42.459E-08	+42.459E-08	
Io (in ⁴)	+33.434E+01	+13.547E+01	+13.547E+01	
rx (in)	+97.126E-01	+61.725E-01	+61.725E-01	
ry (in)	+45.454E-02	+45.454E-02	+45.454E-02	
ro (in)	+97.233E-01	+61.893E-01	+61.893E-01	
Y top (in)		+74.990E-01	+74.990E-01	
Y bot (in)		+74.990E-01	+74.990E-01	
Sx top (in ³)		+17.967E+00	+17.967E+00	
Sx bot (in ³)		+17.967E+00	+17.967E+00	
X right (in)		+10.107E-01	+10.107E-01	
X left (in)		+10.106E-01	+10.106E-01	
Sy right (in ³)		+72.295E-02	+72.295E-02	
Sy left (in ³)		+72.295E-02	+72.295E-02	
Zpx (in ³)		+20.356E+00	+20.356E+00	
Zpy (in ³)		+11.175E-01	+11.175E-01	
Max Mx (lb.in)		+10.780E+05	+10.780E+05	
Max My (lb.in)		+43.377E+03	+43.377E+03	
Mpx (lb.in)		+12.214E+05	+12.214E+05	
Mpy (lb.in)		+67.053E+03	+67.053E+03	
SFx		+11.330E-01	+11.330E-01	
SFy		+15.458E-01	+15.458E-01	
IMax (in ⁴)			+13.474E+01	
IMin (in ⁴)			+73.065E-02	
Theta (Deg)			+00.000E+00	

Fig. 67 Shape Designer SaaS idealized beam properties

APPENDIX D A-10 DTA GROUND RULES FOR A-10A
RECONFIGURED POST DESERT STORM

DTA/ FSMP Update	PREPARED BY:	PREPARED BY 2:	DATE:	REV.	
	Robert Pilarczyk	Tim Allred	Sep 22, 2010	W	
	CHECKED BY:	APPROVED BY:	DATE:	REPORT NO:	
		Paul Clark	Sep 22, 2010	Rev. W	
TITLE:	Damage Tolerance Analysis Ground Rules for A-10A Reconfigured Post Desert Storm				

This document outlines the approach for conducting damage tolerance analyses to support the A-10 Damage Tolerance Re-Assessment and resultant Force Structural Maintenance Plan (FSMP) update as well as any field or depot repair actions. These ground rules apply to analyses using the USAF crack growth software AFGROW.

1. Version 4.12.15.0 of AFGROW released 08/11/2009, or version 5.1.3.16 released 06/13/2010.
 - a. Prepare AFGROW Electronic Input file (.dax) as part of deliverable.
2. Title: Brief description of model.
3. Material: reference RPDS DTR Master Document for guidance related to material model (Forman Lookup or Tabular Lookup) as well as material properties for cp locations. Reference "A-10 Material Reference" document for new analysis not covered by the RPDS Master Document. This document is a general guide and some material properties may need to be adjusted based on manufacturing thicknesses or other factors. Reference the RPDS DTR Master Document and the "Metallic Materials Properties Development and Standardization" (formerly MIL HNDBK 5) document to verify correct material properties.
 - a. Tabular Lookup File
 - i. Select appropriate tabular lookup file from A-10 Materials Folder.
 1. **Verify** correct material properties *for each control point* as prescribed in RPDS DTR Master Document.

NOTE: Ultimate strength and R_{LO} default to 66ksi and -1.0; these values will need to be modified in accordance with the RPDS DTR Master Document. Altering the ultimate strength does not seem to affect the result from AFGROW.

- b. Forman Lookup File
 - i. Select appropriate Forman lookup file from A-10 Materials Folder.
 1. **Verify** correct material properties *for each control point* as prescribed in RPDS DTR Master Document
 2. Special note: Fracture Toughness

DTA/ FSMP Update	PREPARED BY:	PREPARED BY 2:	DATE:	REV.	
	Robert Pilarczyk	Tim Allred	Sep 22, 2010	W	
	CHECKED BY:	APPROVED BY:	DATE:	REPORT NO:	
		Paul Clark	Sep 22, 2010	Rev. W	
TITLE:	Damage Tolerance Analysis Ground Rules for A-10A Reconfigured Post Desert Storm				

- a. "K_c" from RPDS DTR Master Document must be entered into AFGROW → Predict Function Preferences → Propagation Limits → User Defined 'K_{max}'

NOTE: R_{LO} defaults to -1.0; this value will need to be modified in accordance with the RPDS DTR Master Document, typically -0.3

c. Material Properties

- i. Select from RPDS DTR Master Document.

4. Model:

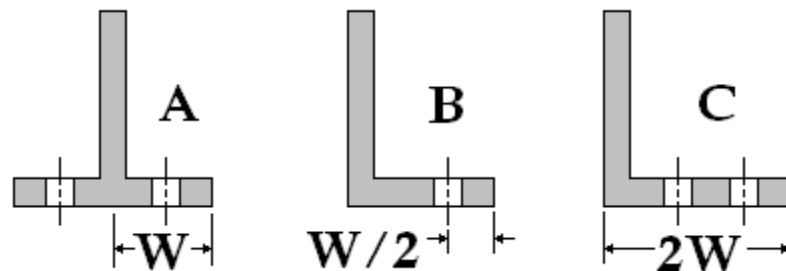
a. Classic models

- i. Select appropriate geometric model
- ii. Enter problem geometric factors including: thickness, width, hole diameter, initial flaw size (IFS), offset, etc
 - 1. Keep A/C constant=YES (checked)
 - a. Note: Keep A/C constant=NO [For surface flaws and in specific cases as noted in SA220R0207 (2nd 6000 Hour DTR)]
 - 2. Oblique through crack=NO (unchecked)
 - 3. Initial Flaw Size: Unless otherwise specified, the initial flaw size should be the same in both the "A" & "C" directions. See Section 10 for appropriate initial flaw sizes.
- 4. Countersunk Holes:
 - a. A stress concentration (K_t), as calculated by Shavikumar and Newman (NASA TP-3192, 1992), is used to calculate beta corrections to be used for countersunk holes.
 - b. The A-10 countersunk hole macro can be used to calculate beta corrections for a given model and countersink geometry.
 - c. The shank diameter of the hole should be used in the analysis.
 - d. A reduced model thickness should be used in the analysis (true thickness minus the depth of the countersink).

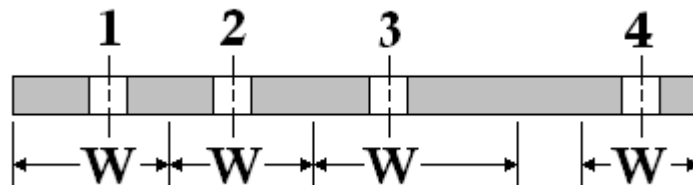
DTA/ FSMP Update	PREPARED BY:	PREPARED BY 2:	DATE:	REV.	
	Robert Pilarczyk	Tim Allred	Sep 22, 2010	W	
	CHECKED BY:	APPROVED BY:	DATE:	REPORT NO:	
		Paul Clark	Sep 22, 2010	Rev. W	
TITLE:	Damage Tolerance Analysis Ground Rules for A-10A Reconfigured Post Desert Storm				

- i. For materials where SOLR changes with thickness, assume the full thickness in determining SOLR.
 - e. For locations with load transfer, the shank diameter and full thickness of the component should be used to calculate the bearing stress fraction.
 - f. Reference SA220R0207, Rev. C, Appendix J for fastener head size information.
 - g. Knife edge fasteners ($t_{CS} \geq t$) are not allowed in airframe design because of fatigue requirements. The maximum countersink depth is $t_{cs} = \frac{2}{3}(t)$
- iii. Load: Ratio of tension or bearing stress to reference stress must be input for each load case (tension stress fraction = 1.0, if bearing stress is zero).
- iv. For pin loaded fastener holes, the tension stress fraction should reflect the reduced bypass stress fraction (i.e.: 20% load transfer equates to 80% tension stress fraction).
 - 1. Effective Widths: Refer to RPDS DTR Master Document for appropriate Effective Width for each CP.
 - a. New analysis: For the purpose of determining the Bearing Stress Fraction (BrSF) in AFGROW the following approach should be used.
 - b. For all capstrips, angles etc., the effective width as shown in the figure below: A) the length of the leg, B) the offset doubled, or C) one-half the leg length as in the case of a leg with a double row of fasteners. In cases where multiple cases could be applicable, use the smallest effective width.

DTA/ FSMP Update	PREPARED BY:	PREPARED BY 2:	DATE:	REV.	
	Robert Pilarczyk	Tim Allred	Sep 22, 2010	W	
	CHECKED BY:	APPROVED BY:	DATE:	REPORT NO:	
		Paul Clark	Sep 22, 2010	Rev. W	
TITLE:	Damage Tolerance Analysis Ground Rules for A-10A Reconfigured Post Desert Storm				



- c. In situations where there is a line of fasteners the effective width can be taken as 1) offset plus half the distance to the neighboring hole, 2 & 3) the sum of half the distance to the neighboring holes, or 4) offset doubled, which ever is less.



- d. The final method of finding the BrSF is to determine it directly from the load reports. The far field stress is easily determined using the load and the cross-sectional area, the bearing stress is the load taken out by the fastener divided by (width * thickness). Typically, doing this method in lieu of the above technique should result in the same BrSF.
2. Further modeling may be necessary via, FEM, Stress-Check, etc.
- v. The "Filled Unloaded Hole" option is not typically used unless engineering judgment overrides this approach. If used, justification must be provided in the analysis report.
- b. Advanced Model

DTA/ FSMP Update	PREPARED BY:	PREPARED BY 2:	DATE:	REV.	
	Robert Pilarczyk	Tim Allred	Sep 22, 2010	W	
	CHECKED BY:	APPROVED BY:	DATE:	REPORT NO:	
		Paul Clark	Sep 22, 2010	Rev. W	
TITLE:	Damage Tolerance Analysis Ground Rules for A-10A Reconfigured Post Desert Storm				

- i. Advanced models can be used for some situations, i.e. crack growth between adjacent holes. The analyst should ensure the model details are within the bounds of the solutions in AFGROW. The classic model inputs detailed in section 4.a are also applicable for advanced models.
 - ii. Advanced continuing damage model (slot)
 - 1. The in-plane bending constraint option should typically be selected. Some situations, where in plane bending may occur in a continuing damage scenario, may warrant the use of the unconstrained in-plane bending option.
 - c. Lug Model
 - i. Use AFGROW default preferences (see Predict Function Preferences in this document).
- 5. Spectrum:
 - a. Stress Multiplication Factor (SMF)
 - i. Enter maximum stress (normalized spectrum will be used for all analyses).
 - 1. Maximum stresses come from Northrop Grumman stress equations (reference SA220R0474), these values are also listed in the RPDS DTR Master Document.
 - 2. For non-CP locations engineering judgment with referenced justification should be used to select the appropriate SMF.
 - a. For details similar and near a CP location, the SMF for that location may be used when appropriate.
 - b. The ultimate stress reports may be used to scale a known CP location SMF to the location of interest.
 - b. Residual Strength Requirement (P_{xx})
 - i. Enter the higher of either the maximum spectrum stress or the limit stress if known.
 - c. Open existing spectrum file
 - 1. Use only RPDS severe spectrum from approved spectrum folder.
 - a. A common spectrum electronic folder will be utilized.

DTA/ FSMP Update	PREPARED BY:	PREPARED BY 2:	DATE:	REV.	
	Robert Pilarczyk	Tim Allred	Sep 22, 2010	W	
	CHECKED BY:	APPROVED BY:	DATE:	REPORT NO:	
		Paul Clark	Sep 22, 2010	Rev. W	
TITLE:	Damage Tolerance Analysis Ground Rules for A-10A Reconfigured Post Desert Storm				

- b. Spectrum files are:
 - i. Flight-by-flight
 - ii. Base-peak-base converted
 - iii. Normalized
 - 2. In the event an AFGROW ready spectrum file (filename.sp3) is not in existence, use the spectrum converter file to be certain the spectrum file is in the proper format to be read by AFGROW.
- 6. Retardation:
 - a. Generalized Willenborg Retardation
 - i. Turn OFF the “Adjust Yield Zone Size for Compressive Cycles” toggle.
 - ii. For all SOLR values, see the RPDS DTR Master Document and/or Appendix F.
- 7. Predict Function Preferences:
 - a. Growth Increment
 - i. Cycle by Cycle Beta and Spectrum calculation
 - 1. For advanced models use “Cycle by Cycle Spectrum calculation”.
 - a. Use Max. Growth Increment of 0.25%.
 - b. Output Intervals
 - i. Specify Crack Growth Increments. Increment = 0.01”
 - ii. Number of Hours per Pass.
 - 1. Spectra based on 240 hours for all except landing gear
 - 2. Landing gear spectra based on 250 landings (assumes 1.5 hours per landing).
 - c. Output Options (AFGROW output files are part of deliverables).
 - i. Output
 - 1. Data File
 - 2. Plot File
 - d. Propagation Limits
 - i. K_{max} failure criteria (If using Forman: see 3.b.i.2.a of these ground rules)
 - ii. Net section yield: to be evaluated on a case-by-case basis
 - e. Transition to Through Crack
 - i. Default = 95% (Stick with default unless documented otherwise.)
 - f. Lug Boundary Conditions

DTA/ FSMP Update	PREPARED BY:	PREPARED BY 2:	DATE:	REV.	
	Robert Pilarczyk	Tim Allred	Sep 22, 2010	W	
	CHECKED BY:	APPROVED BY:	DATE:	REPORT NO:	
		Paul Clark	Sep 22, 2010	Rev. W	
TITLE:	Damage Tolerance Analysis Ground Rules for A-10A Reconfigured Post Desert Storm				

- i. Use default of combined bearing and spring solution and default values:
 - 1. Bearing: 70%
 - 2. Spring 80%
 - ii. Use Spring Boundary Condition for applications with an interference fit fastener or interference fit bushing where fastener/bushing is steel in aluminum lug.
 - 8. Stress State
 - a. Use Stress State to be determined automatically.
 - 9. Betas
 - a. Use AFGROW standard solution betas for standard geometries.
 - b. Non-standard geometries shall be dealt with on a case-by-case basis (User Defined Betas: Legacy, StressCheck, etc.)
 - 10. Inspection intervals
 - a. Initial inspection intervals based upon the safety limit (Initial Flaw Size** to fracture) divided by 2.
**Ref: JSSG-2006 Table XXX, page 449.
 - i. New Structure Initial Flaw Sizes (IFS)
 - 1. Non-Cold Worked Holes:
 - a. Aluminum: IFS = 0.050"
 - b. Steel: IFS = 0.050"
 - 2. Cold Worked Holes:
 - a. Aluminum: IFS = 0.005"
 - b. Steel: IFS = 0.005"
 - 3. Surface Flaws
 - a. IFS = 0.100" = 2c (This is the total crack length)
 - b. Recurring inspection intervals based upon the field safety limit (Detectable Flaw Size** to fracture) divided by 3.
**Ref: Structures Bulletin EN-SB-08-012, Revision A.
 - i. Field safety limit detectable flaw sizes (DFS)
 - 1. For Bolt Hole Eddy-Current inspections
 - a. Aluminum: DFS = 0.050"
 - b. Stainless & Ni-Co Steels: DFS = 0.060"
 - c. 4000 Series Steel: DFS = 0.100"
 - d. Note: minimum part thickness of 0.040" is required

DTA/ FSMP Update	PREPARED BY:	PREPARED BY 2:	DATE:	REV.	
	Robert Pilarczyk	Tim Allred	Sep 22, 2010	W	
	CHECKED BY:	APPROVED BY:	DATE:	REPORT NO:	
		Paul Clark	Sep 22, 2010	Rev. W	
TITLE:	Damage Tolerance Analysis Ground Rules for A-10A Reconfigured Post Desert Storm				

- e. The DFS for a coldworked hole using Bolt-Hole Eddy Current inspections is the same as a non-coldworked hole, however, the recurring inspection intervals should be based upon the field safety limit divided by 2.
2. Eddy Current Surface Scan
 - a. Flat Open Surface--Free Hand Scanning—Radius of Curvature > 1.0"
 - i. Aluminum: DFS = 0.250" = 2c
 - b. Radii
 - i. Free Hand Scanning—Radius of Curvature < 1.0"
 1. Aluminum: DFS = 0.500" = 2c
 - ii. Conformal Radius Probe (specialty probe)
 1. Aluminum: DFS = 0.150" = 2c
 - c. Edges
 - i. Free Hand Scanning
 1. Aluminum: DFS = 0.250"
 - ii. Articulating Edge Probe (specialty probe)
 1. Aluminum: DFS = 0.150"
 - d. Around Raised Fastener Heads (or Collars)
 - i. Fastener Head as Guide
 1. Aluminum: DFS = 0.200" + fastener head (or collar) overlap
 2. Reference SA220R0207, Rev. C, Appendix J for fastener head size information.
 - ii. Socket Scanner Probes (specialty probe)
 1. Aluminum: DFS = 0.150" + fastener head (or collar) overlap
 2. Reference SA220R0207, Rev. C, Appendix J for fastener head size information.
 - e. Around Countersunk Fastener Heads
 - i. Aluminum: DFS = 0.250" + fastener head overlap

DTA/ FSMP Update	PREPARED BY:	PREPARED BY 2:	DATE:	REV.	
	Robert Pilarczyk	Tim Allred	Sep 22, 2010	W	
	CHECKED BY:	APPROVED BY:	DATE:	REPORT NO:	
		Paul Clark	Sep 22, 2010	Rev. W	
TITLE:	Damage Tolerance Analysis Ground Rules for A-10A Reconfigured Post Desert Storm				

- ii. Reference SA220R0207, Rev. C, Appendix J for fastener head size information.
 - f. See EN-SB-08-012, Rev A for additional guidance on inspections using guides, fixtures, or specialty probes.
 - g. For inspections of steel components the following DFS guidelines apply:
 - i. Stainless & Ni-Co Steels: $DFS = 1.2 \times DFS \text{ for Aluminum}$
 - ii. 4000 Series Steels: $DFS = 2.0 \times DFS \text{ for Aluminum}$
 - iii. Guidelines were provided by HAFB NDI Program Office.
 - h. Consult the A-10 ASIP group and the HAFB NDI Program Office for additional guidance for other inspection methods.
11. Continuing Damage Option: This section explains some of the common situations for employing continuing damage. Engineering judgment may overrule these guidelines as determined for each situation analyzed. (*e.g.: fleet history may dictate more conservative assumptions than those presented here*)
- a. Use standard Air Force practice when justified.
 - i. JSSG 2006 Table XXXI, page 450
 - b. For continuing damage on diametrically opposite side of hole
 - i. Use advanced AFGROW model with hole and slot
 - ii. Standard holes (Non-Cold Worked holes)
 - 1. IFS: 0.050"x0.050" (primary) and 0.005"x0.005" (secondary)
 - 2. Continuing damage: Ligament failed and (0.005"x0.005" + Δa^*)
 - 3. Inspection Interval:
 - a. Safety Limit: Total Life divided by two
 - b. Field Safety Limit: Life from DFS divided by three
 - iii. Cold Worked holes (*note: divided by two for FSL, see 11.b.iii.2*)
 - 1. Safety Limit

DTA/ FSMP Update	PREPARED BY:	PREPARED BY 2:	DATE:	REV.	
	Robert Pilarczyk	Tim Allred	Sep 22, 2010	W	
	CHECKED BY:	APPROVED BY:	DATE:	REPORT NO:	
		Paul Clark	Sep 22, 2010	Rev. W	
TITLE:	Damage Tolerance Analysis Ground Rules for A-10A Reconfigured Post Desert Storm				

- a. IFS: 0.005"x0.005" (primary) and 0.005"x0.005" (secondary)
- b. Continuing damage: Ligament failed and (0.005"x0.005" + Δa^*)
- c. Initial Inspection: Total Life divided by two
- 2. Field Safety Limit
 - a. IFS: 0.050"x0.050" (primary) and 0.005"x0.005" (secondary)
 - b. Continuing damage: Ligament failed and (0.005"x0.005" + Δa^*)
 - c. Inspection Interval: Life from DFS **divided by two**

* Δa found with a separate model with one continuing damage flaw on the opposite side of the hole as the primary crack, ran the number of cycles it took the primary crack to grow from the initial flaw to failure. Note: The primary crack is not included in this model

- c. For continuing damage in adjacent structure.
 - i. Continuing damage IFS = 0.005" + Δa
 - ii. Δa should be calculated based on the life in the primary component from IFS to failure.
 - d. Significant detail shall be documented in the write-up to fully explain all details of the analysis.
12. Document analysis using A-10 USAF-SwRI-NGC DTA template.

APPENDIX E AFGROW INPUT FILE SCREENSHOTS

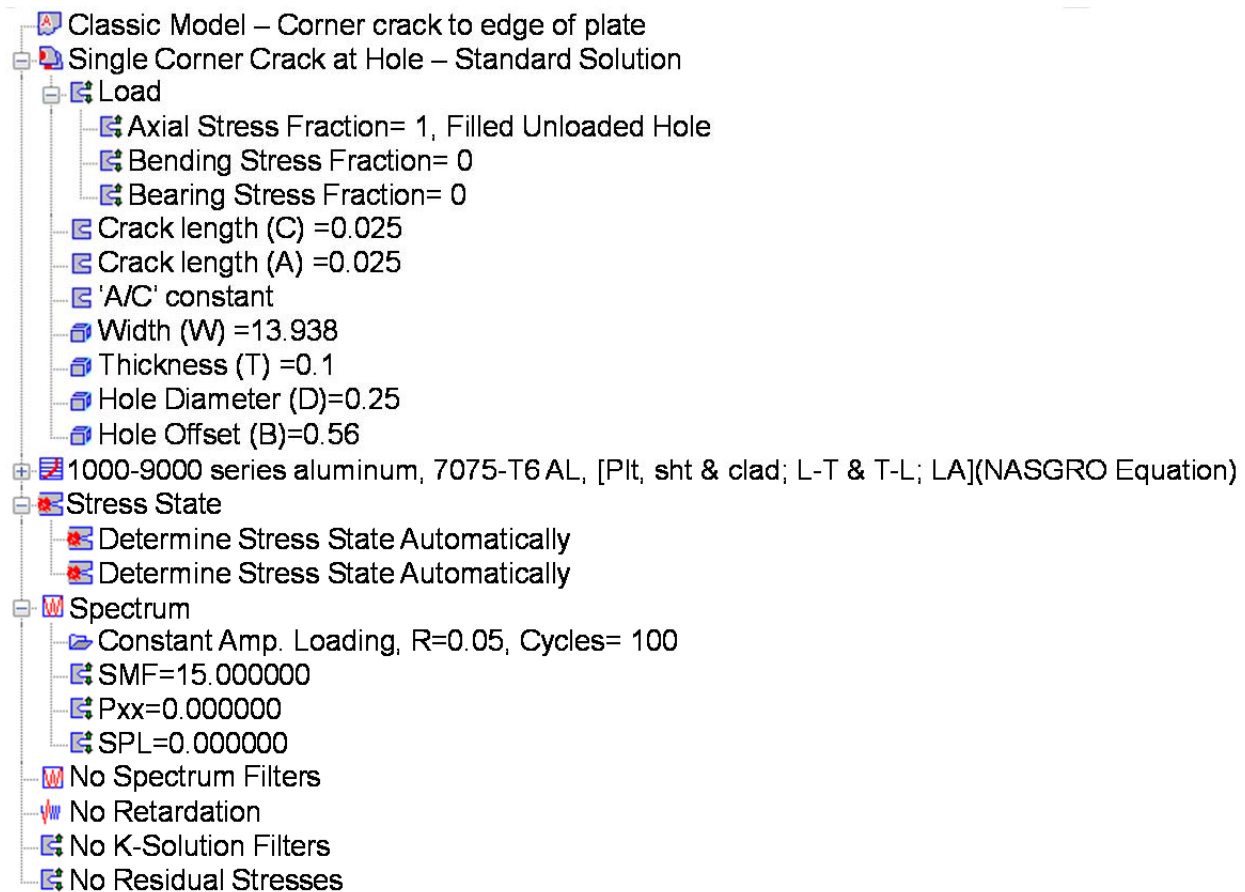


Fig. 68 AFGROW input file – tension model 1 - ligament crack – baseline.

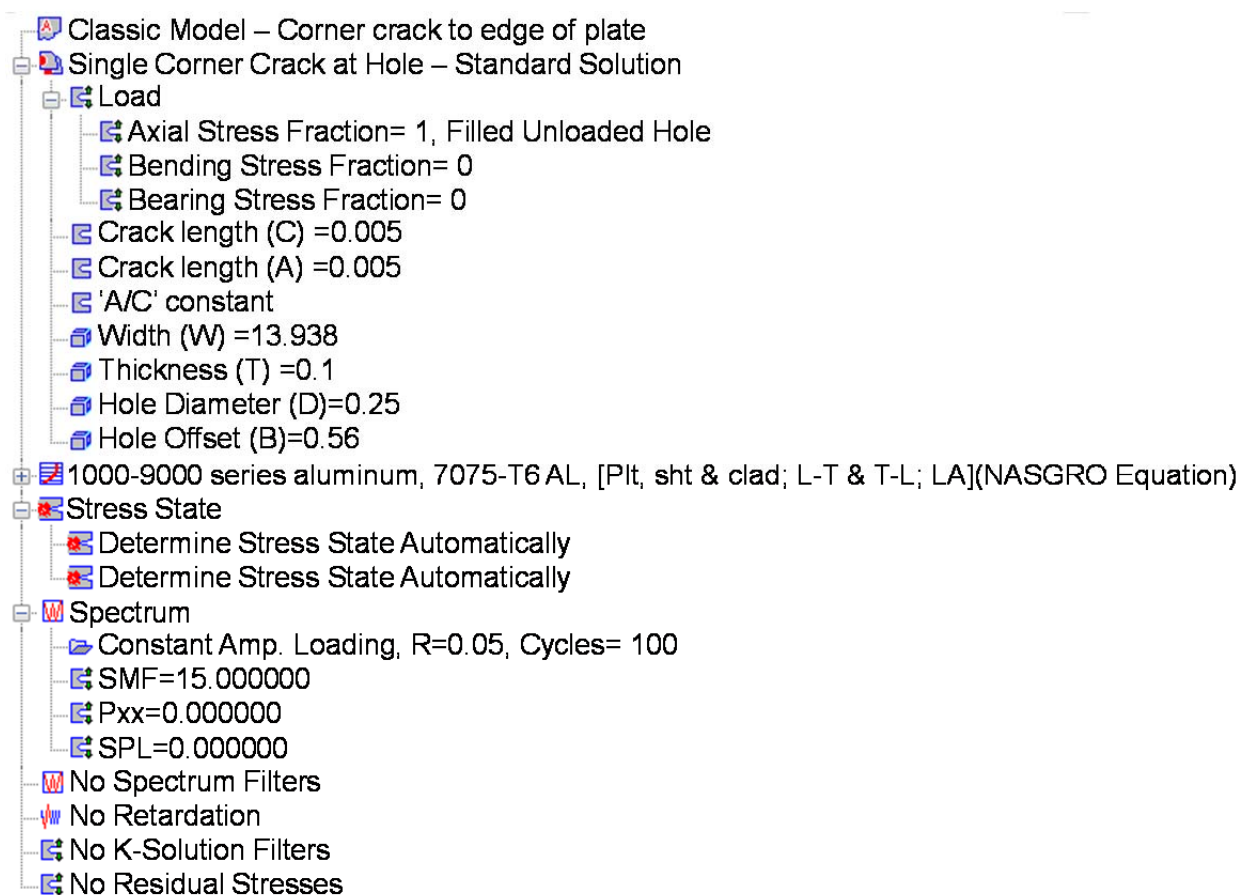


Fig. 69 AFGROW input file – tension model 2 - IFS for secondary crack – baseline.



Fig. 70 AFROW input file – tension model 3 - secondary crack – baseline.

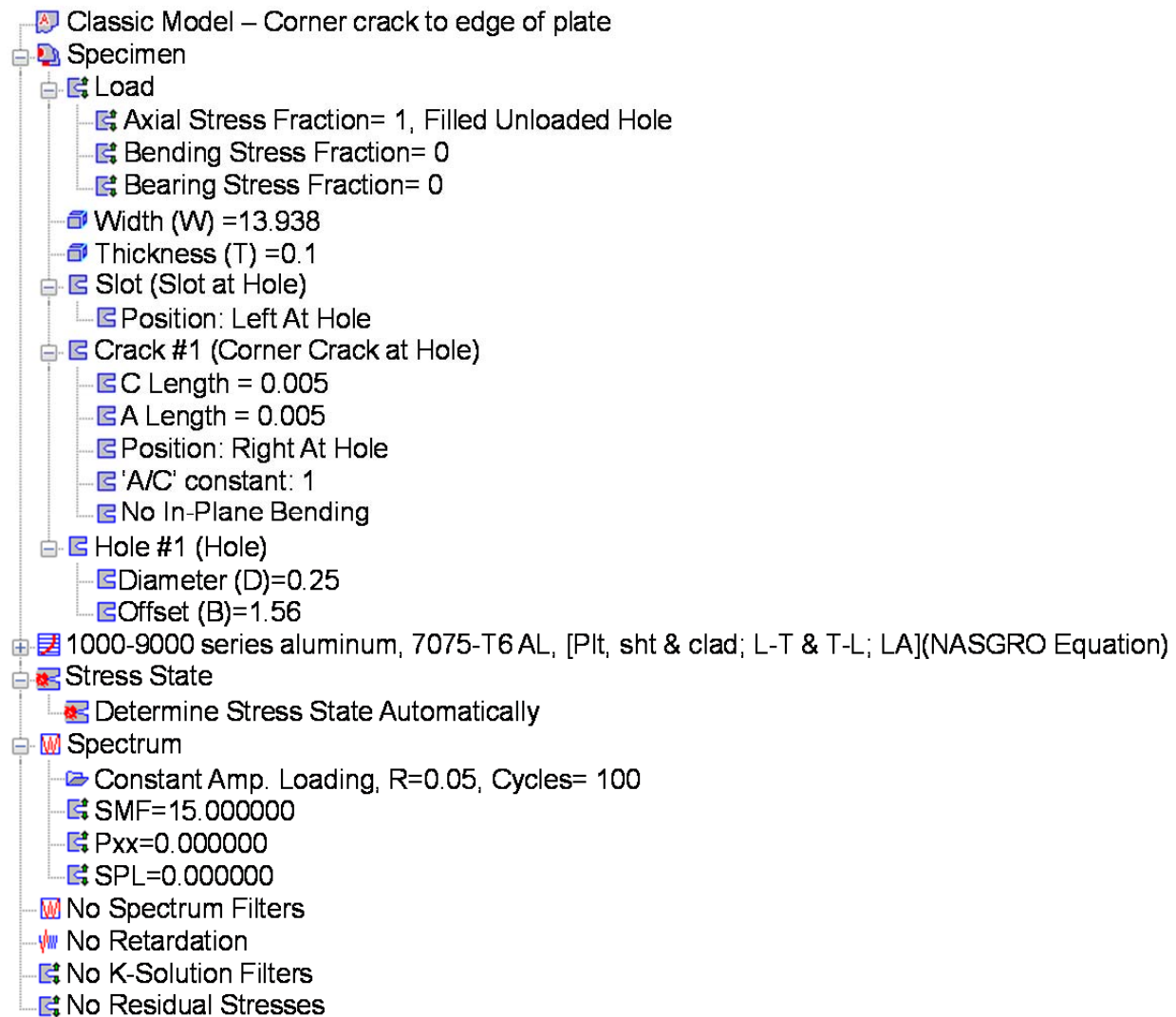


Fig. 71 AFGROW input file – tension model 4 - continuing damage crack – baseline.

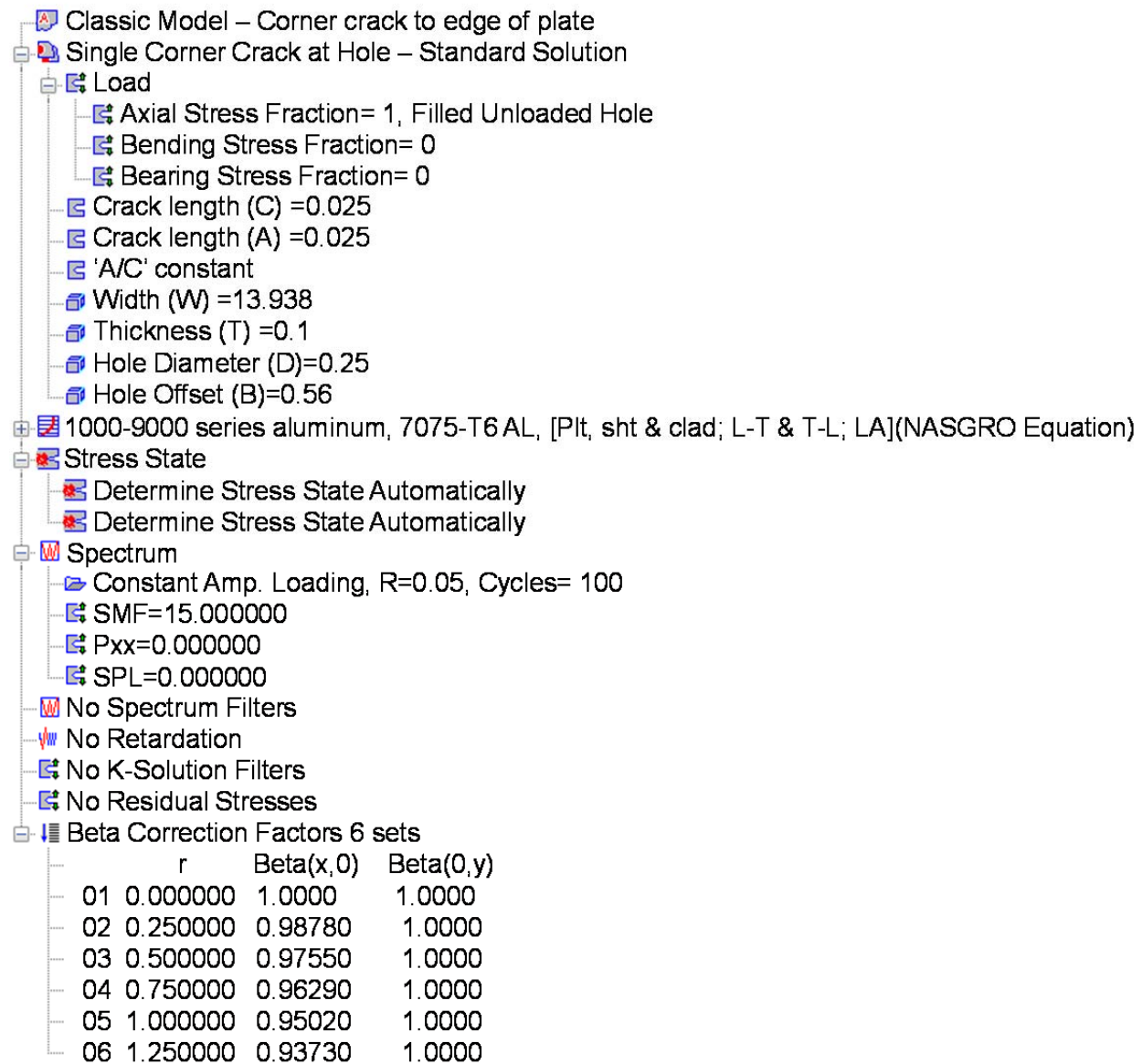


Fig. 72 AFGROW input file – tension model 1 - ligament crack – beta correction.

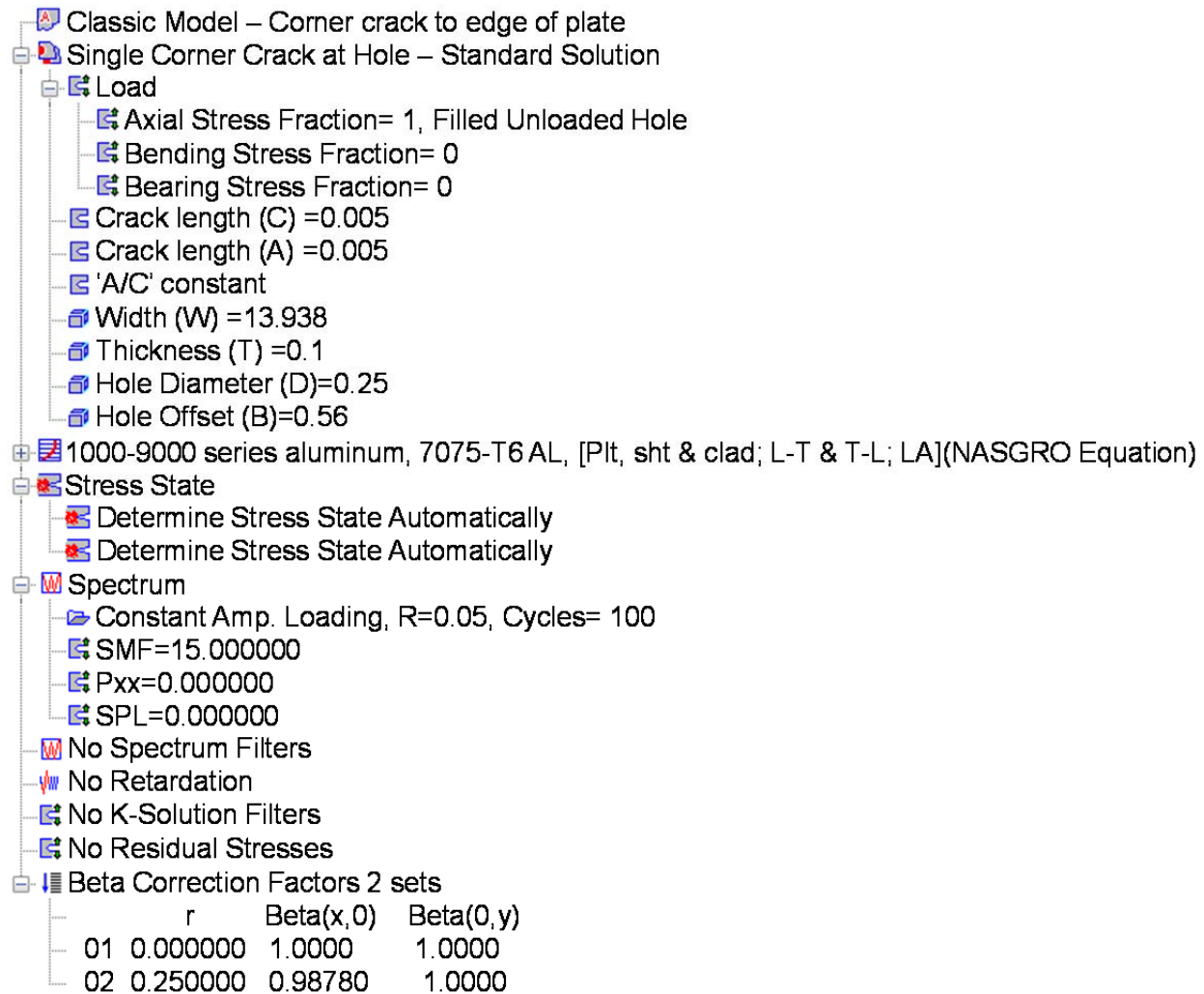


Fig. 73 AFGROW input file – tension model 2 - IFS for secondary crack – beta correction.

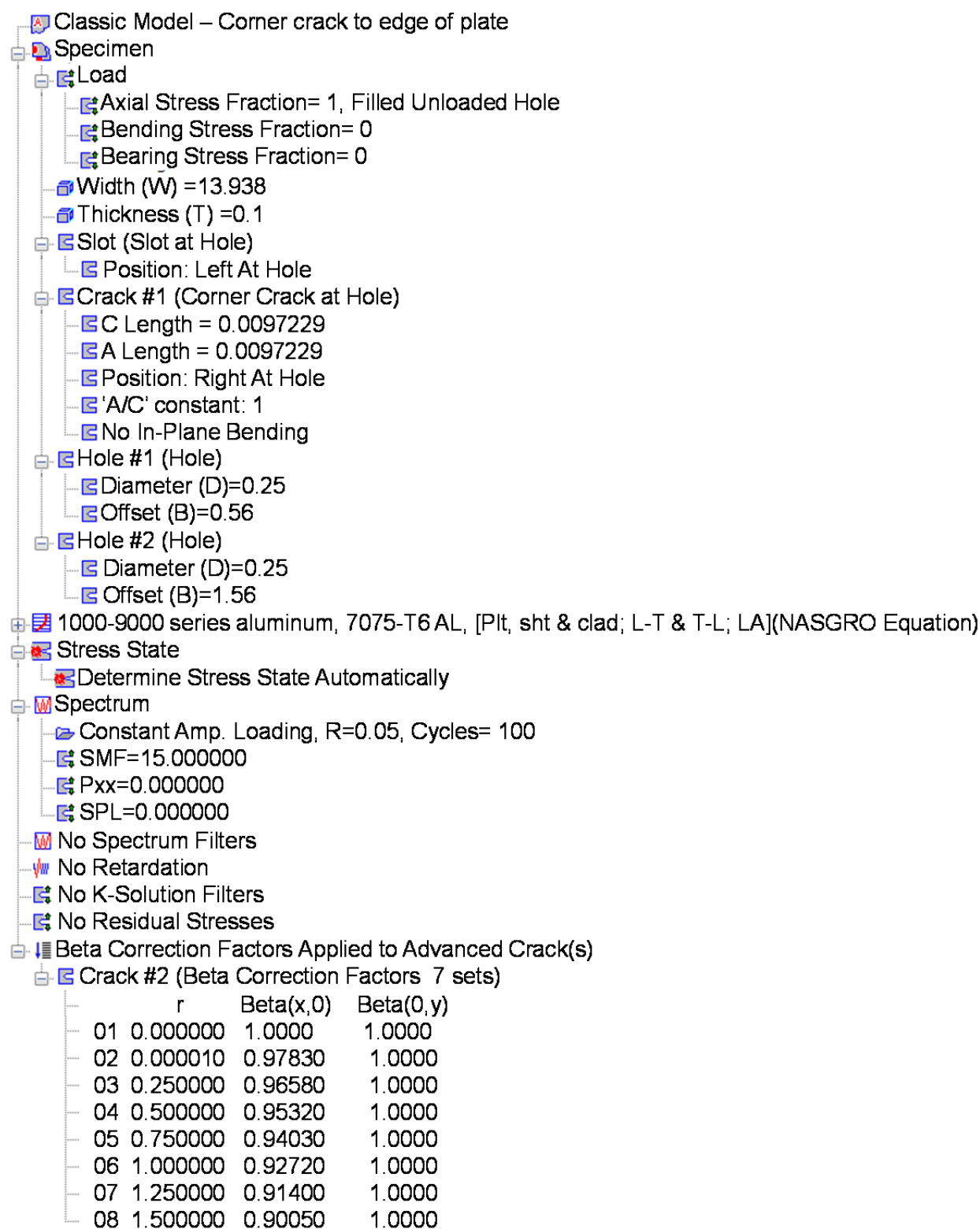


Fig. 74 AFROW input file – tension model 3 - secondary crack – beta correction.

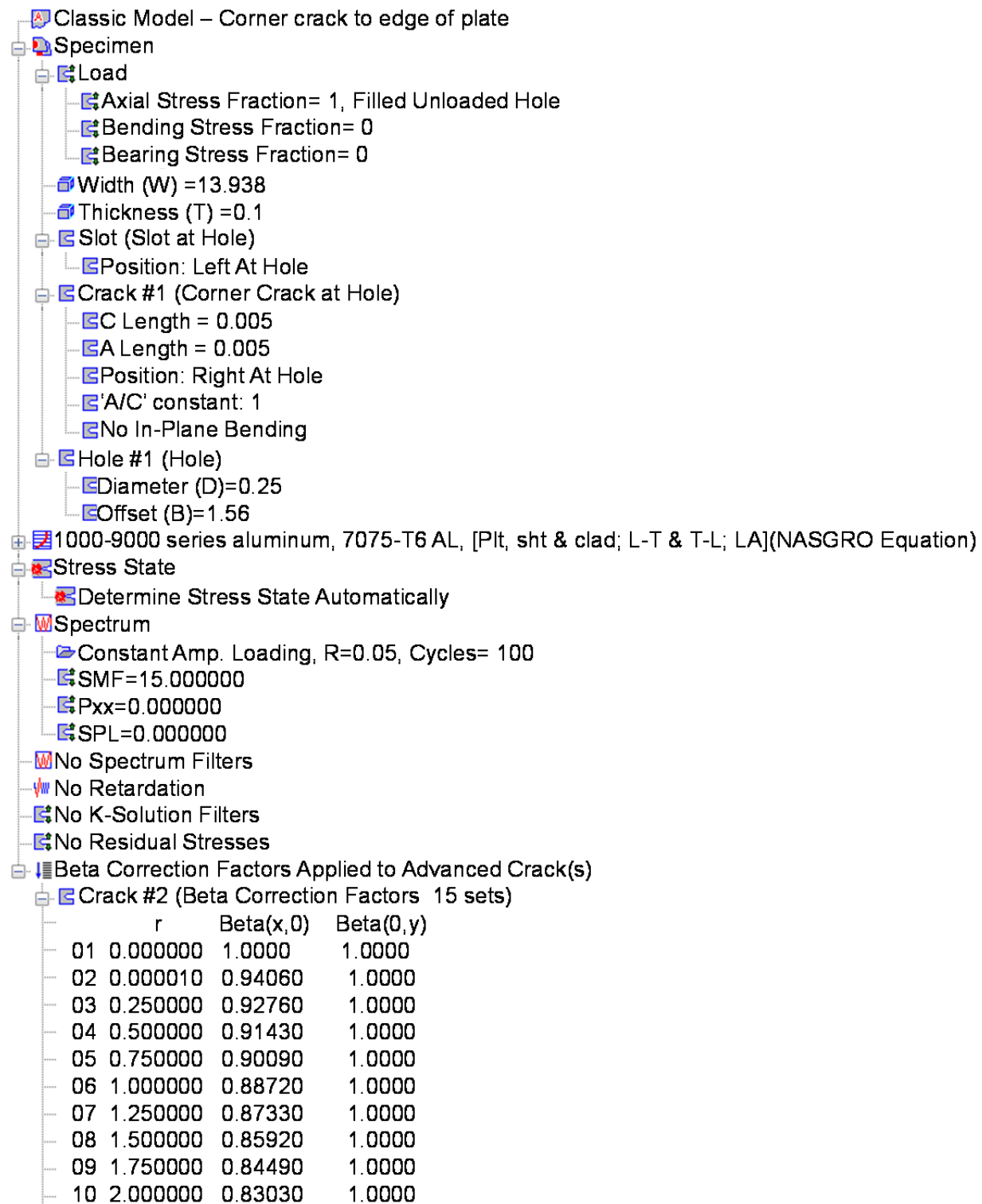


Fig. 75 AFGROW input file – tension model 4 - continuing damage crack – beta correction.

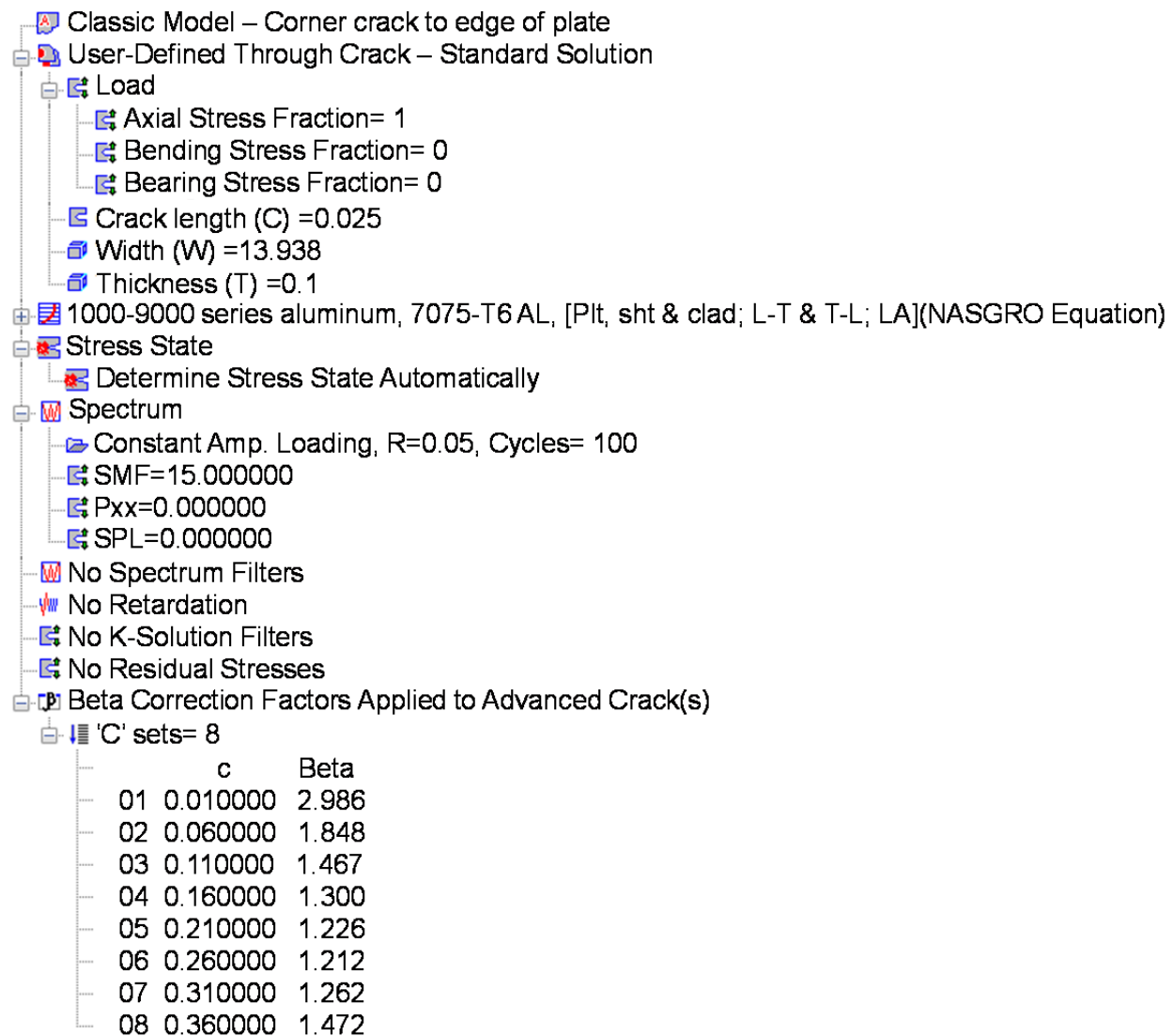


Fig. 76 AFGROW input file – tension model 1 - ligament crack – user-defined beta.

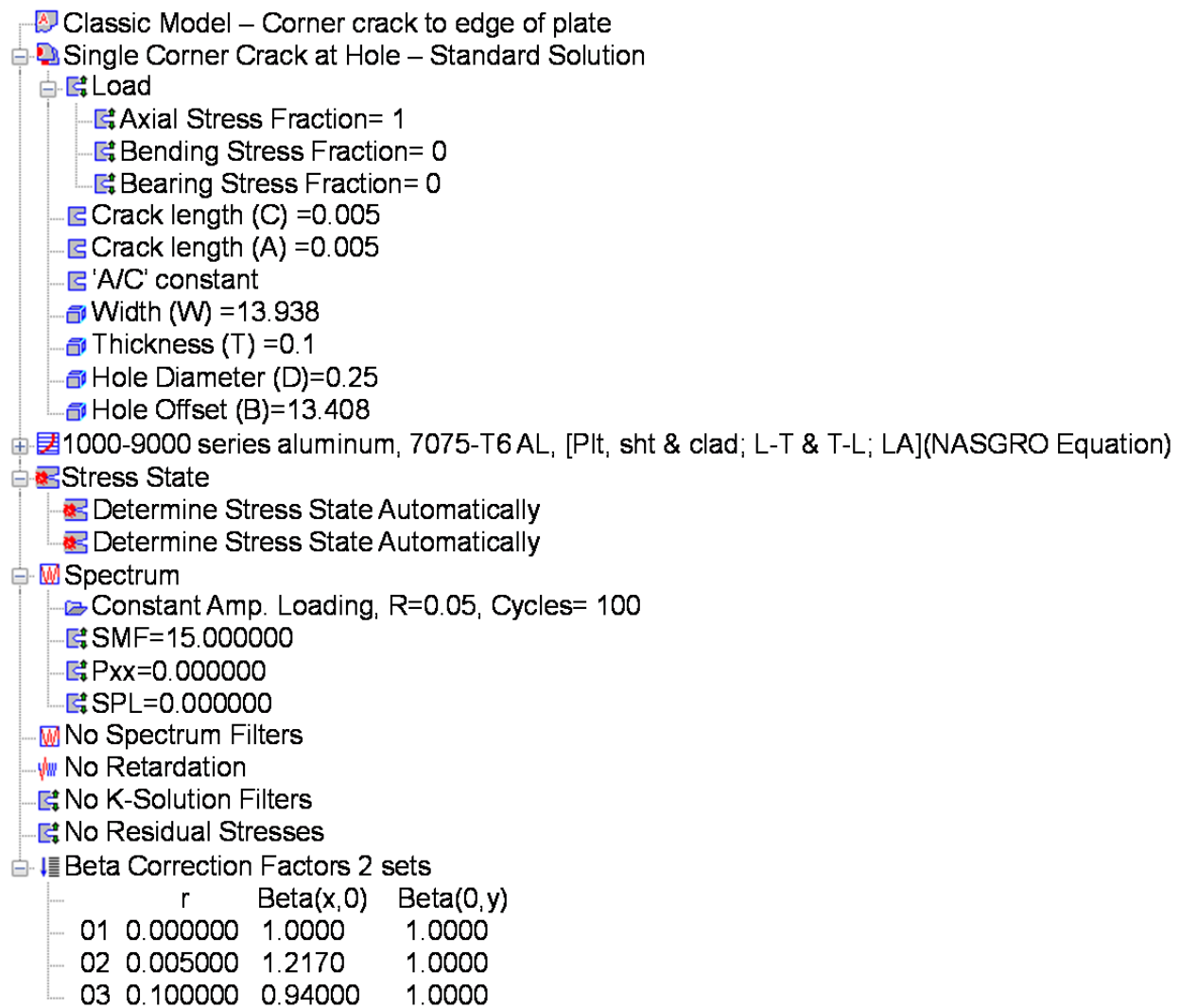


Fig. 77 AFGROW input file – tension model 2 - IFS for secondary crack – user-defined beta.

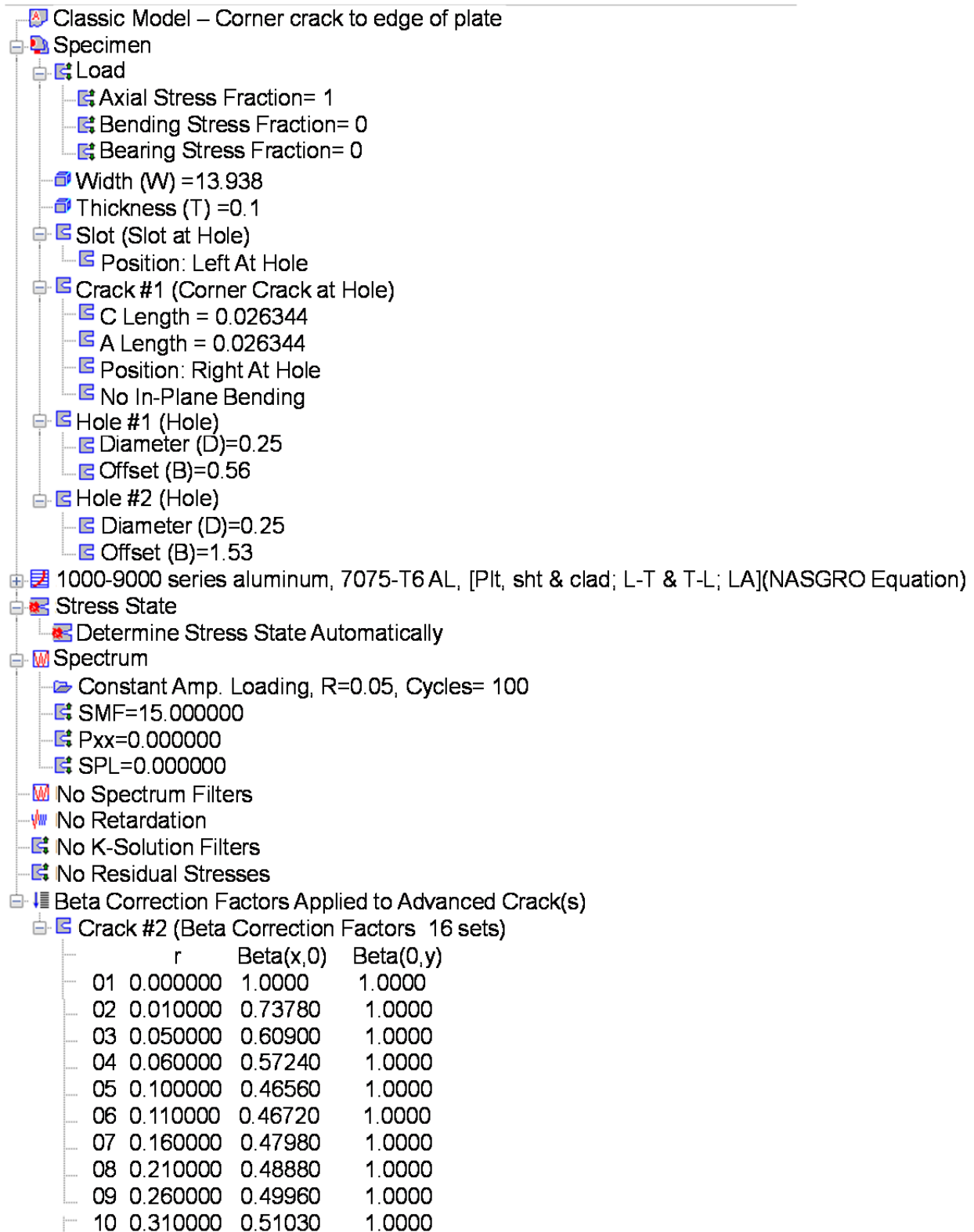


Fig. 78 AFROW input file – tension model 3 - secondary crack – user-defined beta.

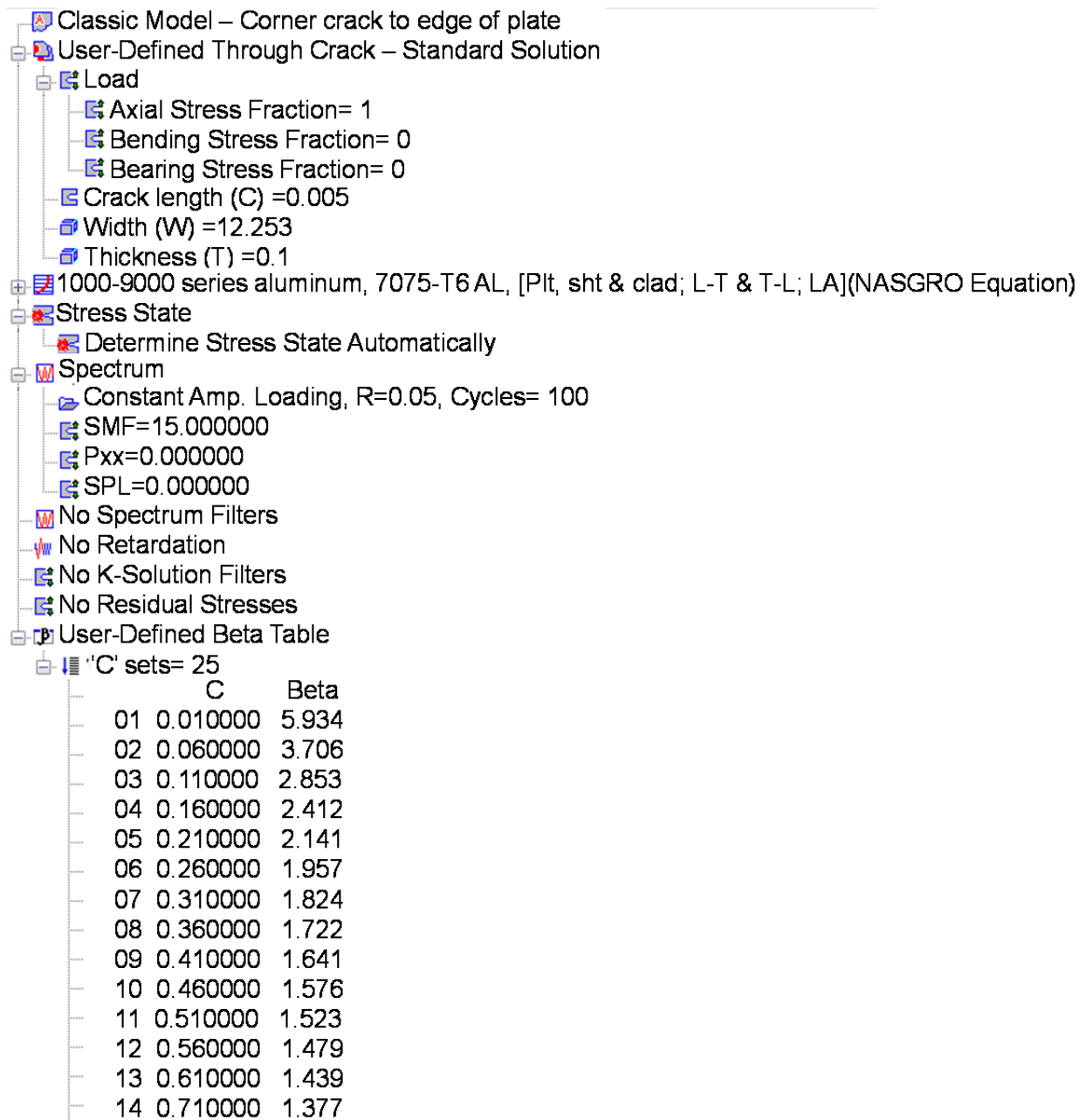


Fig. 79 AFGROW input file – tension model 4 - continuing damage crack – user-defined beta.

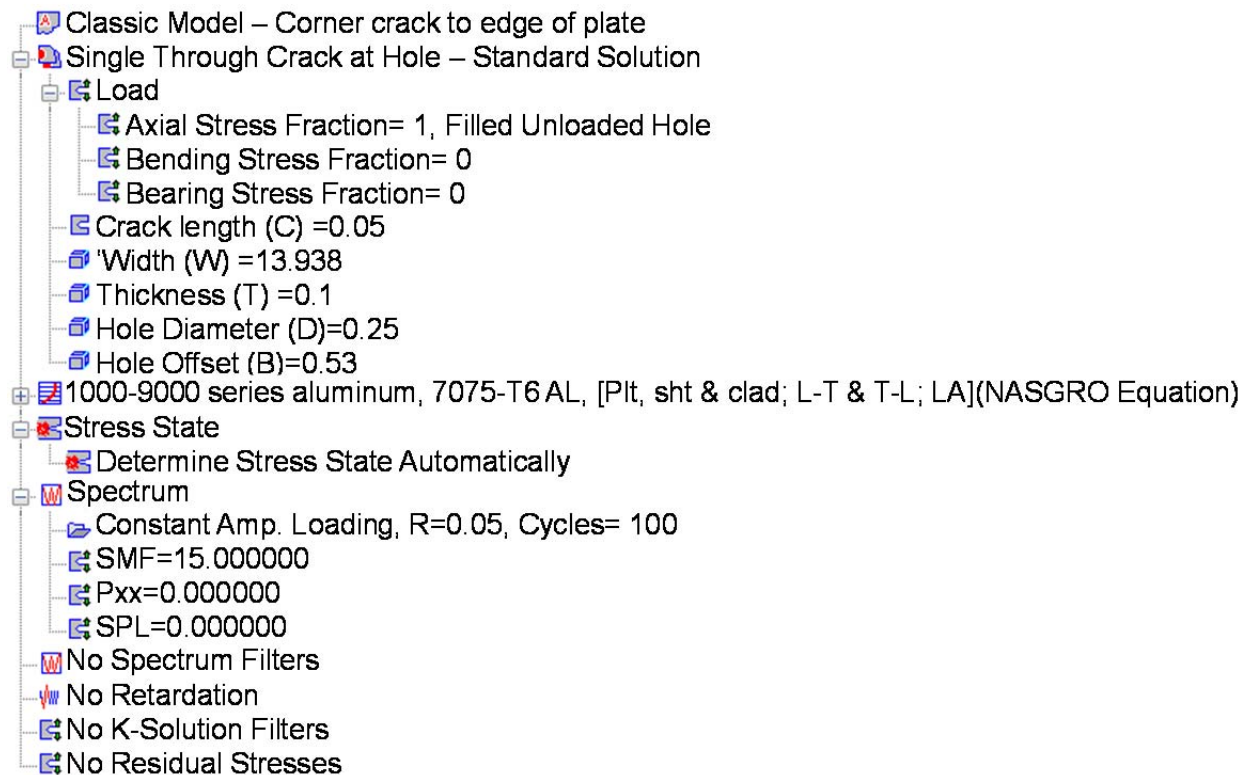


Fig. 80 AFGROW input file – bending model 1 - ligament crack – baseline.

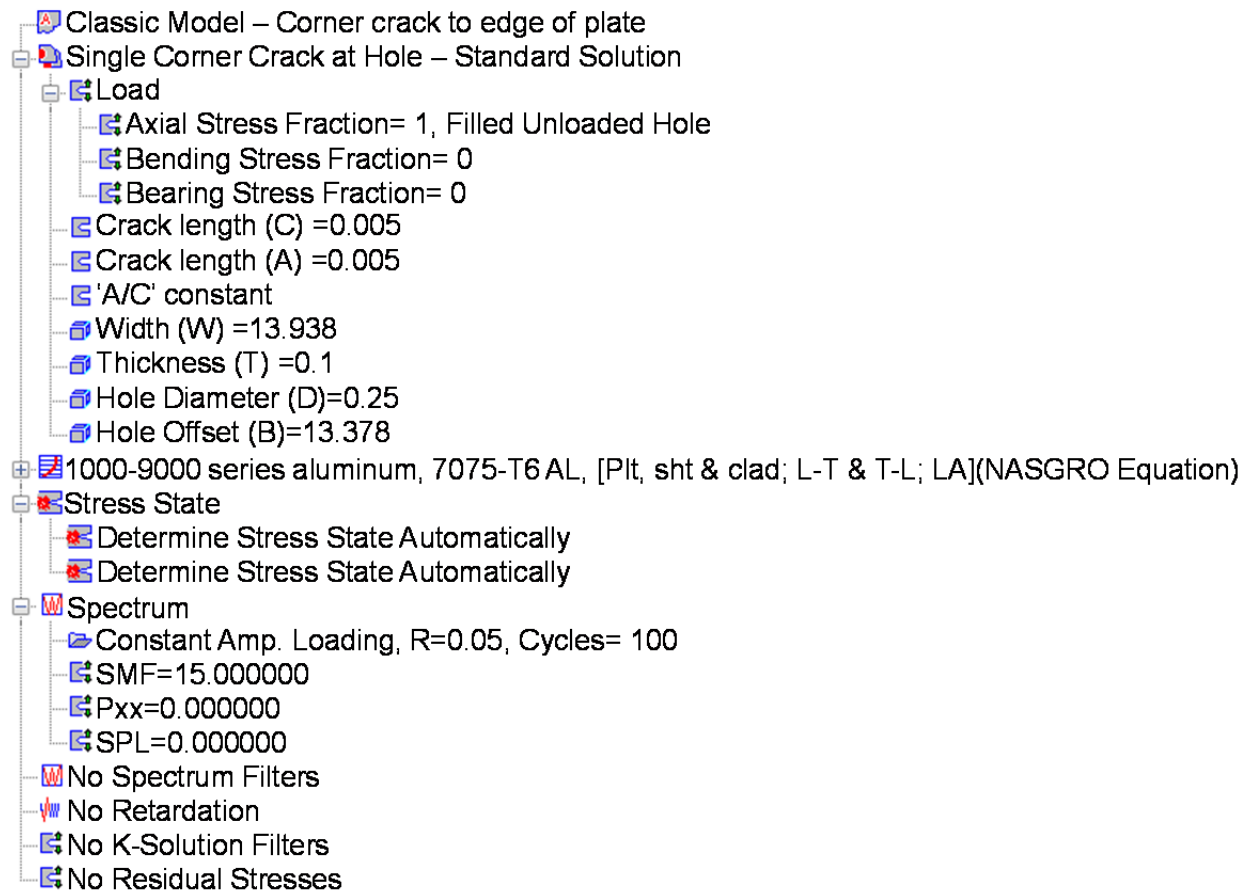


Fig. 81 AFGROW input file – bending model 2 - IFS for secondary crack – baseline.

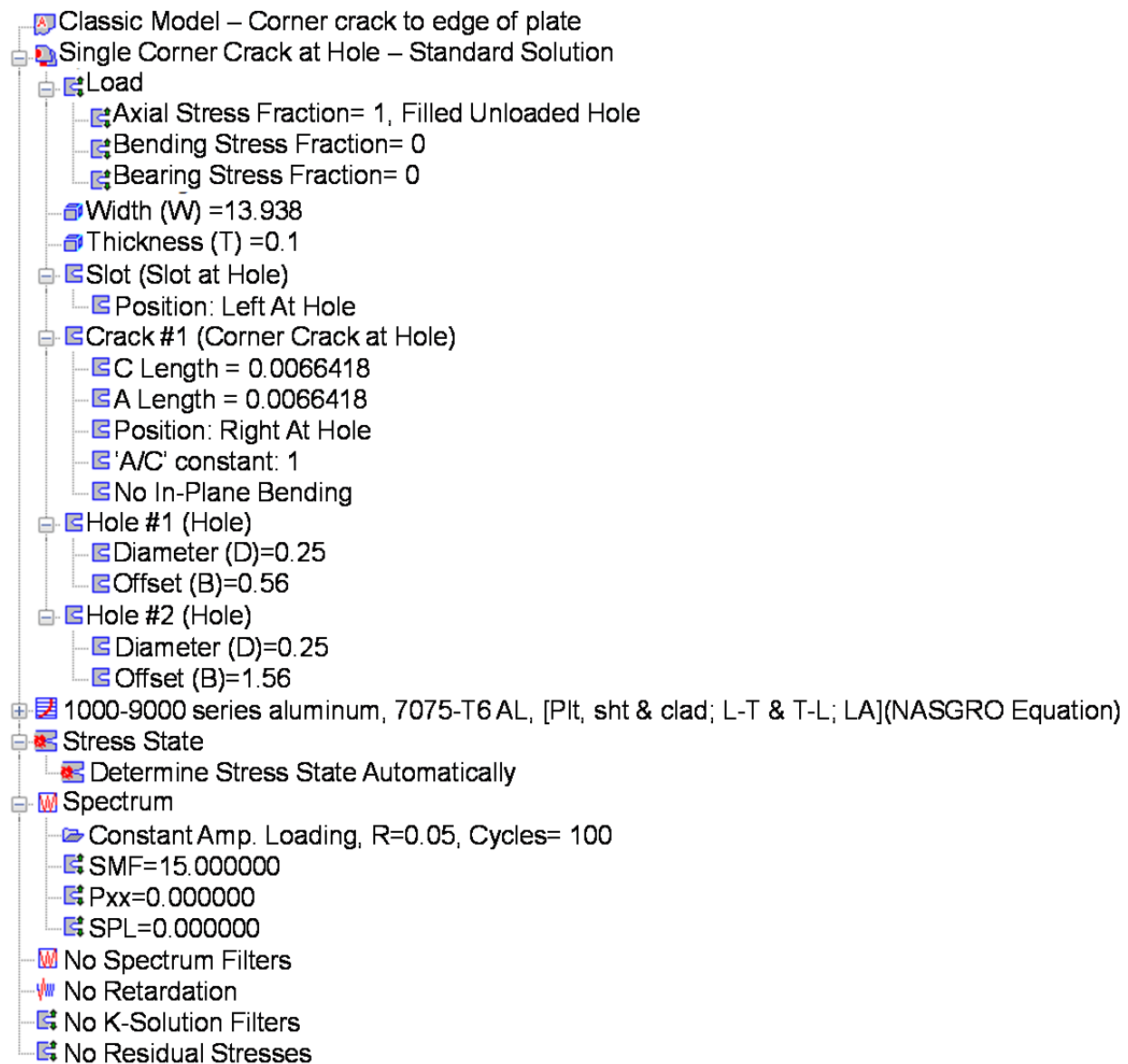


Fig. 82 AFROW input file – bending model 3 - secondary crack – baseline.

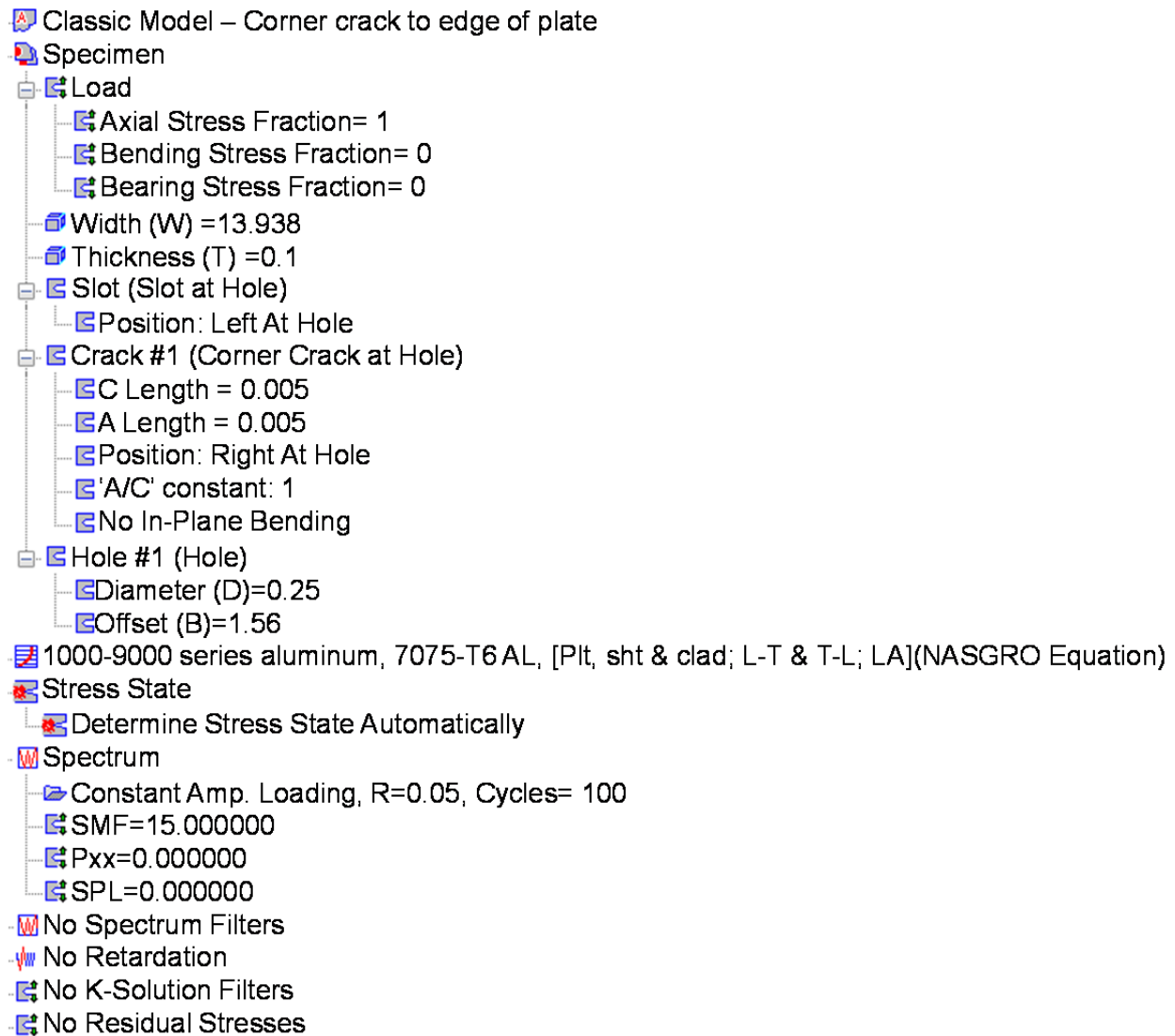


Fig. 83 AFGROW input file – bending model 4 - continuing damage crack – baseline.

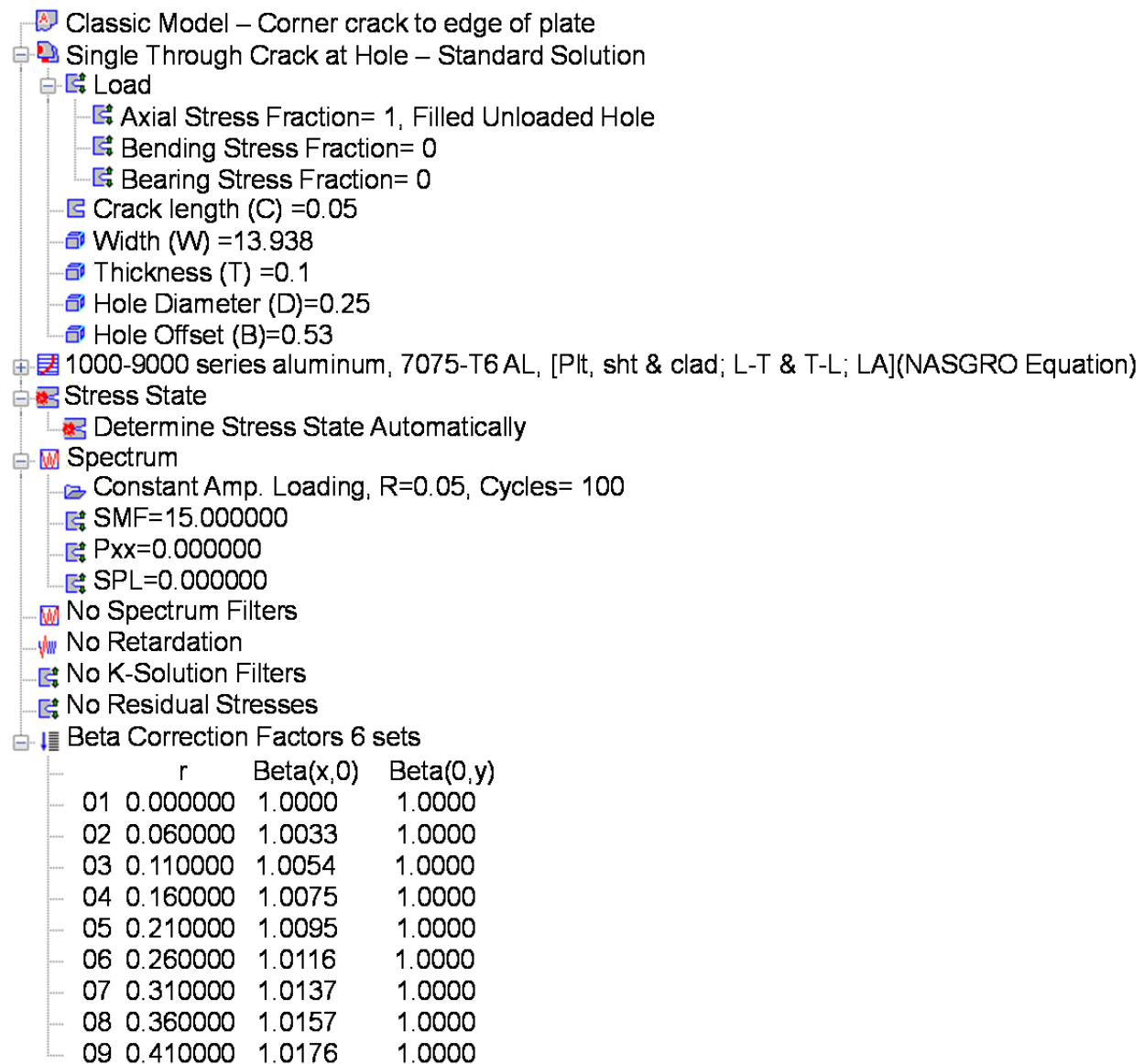


Fig. 84 AFGROW input file – bending model 1 - ligament crack – beta correction.

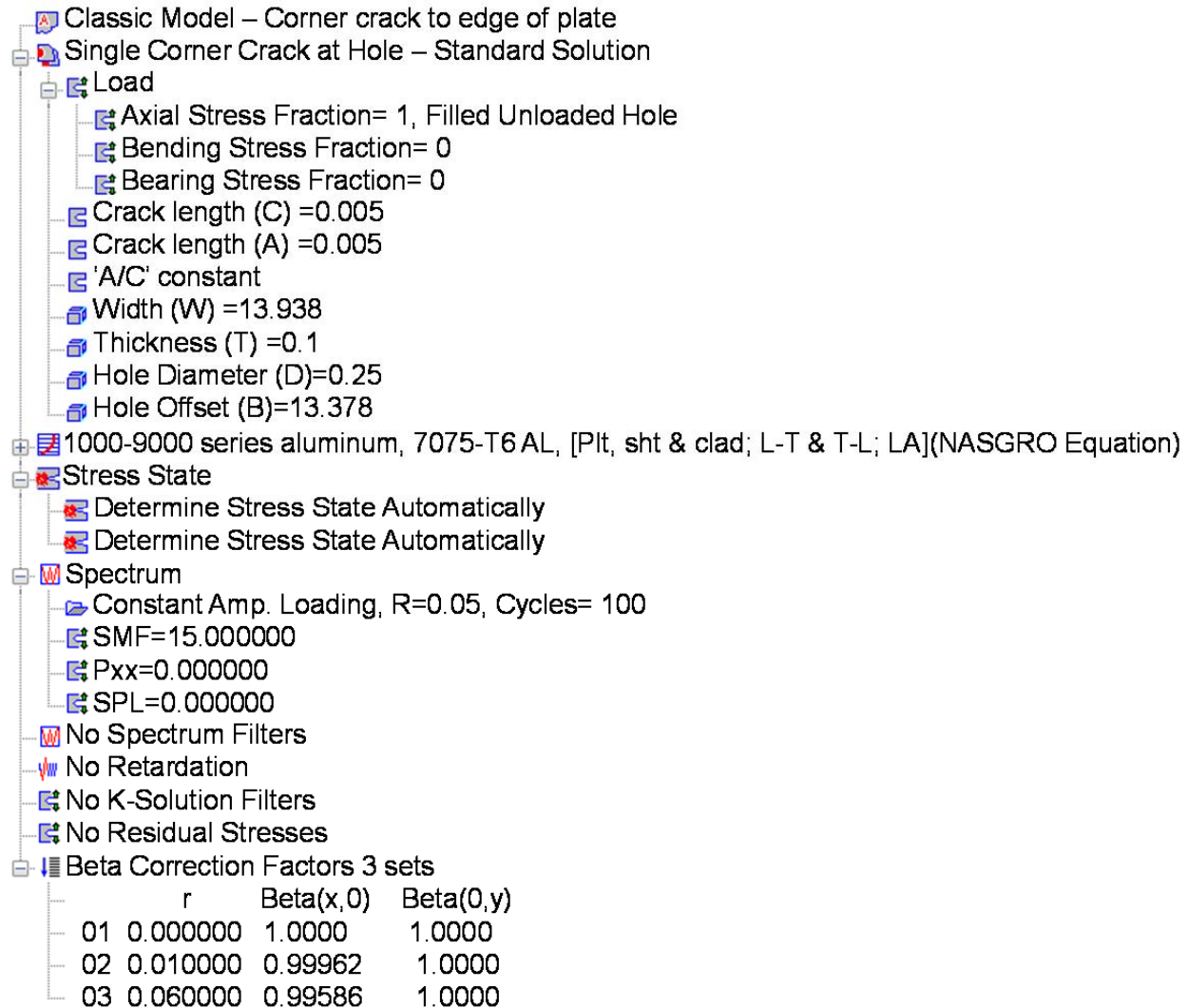


Fig. 85 AFGROW input file – bending model 2 - IFS for secondary crack – beta correction.

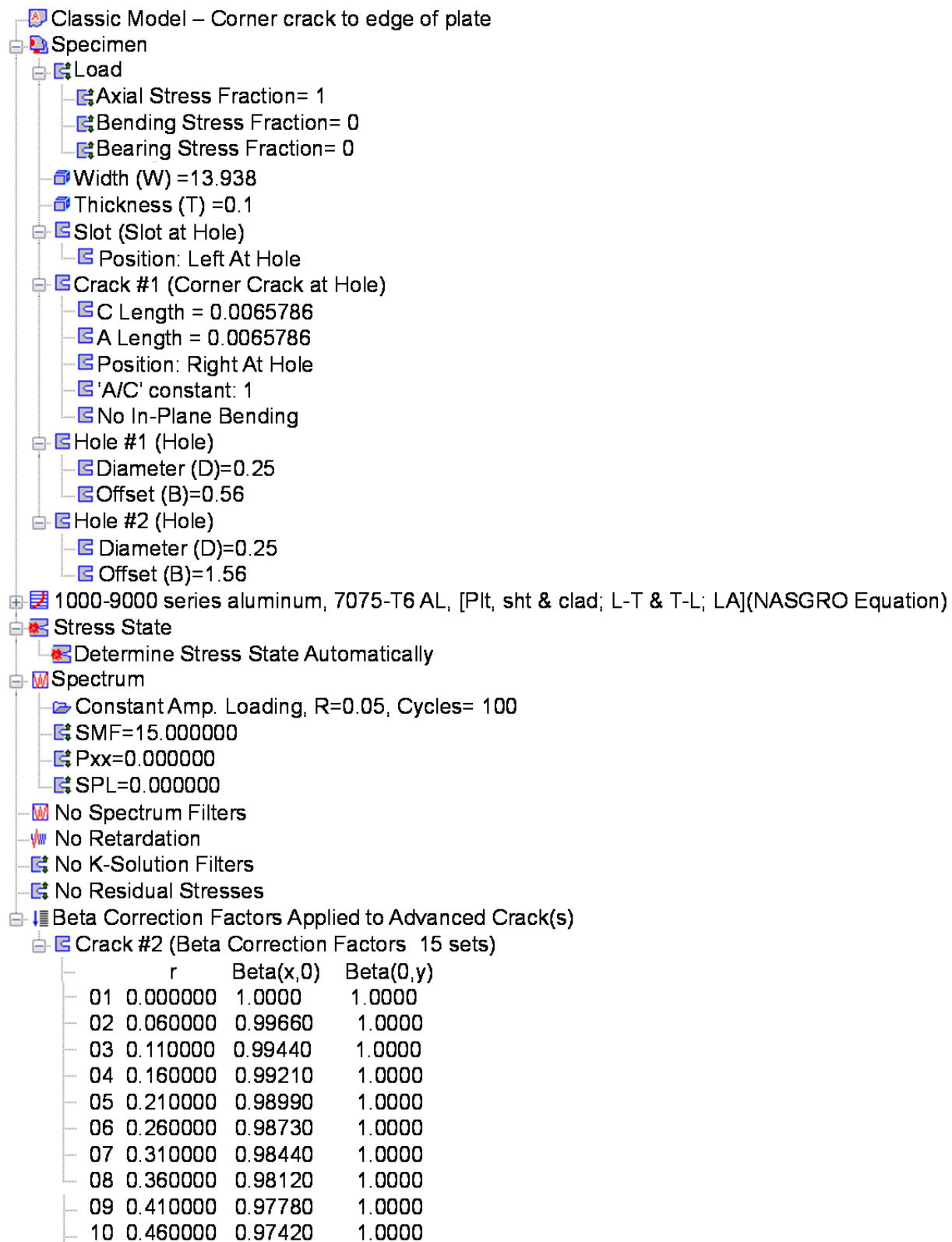


Fig. 86 AFROW input file – bending model 3 - secondary crack – beta correction.

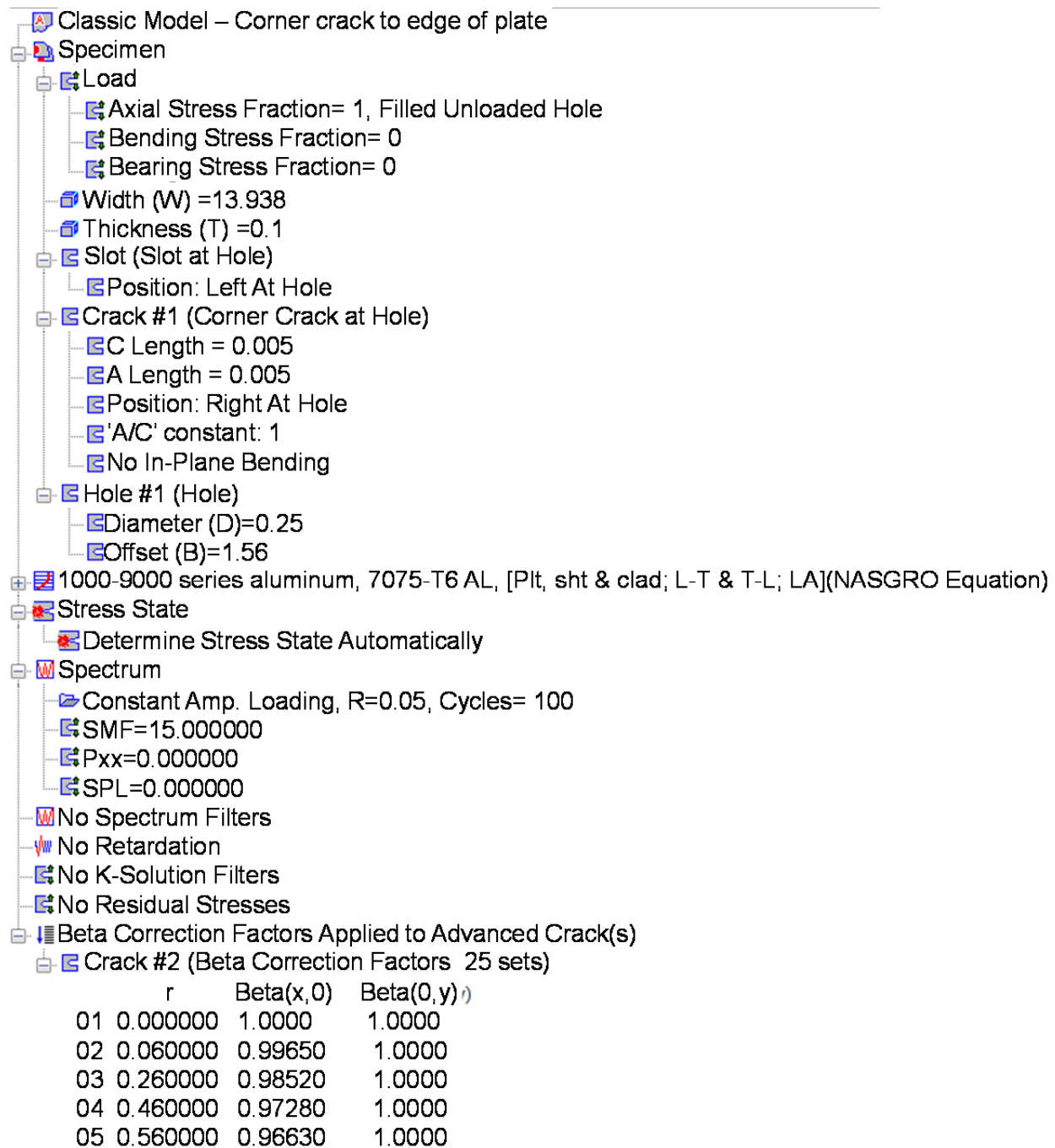


Fig. 87 AFGROW input file – bending model 4 - continuing damage crack – beta correction.

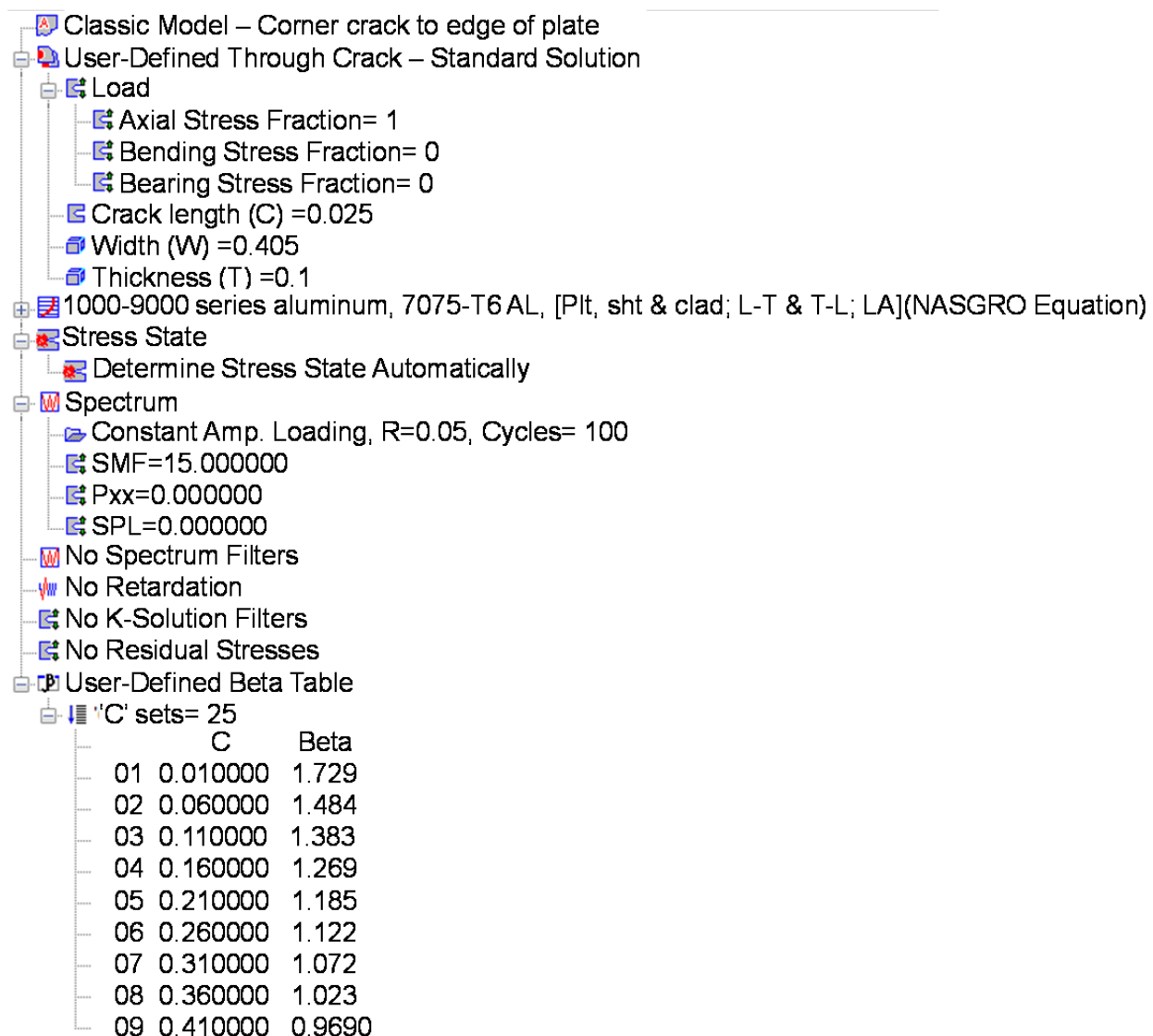


Fig. 88 AFGROW input file – bending model 1 - ligament crack – user-defined beta.

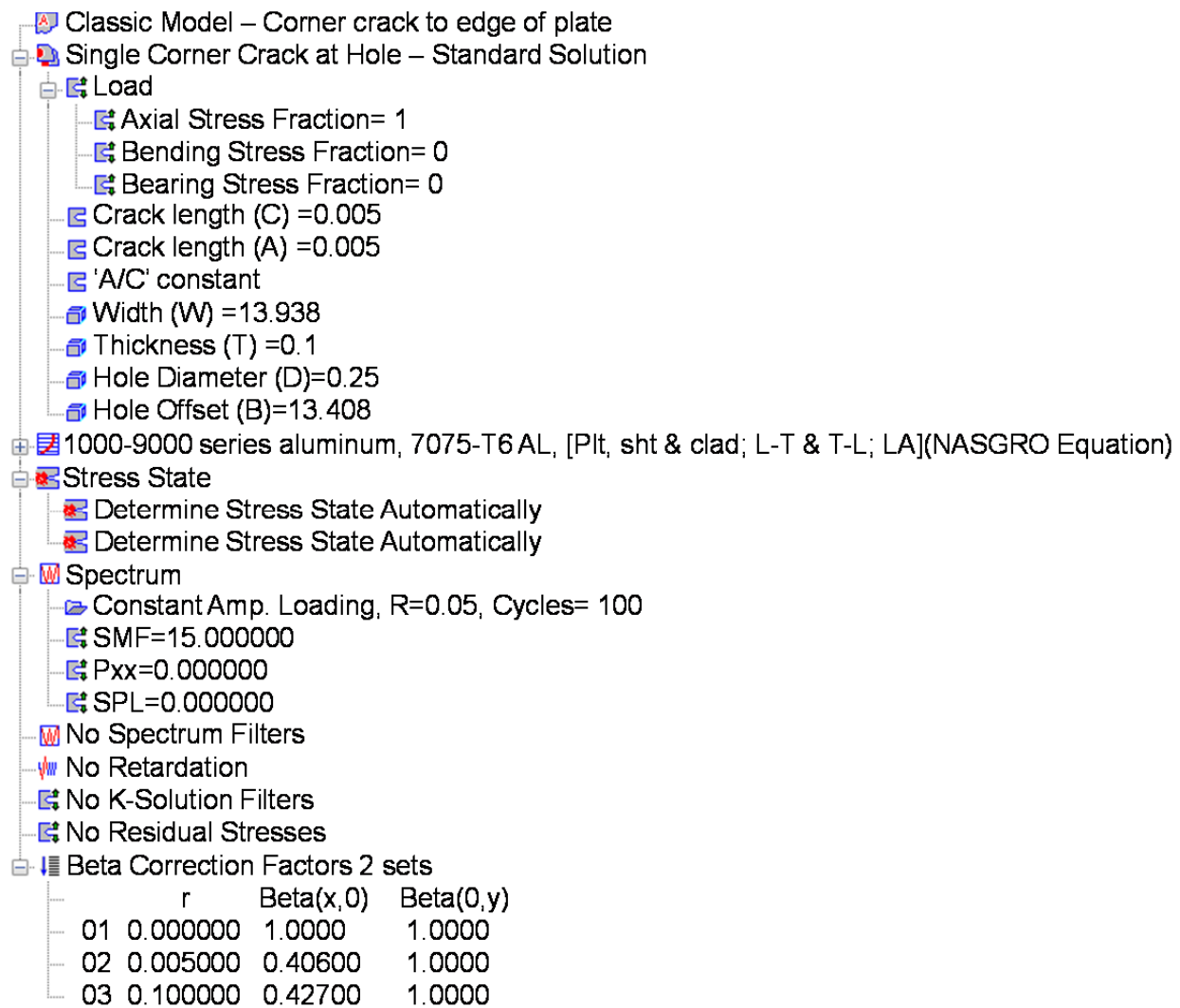


Fig. 89 AFGROW input file – bending model 2 - IFS for secondary crack – user-defined beta.

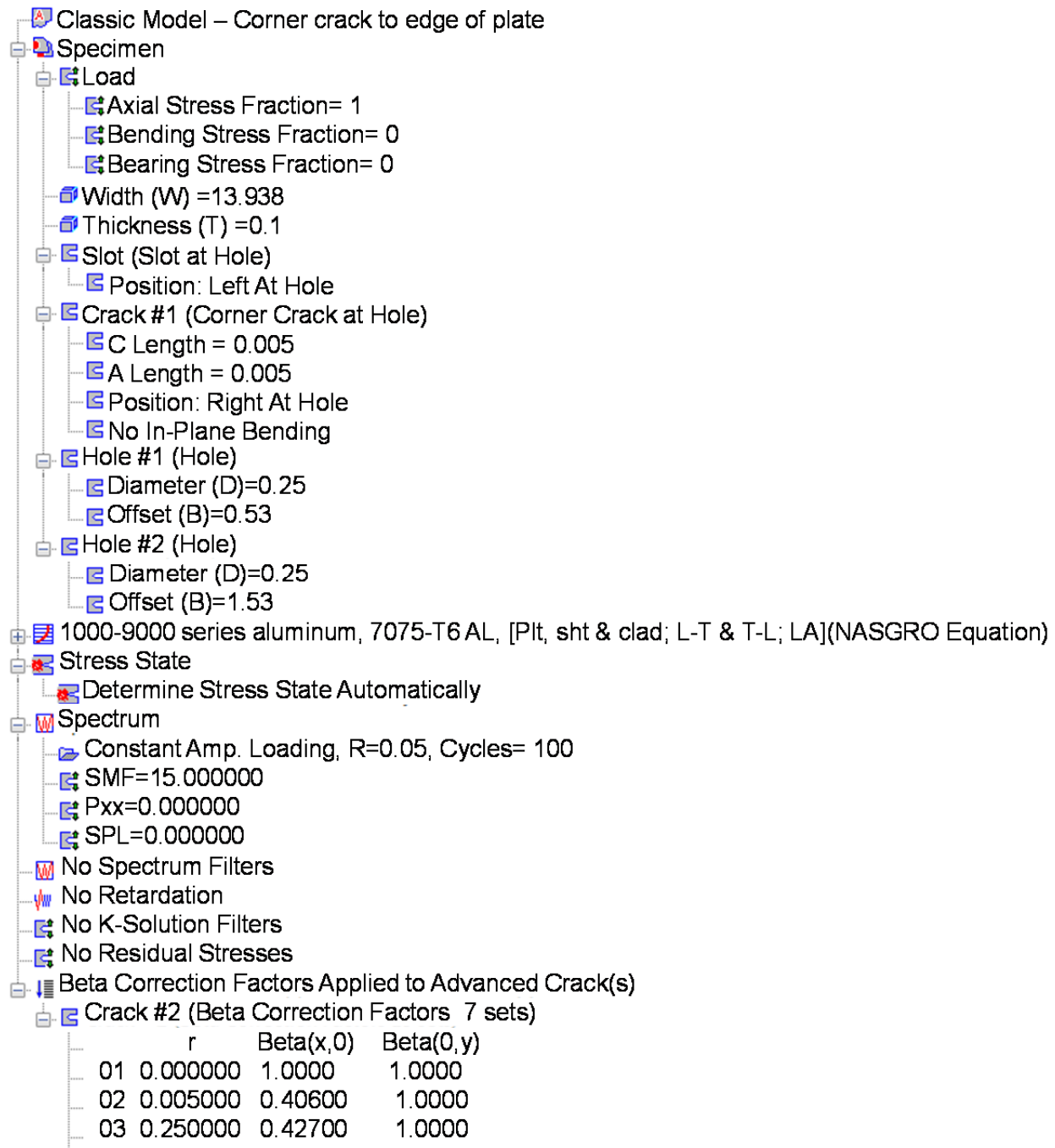


Fig. 90 AFROW input file – bending model 3 - secondary crack – user-defined beta.

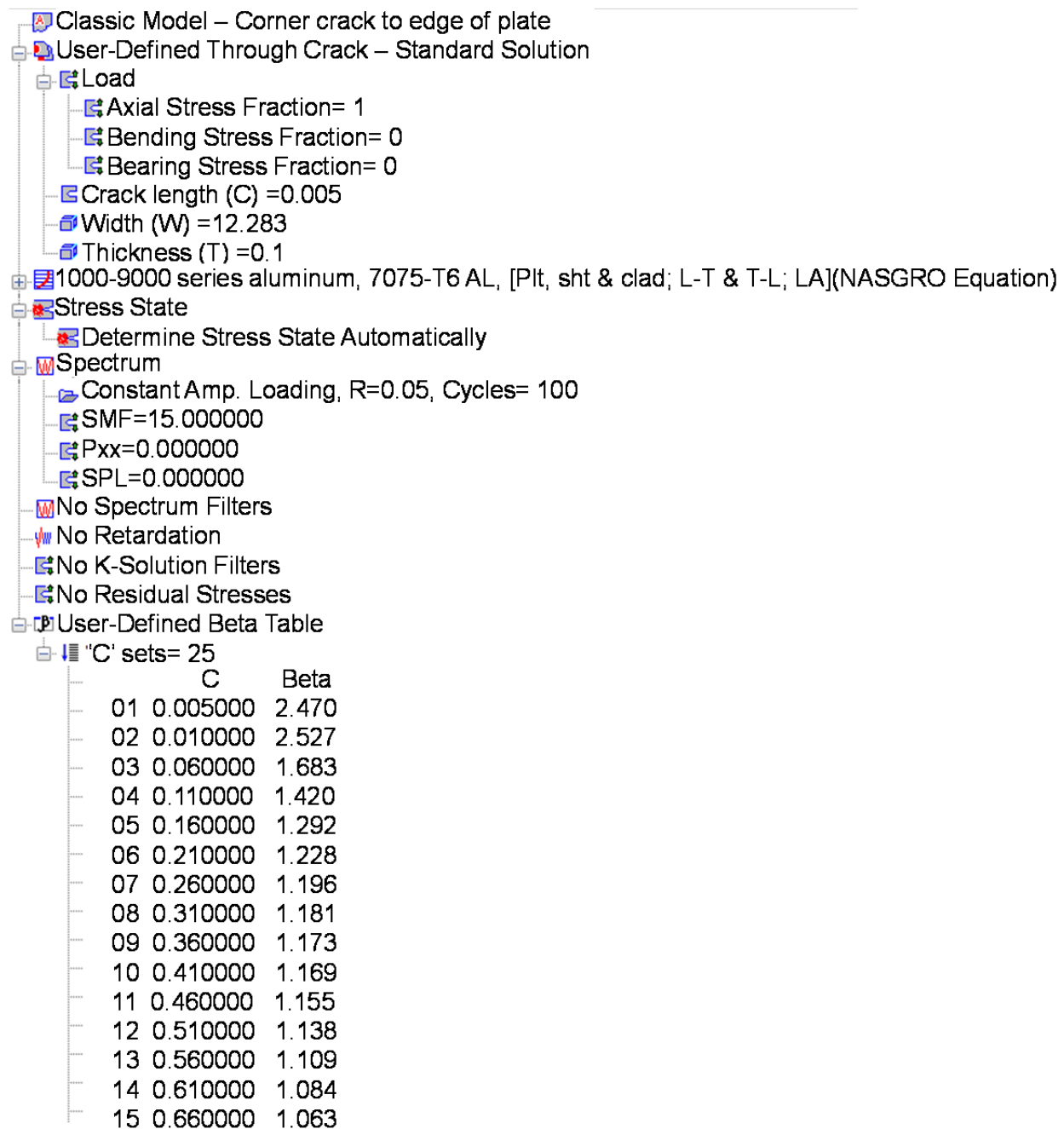


Fig. 91 AFGROW input file – bending model 4 - continuing damage crack – user-defined beta.

REFERENCES

- ¹ Gebman, Jean R. (2009). Challenges and Issues with the Further Aging of U.S. Air Force Aircraft, RAND Corporation, Santa Monica, CA, USA.
- ² Goranson, Ulf G. (1993). Damage Tolerance Facts and Fiction. 17th Symposium of the International Committee on Aeronautical Fatigue, Stockholm, Sweden.
- ³ Kaplan, Mitchell P., Lincoln, John W. (1996) The U.S. Air Force Approach to Aircraft Damage Tolerant Design. *ASM Handbook, Volume 19: Fatigue and Fracture*. ASM International, Materials Park, OH, USA.
- ⁴ Tong, Yu C. (2001) Literature Review on Aircraft Structural Risk and Reliability Analysis. *Defence Science & Technology Organisation* DTSO-TR-1110, 1-3.
- ⁵ Schutz, W. (1996) *A History of Fatigue*. *Engineering Fracture Mechanics*, **54**, 2. pp263-300.
- ⁶ Buntin, W.D. (1969). *Concept and Conduct of Proof Test of F-111 Production Aircraft*, United States Air Force.
- ⁷ Gallagher, J.P. (2007). A Review of Philosophies, Processes, Methods and Approaches that Protect In-Service Aircraft from the Scourge of Fatigue Failures. *ICAF '07 International Committee of Aeronautical Fatigue*, Naples, Italy. p.2
- ⁸ Cameron, D.W, Hoepfner, D.W. (1996). Fatigue Properties in Engineering. *ASM Handbook, Volume 19: Fatigue and Fracture*. ASM International, Materials Park, OH, USA.
- ⁹ United States Department of Defense. (1998) Joint Service Specification Guide Aircraft Structures. JSSG-2006.
- ¹⁰ United States Department of Defense. (2005). Aircraft Structural Integrity Program (ASIP). MIL-STD-1530C.
- ¹¹ Schijve, J. (2001) *Fatigue of Structures and Materials*. Kluwer Academic Publishers, Norwell, MA, USA.
- ¹² Grandt, A.F. (2004). Fundamentals of Structural Integrity Damage Tolerant Design and Nondestructive Evaluation. John Wiley & Sons, Hoboken, NJ, USA. p.482, 494.
- ¹³ Committee on Aging of U.S. Air Force Aircraft. (1997). Aging of U.S. Air Force Aircraft Final Report. (NMAB-488-2). National Materials Advisory Board, Commission on Engineering and Technical Systems, National Research Council. National Academy Press, Washington D.C., USA.

- ¹⁴ Hovey, P.W., Berens, A.P., Skinn, D.A. (1991). Risk Analysis for Aging Aircraft Volume 1 – Analysis. WL-TR-91-3066. Flight Dynamics Directorate, Wright Laboratory, Wright-Patterson AFB, OH 45433.
- ¹⁵ United States Air Force website. Available at <http://www.af.mil/shared/media/photodb/photos/081107-F-7823A-979.jpg> [Accessed 03 October 2011].
- ¹⁶ Grube, K., Burnside, H., Clark, P. (2006) Damage Tolerance Reassessment: Reconfigured Post Desert Storm Severe Spectrum. SA220R0207. Northrop Grumman Corporation, Bethpage, NY, USA.
- ¹⁷ King, C. (2007). Spar Web Continuing Damage Study. A3G-2007-178864. United States Air Force.
- ¹⁸ Rouse, Marshall, Jegley, Dawn, McGowan, David, Bush, Harold, Waters, W.A. (2005). Utilization of the Building-Block Approach in Structural Mechanics Research. NASA
- ¹⁹ Kokoris, J., Smith, R., Grube, K. (2009). Final Engineering Report A-10A Damage Tolerance Analysis Summary of Control Point Stress Equations and Reconfigured Post-Desert Storm Severe Spectrum Maximum Stresses. SA220R0474, Rev. C. Northrop Grumman Corporation, Bethpage, NY, USA.
- ²⁰ Northrop Grumman Systems Corporation. (2009). Spar Web Component Test Specimen A-10 Spar Web Damage Tolerance Analysis Validation, Rev -, GT264KA001.
- ²¹ Grasso, S., Miro, S., Grube, K. (2008) A-10A Simulated Spar Web Component Crack Growth Test Planning Document. GT220W0311. Northrop Grumman Corporation. Bethpage, NY, USA.
- ²² Levy, M., Miro, S., Kassinger, M., Grube, K. (2011). Spar Web Damage Tolerance Analysis Validation Test Results Report. GT200R0314. Northrop Grumman Corporation. Bethpage, NY, USA.
- ²³ American Society for Testing and Materials (ASTM) Committee E08. (2007). *Standard Terminology Relating to Fatigue and Fracture Testing (E 1823-07a)*, ASTM, West Conshohocken, PA, USA.
- ²⁴ Broek, D. (1989). *The Practical Use of Fracture Mechanics*. Kluwer Academic Publishers, Norwell, MA, USA.
- ²⁵ Northrop Grumman Systems Corporation. (2009). Fixture Spar Web Component Test Specimen, Rev. -. GT264KB001.

²⁶Reams, R., Babish, C.A. (2011). Revised Damage Tolerance Requirements and Determination of Operational Life Limits for Slow Crack Growth Metallic Structures (EN-SB-08-002, Revision A). United States Air Force.